2008

Hydrogenase Inhibition by O2: Density Functional Theory/Molecular Mechanics Investigation

Daniela Dogaru
Cleveland State University

HYDROGENASE INHIBITION BY O_2: DENSITY FUNCTIONAL THEORY/MOLECULAR MECHANICS INVESTIGATION

DANIELA B. DOGARU

Bachelor of Science in Chemistry

University of Bucharest, Romania

July, 2000

Master of Science in Chemistry

University of Bucharest, Romania

July, 2002

submitted in partial fulfillment of requirements for the degree

DOCTOR OF PHILOSOPHY IN CLINICAL AND BIOANALYTICAL CHEMISTRY

at the

CLEVELAND STATE UNIVERSITY

December, 2008

In Memoriam – My Dear Aunt Mariana Bobarnac Dogaru

HYDROGENASE INHIBITION BY O_2: DENSITY FUNCTIONAL THEORY/MOLECULAR MECHANICS INVESTIGATION

DANIELA B. DOGARU

ABSTRACT

[Fe-Fe]-hydrogenases are enzymes that reversibly catalyze the reduction of protons to molecular hydrogen, which occurs in anaerobic media. In living systems, [Fe-Fe]-hydrogenases shift the reversible reaction towards H_2 formation. The [Fe-Fe]-hydrogenase H-cluster is the active site, which contains two iron atoms (Fe_p-Fe_d, i.e., proximal and distal iron). Because most experimental and theoretical investigations confirm that the structure of di-iron air inhibited species is Fe_p^{II}-Fe_d^{II}-O-O-H^-, O_2 has to be prevented from binding to Fe_d in all di-iron subcluster oxidation states in order to retain a catalytically active enzyme. By understanding the catalytic processes of metalloenzymes, researches are enabled to produce an excellent source of fuel and energy storage (H_2) for the future, which is clean and highly energetic when reacted with oxygen.

H-cluster oxidation in gas phase, and in aqueous enzyme phase, has been investigated by means of quantum mechanics (QM) and combined quantum mechanics-molecular mechanics (QM/MM).

The inhibitory process occurs at the coordination site, distal iron (Fe_d), of the catalytic H-cluster. The processes involved in the H-cluster oxidative pathways are O_2

binding, e^- transfer, protonation, and H_2O removal. We found that oxygen binding is non-spontaneous in gas phase, and spontaneous for aqueous enzyme phase where both Fe atoms have oxidation state II; however, it is spontaneous for the partially oxidized and reduced clusters in both phases. Hence, in the protein environment the O_2-inhibited H-cluster is obtained by means of exergonic reaction pathways.

A unifying endeavor has been carried out for the purpose of understanding the thermodynamic results vis-à-vis several other performed electronic structural methods, such as frontier molecular orbitals (FMO), natural bond orbital partial charges (NBO), and H-cluster geometrical analysis.

Since hydrogenases become O_2 inactivated, residue mutations were carried out in order to make them O_2 resistant. Residue mutations consist of deletions and substitutions 8 Å radially outward from Fe_d. In order to screen the polar residues (in the 8 Å apoenzyme layer), individual residue deletions were carried out to determine what residue substitutions should be made to improve O_2 inhibition. Residue deletions and substitutions were performed for three di-iron subcluster oxidation states, Fe_p^{II}-Fe_d^{II}, Fe_p^{II}-Fe_d^{I}, and Fe_p^{I}-Fe_d^{I} of [Fe-Fe]-hydrogenase. From the screened residues, two deletions (ΔThr^{152}, and ΔSer^{202}) were found most effective in hindering O_2 binding to Fe_d. The two-residue deletions, $\Delta Thr^{152}$and ΔSer^{202}, on Fe_p^{II}-Fe_d^{II} hydrogenase, gave $\Delta G_{QM/MM}$ = +5.4 kcal/mol, which evidently hinders O_2 binding. An improvement in Gibbs' energy (+4.4 kcal/mol) has also been found for Fe_p^{I}-Fe_d^{I} hydrogenase. Comparing the simultaneous residue deletions (ΔThr^{152} and ΔSer^{202}) with the dual residue substitutions (Thr^{152}Ala, and Ser^{202}Ala), a small difference in Gibbs' energy has been found ($\Delta G_{QM/MM} \sim$ +2 kcal/mol), for O_2 binding, which is attributed to an overall charge

of approximately zero for alanine. The eventual propose hydrogenase mutation in molecular biology laboratory should avail researchers in using it for the full cells of the future.

TABLE OF CONTENTS

LIST OF TABLES

LIST OF FIGURES

CHAPTER I

THE CHEMISTRY OF THE H-CLUSTER INHIBITION BY O_2

1.1. General Considerations

The goal of the present research is to engineer an O_2 resistant (H_2 producing) hydrogenase that is found in Desulfovibrio desulfuricans (DdH). Moreover, the endeavour is to understand the chemistry of O_2 inhibition of [Fe-Fe]-hydrogenase H-cluster (where the latter is the active site), by identifying the chemical species involved in the aerobic inhibition:

1. Finding reaction intermediates, their molecular structure (bond lengths, angles, dihedrals, etc.), thermodynamic functions for different reaction steps (reaction

enthalpies,), i.e., investigate the potential energy surface of H-cluster inhibition by O_2 in vacuum.

2. Investigating the potential energy surface of H-cluster inhibition by O_2 in solution.
3. Identifying the essential structural moieties of the enzyme (e.g., amino acid residues), which are responsible for the enzymatic inhibition.

The current undertaking ensues because DdH has a great turnover number in an anaerobic milieu[1] (9000 s^{-1}). However, it is economically desirable to set off DdH to function aerobically for the purpose of H_2 evolution[*].

Finally, burning hydrogen as fuel will benefit our convalescing planet from the current deleterious plight is currently in.

Calculations in vacuum yield basic information regarding the reaction steps and intermediates i.e., molecular geometry, electronic structure (e.g., partial charges), vibrational frequencies, and thermodynamic functions. Moreover, such calculations provide an expedient way of mapping the potential energy surfaces of the reaction mechanisms. Because the in-vacuum (or, gas phase) calculations are inexpensive relative to the enzyme matrix calculations, it is reasonable that the initial calculations be carried out in gas phase. To achieve the current aim, the following studies are performed:

1. Thermodynamic analysis of H-cluster and O_2 inhibitory process in gas phase and water.
2. Electronic structure examination of the H-cluster in order to ascertain the thermodynamics analysis.

[*] It is cost effective to work in the ambient atmosphere rather then an artificial (N_2) atmosphere.

Furthermore, since gas phase results (Chapter I and II) confirm that the reaction mechanism of H-cluster and O_2 is reversible, the next investigation shall perforce deal with the inhibitory mechanism of H-cluster by O_2 using hybrid classical mechanics and quantum mechanics calculations for the enzyme matrix. Thus, three examinations need to be performed, i.e., Chapter 3 and 4.

1. Perform calculations on the inhibitory mechanism of [Fe-Fe]-hydrogenase by O_2.
2. Evaluate the inhibitory effect of O_2 for the wild type hydrogenase.
3. Engineer an [FeFe]-hydrogenase, which shall not react with O_2, via residue mutations.

1.2. Background and Significance

1.2.1. Hydrogenases Structure and Function

[Fe-Fe]-hydrogenases as well as [Ni-Fe]-hydrogenases are enzymes that are implicated in H_2 metabolism ($2H^+ + 2e^- \rightleftarrows H_2$), which occurs in anaerobic media. Of these two bi-metal enzymes, [Fe-Fe]-hydrogenases are most attractive for H_2 production, with a reactivity of up to 2 orders of magnitude larger than [Ni-Fe]- hydrogenases [1,2]. In hydrogenases, H_2 evolution, emerging from proton reduction ($2H^+ + 2e^- \rightarrow H_2$), is essential in the disposal of excess electrons*. Low-molecular weight biomolecules such as

* The excess electrons are generally low potential electrons that are also involved in fermentation.

ferredoxins, cytochrome c3, and cytochrome c6 can act as physiological electron acceptors or donors[3].

The hydrogenase H-cluster is the active site and is comprised of two subunits, the 2Fe subunit, and the cubane, $[Fe_4\text{-}S_4]^{2+}$, subunit. The 2Fe subunit is composed of two iron atoms (Fe_p-Fe_d, i.e., proximal and distal iron) that are bridged by 1,3-di(thiomethyl)amine (DTMA) chain, and are coordinated by endogenous ligands, i.e., two cyanides, two terminal carbonyls, and a bridging carbonyl (CO_b). Moreover, the S_γ (of Cys^{382}) is the connecting atom from an Fe atom of the (proximal) cubane subunit and the Fe_p of the 2Fe subunit.

The reason for studying biological H_2 production is because the eventual elucidation of the mechanism (for hydrogen synthesis) may help researchers to produce clean fuel through using certain anaerobic prokaryotes[4-8].

Previous Density Functional Theory (DFT) as well as hybrid quantum mechanics/ molecular mechanics (QM/MM) calculations[2,9-16] have been successful in clarifying some aspects of the catalytic properties of the H-cluster.

As in similar computational studies[2,9], cysteine is substituted with $CH_3\text{-}S^-$, whereas cubane is replaced* with a H^+.

Furthermore, computational and experimental[2,9,14,16-41] [Fe-Fe]-hydrogenase H-cluster (and synthetic H-cluster-like compounds) research sheds light on the potential redox states of the 2Fe H-cluster subunit, Fe_p-Fe_d, where Fe_p^I-Fe_d^I is the reduced 2Fe H-

* The truncation of the cubane, $[Fe_4\text{-}S_4]^{2+}$, and its replacement by a H^+ (as well as the replacement of $CH_3\text{-}S^-$ for cysteine-S) had been done in order to obtain the best compromise with regard to the computational cost.

cluster subunit, Fe_p^{II}-Fe_d^{I} is the partially oxidized enzyme subunit, and Fe_p^{II}-Fe_d^{II} is the fully oxidized, inactive enzyme H-cluster subunit.

The fully oxidized H-cluster, Fe_p^{II}-Fe_d^{II}, has a H_2O molecule, OOH^- or an OH^- bound to the Fe_d^{II}. In our previous investigation[21], we have inferred that a vacant (fully oxidized) Fe_p^{II}-Fe_d^{II} (Figure 1-1) could also be a viable intermediate in H_2 synthesis. Regardless of the 2Fe H-cluster subunit redox states, the proximal cubane – or more precisely a cuboid (point group: D_2d) – always retains a 2+ oxidation state, $[Fe_4\text{-}S_4]^{2+}$.

The partially oxidized H-cluster (Fe_p^{II}-Fe_d^{I}, Figure 1-1), H_{ox}, is the active form of the hydrogenase enzyme*. The reduced H-cluster (Fe_p^{I}-Fe_d^{I}, Figure 1-1) has both iron atoms in oxidation states I (being an intermediate in H_2 metabolism). According to Liu and Hu[9], 6 is the cluster having great affinity for protonation (6 → 8), in capturing a proton from the side chain of a near by amino-acid, such as Lys^{237}.

X-ray crystallography and spectroscopic studies of hydrogenases, with the latter having been obtained from *Clostridium pasteurianum* (CPI)[43] and *Desulfovibrio desulfuricans* (DdH)[31] (Figure 1-1), led to a better understanding of the biochemical roles of these enzymes. The X-ray crystal structure of CPI hydrogenase shows an oxygen species that may be OH^-, or H_2O bound to the Fe_d of the H-cluster. Based on the computational results of Liu and Hu[2] (CPI has OH^- in its inactive form according to X-ray crystal structure), we try to ascertain whether the air oxidized H-cluster (Fe_p-Fe_d-O_2) converts to Fe_p-Fe_d-OH species[21].

---

* Voltametric[42] studies show the transition of H_{ox}^{inact} to H_{ox}^{cat} occurring via a reversible e^- transfer process to the hydrogenase transient state followed by a putative two e^- transfer (with the latter not reaching the bimetals of the H-cluster).

1.2.2. *Desulfovibrio Desulfuricans* Hydrogenase Structure

DdH[31] is an enzyme comprised of two types of FeS clusters, i.e., an H-cluster (Fe_4S_4-Fe_2S_2) and two cubanes (Fe_4S_4). It also consists of 511 amino acids (amino acids) with an approximate molecular weight of 53,000 g/mol. Furthermore, DdH consist of two chains, one being light and the other heavy (Figure 2-1).

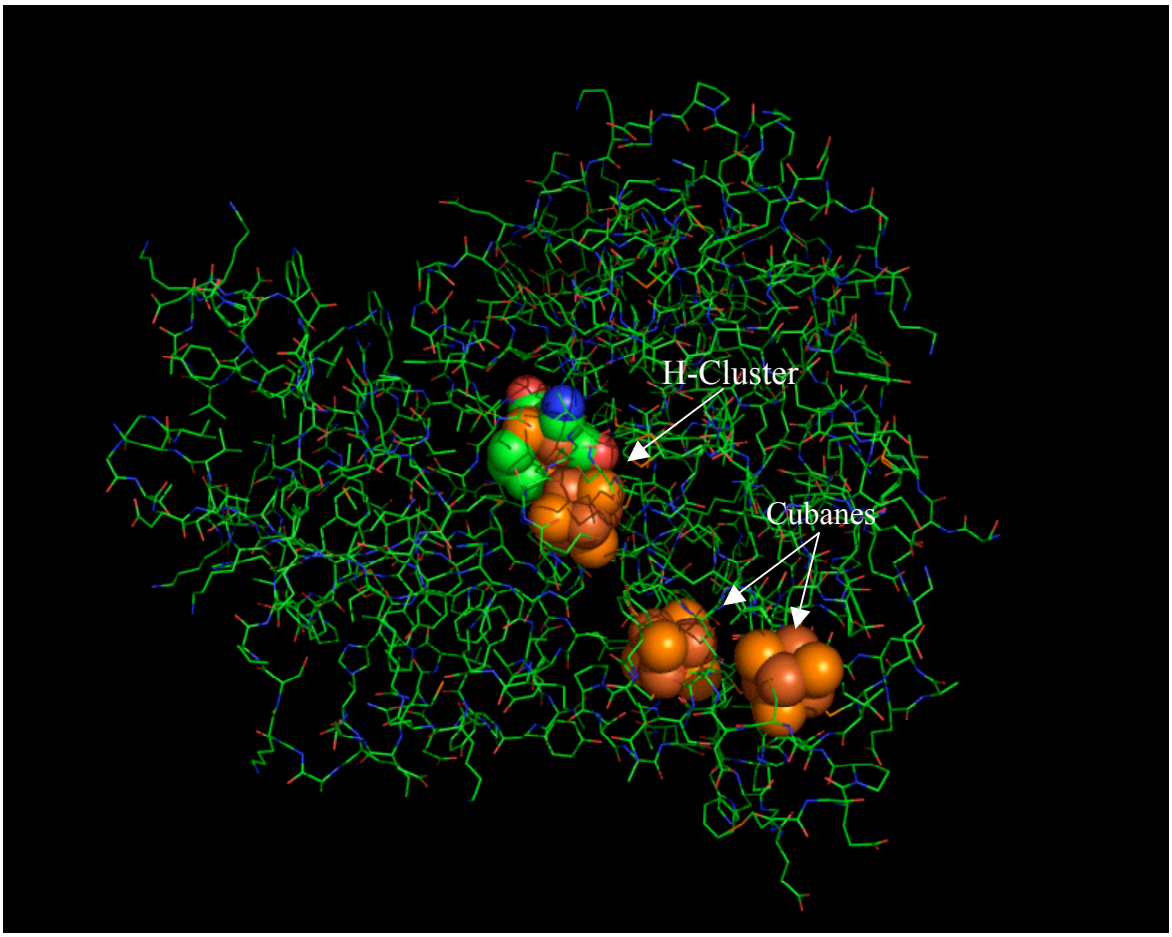

Figure 1-1. A depiction of the prosthetic groups located in [Fe-Fe]-hydrogenase H-cluster, and cubanes, where the atom colors, for the H-cluster and cubanes, are red = O, green = C, blue = N, lighter orange = S, and darker orange = Fe (from the X-ray crystal structure protein data bank code 1HFE[31]).

Theses FeS clusters are situated in the heavy chain and are bound to twelve cysteines, i.e., four cysteines are bound to each FeS cluster and bridge the gap between the polypeptide (heavy) chain and the FeS clusters groups.

Hydrogenases catalyze the reversible reduction of protons to hydrogen molecules ($2H^+ + 2e^- \rightleftarrows H_2$) in anaerobic media. The hydrogen molecule acts as physiological energy storage. One way to produce hydrogen is by harnessing the hydrogenase enzyme. The eventual elucidation of the catalytic mechanism of hydrogen synthesis may help researchers to produce clean hydrogen fuel for the future using certain organisms[*4-8].

1.2.3. *Desulfivibrio Desulfuricans* Hydrogenase Biosynthesis

The translation of DdH occurs mostly on the ribosomes of the rough endoplasmic reticulum, where the FeS clusters are covalently bound to the rest of the polypeptide, which is mediated by certain enzymes called accessory proteins. The FeS-polypeptide joining occurs during the enzymatic folding while the FeS cluster groups are buried inside DdH. Molecular chaperons also contribute to the folding of DdH[44,45]. Furthermore, after being assembled and folded, the (periplasmic) DdH enzyme is delivered to the cell membrane.

[*] Hydrogenases are ubiquitous; they are encountered from the depths of the ocean to the surface of the earth (e.g. in eukaryotes like green algae).

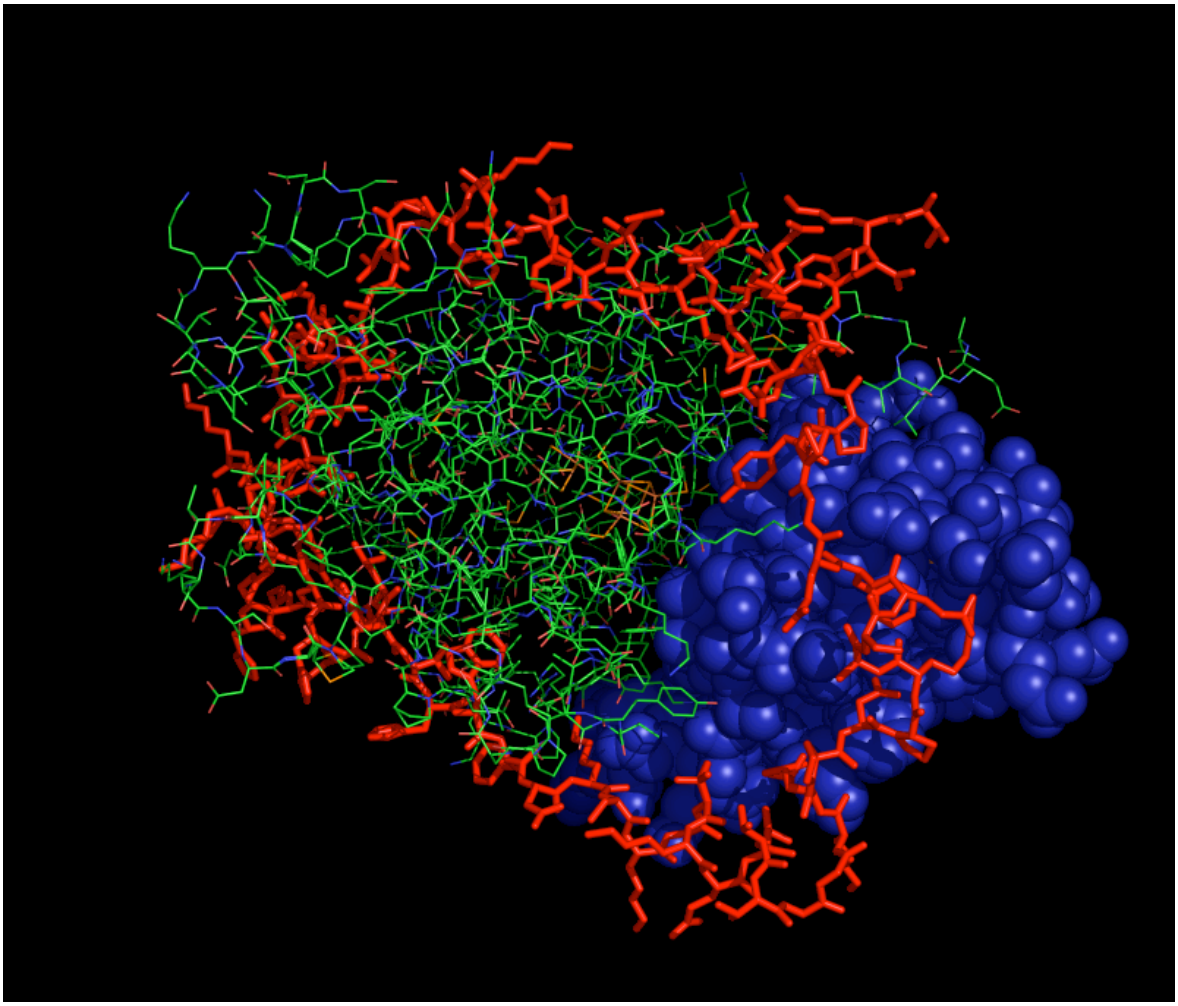

Figure 1-2. DdH is comprised of the ferrodoxin-like domains (blue spheres), and of the H-domain (greenish background), with the small, red chain surrounding the former domains (from the X-ray crystal structure protein data bank code 1HFE[31]).

1.2.4. *Desulfivibrio Desulfuricans* Hydrogenase Main Domains

The active domain (H-domain) has a hydrogen-bond network extending from the H-cluster to the surface of the molecule (Figure 1-3). This hydrogen-bond network is potentially involved in the H^+ transfer, which is a vital step in H_2 synthesis ($2H^+ + 2e^- \rightleftarrows H_2$).

The cubane clusters are found buried inside ferrodoxin-like domains. These cubane clusters, as well as the small chain, are crucial in the electron transfer mechanism and are interconnected with redox partners[1,46] such as cytochrome c3 or c6.

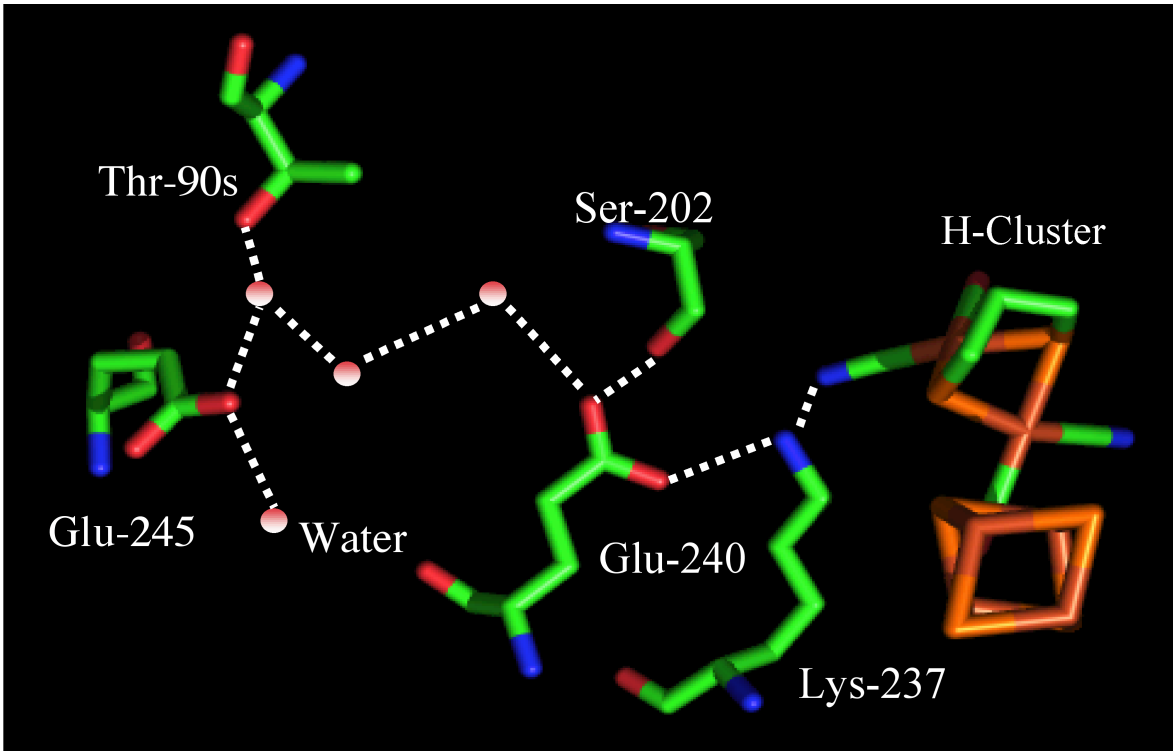

Figure 1-3. Hydrogen-bond network (dashed lines) extends from the H-cluster to the surface of the [Fe-Fe]-hydrogenase; Thr-90 residue belongs to the small chain, while the visible amino acid residues consist of the large chain (as presented in references 29 and 31).

References

(1) Das, D.; Dutta, T.; Nath, K.; Kotay, S. M.; Das, A. K.; Veziroglu, T. N. *Curr. Sci.* **2006**, *90*, 1627.

(2) Liu, Z.-P.; Hu, P. *J. Am. Chem. Soc.* **2002**, *124*, 5175.

(3) Vignais, P. M.; Billoud, B.; Meyer, J. *FEMS Microbiol. Rev.* **2001**, *25*, 455–501.

(4) Melis, A.; Zhang, L.; Forestier, M.; Ghirardi, M. L.; Seibert, M. *Plant Physiol.* **2000**, *122*, 127.

(5) Albracht, S. P. J. *Biochim. Biophys. Acta* **1994**, *1118*, 167.

(6) Adams, M. W. W. *Biochim. Biophys. Acta* **1990**, *1020*, 115.

(7) Adams, M. W. W.; Stiefel, E. I. *Science* **1998**, *282*, 1842.

(8) Happe, R. P.; Roseboom, W.; Pierik, A. J.; Albracht, S. P.; Bagley, K. A. *Nature* **1997**, *385*, 126.

(9) Liu, Z.-P.; Hu, P. *J. Chem. Phys.* **2002**, *117*, 8177.

(10) Bruschi, M.; Fantucci, P.; De Gioia, L. *Inorg. Chem.* **2002**, *41*, 1421.

(11) Bruschi, M.; Fantucci, P.; De Gioia, L. *Inorg. Chem.* **2003**, *42*, 4773.

(12) Bruschi, M.; Fantucci, P.; De Gioia, L. *Inorg. Chem.* **2004**, *43*, 3733.

(13) Zampella, G.; Bruschi, M.; Fantucci, P.; Razavet, M.; Pickett, C. J.; De Gioia, L. *Chem. Eur. J.* **2005**, *11*, 509.

(14) Cao, Z.; Hall, M. B. *J. Am. Chem. Soc.* **2001**, *123*, 3734.

(15) Fan, H.-J.; Hall, M. B. *J. Am. Chem. Soc.* **2001**, *123*, 3828.

(16) Greco, C.; Bruschi, M.; De Gioia, L.; Ryde, U. *Inorg. Chem.* **2007**, *46*, 5911.

(17) Trohalaki, S.; Pachter, R. *ENERG. FUEL.* **2007**, *21*, 2278.

(18) Greco, C.; Bruschi, M.; Heimdal, J.; Fantucci, P.; De Gioia, L.; Ryde, U. *Inorg. Chem.* **2007**, *46*, 7256.

(19) Greco, C.; Bruschi, M.; Fantucci, P.; De Gioia, L. *Eur. J. Inorg. Chem.* **2007**, *13*, 1835.

(20) Greco, C.; Zampella, G.; Bertini, L.; Bruschi, M.; Fantucci, P.; De Gioia, L. *Inorg. Chem.* **2007**, *46*, 108.

(21) Motiu, S.; Dogaru, D.; Gogonea, V. *Int. J. Quantum Chem.* **2007**, *107*, 1248.

(22) Bruschi, M.; Zampella, G.; Fantucci, P.; De Gioia, L. *Coord. Chem. Rev.* **2005**, *15-16*, 1620.

(23) Liu, X.; Ibrahim, S. K.; Tard, C.; Pickett, C. J. *Coord. Chem. Rev.* **2005**, *15-16*, 1641.

(24) Armstrong, F. A. *Curr. Opin. Chem. Biol.* **2004**, *8*, 133.

(25) Rauchfuss, T. B. *Inorg. Chem.* **2004**, *43*, 14.

(26) Evans, D. J.; Pickett, C. J. *Chem. Soc. Rev.* **2003**, *35*, 268.

(27) Chen, Z.; Lemon, B. J.; Huang, S.; Swartz, D. J.; Peters, J. W.; Bagley, K. A. *Biochemistry* **2002**, *41*, 2036.

(28) Horner, D. S.; Heil, B.; Happe, T.; Embley, T. M. *Trends Biochem. Sci.* **2002**, *27*, 148.

(29) Nicolet, Y.; Cavazza, C.; Fontecilla-Camps, J. C. *J. Inorg. Biochem.* **2002**, 1.

(30) Lyon, E. J.; Georgakaki, I. P.; Reibenspies, J. H.; Darensbourg, M. Y. *Angew. Chem., Int. Ed.* **1999**, *38*, 3178.

(31) Nicolet, Y.; Piras, C.; Legrand, P.; Hatchikian, E. C.; Fontecilla-Camps, J. C. *Structure* **1999**, *7*, 13.

(32) Cloirec, A. L.; Best, S. P.; Borg, S.; Davies, S. C.; Evans, D. J.; Hughes, D. L.; Pickett, C. J. *Chem. Commun.* **1999**, 2285.

(33) Rauchfuss, T. B.; Contakes, S. M.; Schmidt, M. *J. Am. Chem. Soc.* **1999**, *121*, 9736.

(34) Lai, C.-H.; Lee, W.-Z.; Miller, M. L.; Reibenspies, J. H.; Darensbourg, D. J.; Darensbourg, M. Y. *J. Am. Chem. Soc.* **1998**, *120*, 10103.

(35) Pierik, A. J.; Hulstein, M.; Hagen, W. R.; Albracht, S. P. *Eur. J. Biochem.* **1998**, *258*, 572.

(36) Pierik, A. J.; Hagen, W. R.; Redeker, J. S.; Wolbert, R. B. G.; Boersma, M.; Verhagen, M. F.; Grande, H. J.; Veeger, C.; Mustsaers, P. H. A.; Sand, R. H.; Dunham, W. R. *Eur. J. Biochem.* **1992**, *209*, 63.

(37) Zambrano, I. C.; Kowal, A. T.; Mortenson, L. E.; Adams, M. W. W.; Johnson, M. K. *J. Biol. Chem.* **1989**, *264*, 20974.

(38) Patil, D. S.; Moura, J. J. G.; He, S. H.; Teixeira, M.; Prickril, B. C.; Der Vartanian, D. V.; Peck, H. D., Jr.; Legall, J.; Huynh, B. H. *J. Biol. Chem.* **1988**, *263*, 18732.

(39) Rusnak, F. M.; Adams, M. W. W.; Mortenson, L. E.; Munck, E. *J. Biol. Chem.* **1987**, *262*, 38.

(40) Adams, M. W. W. *J. Biol. Chem.* **1987**, *262*, 15054.

(41) Adams, M. W. W.; Mortenson, L. E. *J. Biol. Chem.* **1984**, *259*, 7045.

(42) Roseboom, W.; De Lacey, A. L.; Fernandez, V. M.; Hatchikian, E. C.; Albracht, S. P. J. *J. Biol. Inorg. Chem.* **2006**, *11*, 102.

(43) Peters, J. W.; Lanzilotta, W. N.; Lemon, B. J.; Seefeldt, L. C. *Science* **1998**, *282*,

(44) Cammack, R. *Nature* **1999**, *397*, 214.

(45) Cammack, R.; Frey, M.; R., R. *Hydrogen as a Fuel: Learning from the Nature*; CRC Press, 2001.

(46) Morelli, X.; Czjzek, M.; Hatchikian, E. C.; Bornet, O.; Fontecilla-Camps, J. C.; Palma, N. P.; Moura, J. J. G.; Guerlesquin, F. *J. Biol. Chem.* **2000**, *275*, 23204.

CHAPTER II

COMPUTATIONAL ANALYSIS OF H-CLUSTER AND O_2 INHIBITORY PROCESS IN GAS PHASE AND WATER

2.1. General Considerations

Computational and experimental[1-23] [Fe-Fe]-hydrogenase H-cluster (and synthetic H-cluster-like compounds) research elucidates the potential hydrogenase O_2 inhibition pathways.

Density Functional Theory* (DFT[24-28]) methodology is used to calculate the geometry and the electronic structure of the intermediates in the O_2 inhibition pathways. Previous calculations[29-34] using DFT have also been successful in elucidating some

* Density functional theory (DFT) is a quantum mechanical method, which studies the electronic structure of many-body systems, specifically molecules and the condensed phases.

aspects of the catalytic properties of H-cluster.

2.2. Methodology

The electronic structure of the hydrogenase active site is investigated by the B3LYP functional of DFT, with 6-31+G(d,p)** basis set (implemented in Gaussian[35] software). For Fe an effective-core[36-38] potential with a double zeta polarization basis set (LANL2DZ) was used to replace the interaction of core electrons. In accordance with experimental[39-42] and in-silico data[19], low spin states (singlet, and doublet), and low oxidation states (I, and II) for the iron atoms have been selected.

Finally, calculations are performed for the polarized continuous model*** (PCM[43-45]) of the solvent and then have been checked against the gas phase calculations[46].

2.3. Thermodynamics of the H-cluster Oxidation

Figure 2-4 represents different O_2 inhibition pathways of the hydrogenase H-cluster. Reaction $1 \rightarrow 2$ (path I) is slightly exothermic for the gas phase (ΔH_{gas} = -0.94 kcal/mol;

** B3LYP/6-31+G(d,p) = Becke-style 3-Parameter Density Functional Theory (using the Lee-Yang-Parr correlation functional) with the orbitals 6-31+G(d,p).

*** PCM model performs calculations in the presence of a solvent that uses the Polarized Continuum (overlapping spheres) model of Tomasi et al.

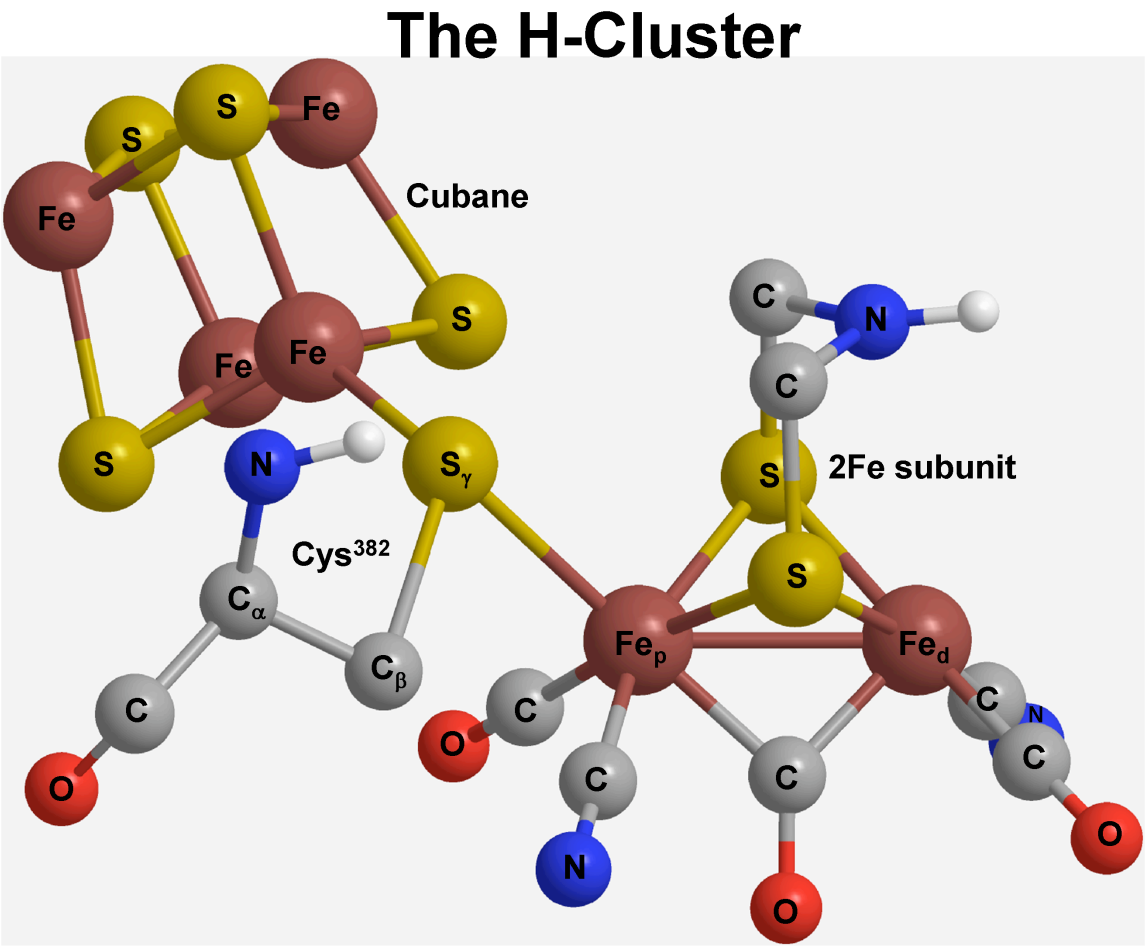

Figure 2-1. The H-cluster and its subunits, i.e., the cubane, and the 2Fe (or di-iron) subunit (as presented in references 17, 19 and 41).

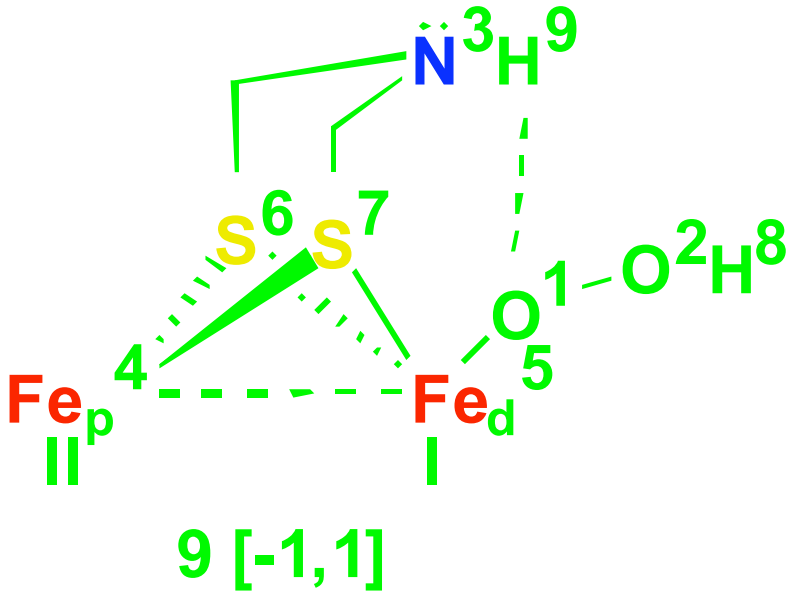

Figure 2-2. Compound 9 is a key compound because it most closely resembles the active site of CPI obtained by X-ray crystallography[17]. Selected distances (Å) of the H-luster, theoretical model vs. X-ray crystallographic structure: Fe_5-Fe_4 2.605 (2.617), S_6-N_3 2.877 (2.702), S_7-N_3 2.848 (2.642), Fe_4-C_b 2.225 (2.100), Fe_5-C_b 1.883 (2.043).

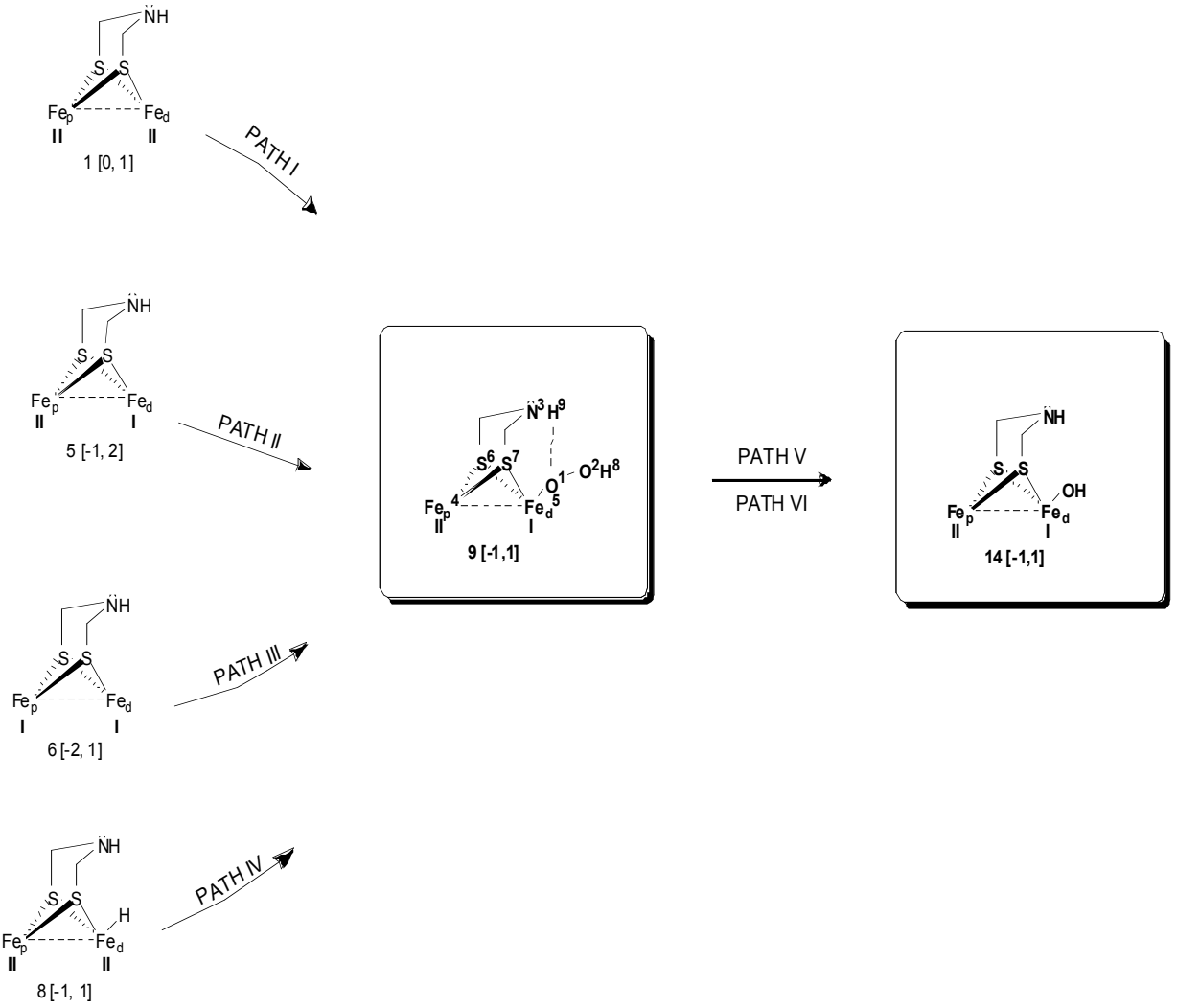

Figure 2-3. The general oxidation mechanisms for H-clusters that are fully oxidized (1), partially oxidized (5), and reduced (6)

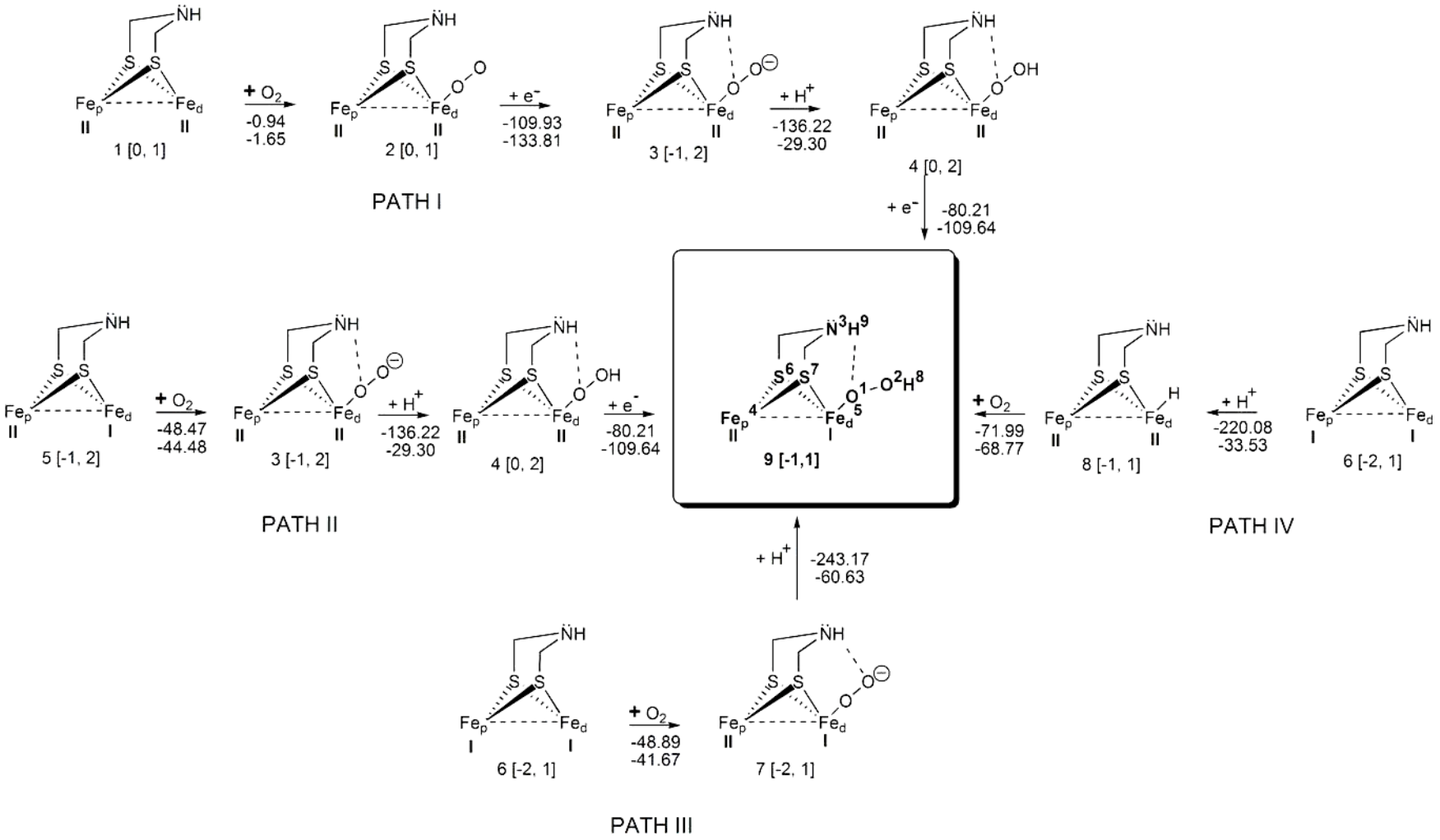

Figure 2-4. O_2 binding mechanisms to H-clusters that are fully oxidized (1), partially oxidized (5) and reduced (6). The charges and multiplicities are given in square brackets. The first enthalpy value (kcal/mol) is for gas phase, and the second is for aqueous phase.

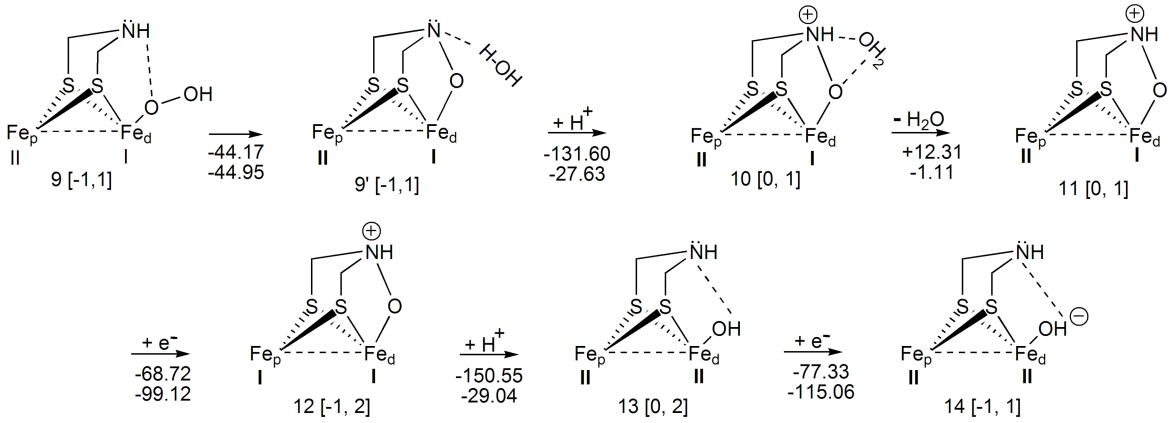

Figure 2-5. Reaction mechanism for H_2O elimination from the inhibited H-cluster. The H_2O is being removed from a closed-shell cluster.

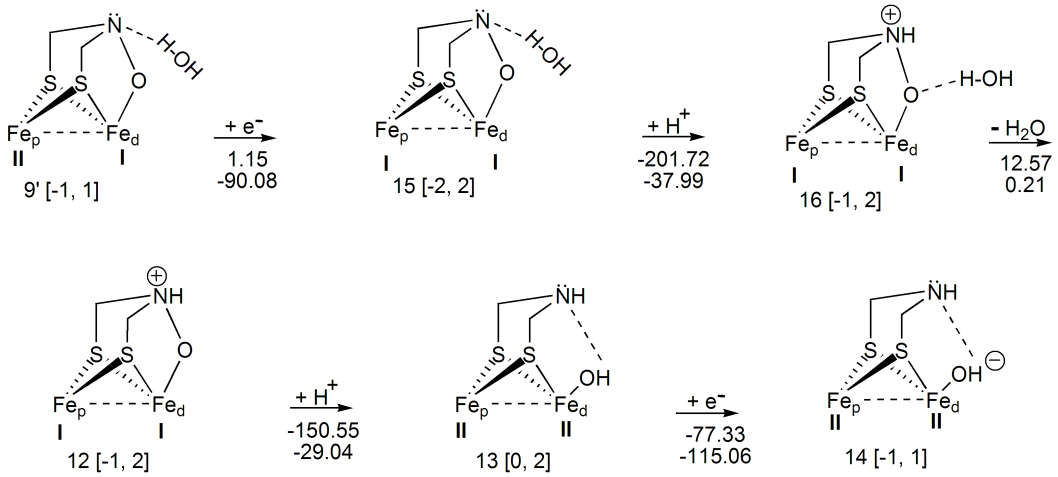

Figure 2-6. Reaction mechanism for H_2O removal from the inhibited H-cluster. The H_2O is eliminated from an open-shell cluster.

gas = gas phase) as well as for the aqueous phase (ΔH_{aq} = -1.65 kcal/mol; aq = aqueous phase) when O_2 binds to the fully oxidized H-cluster (1).

Subsequently, the reduction 2 → 3 (ΔH_{gas} = -109.93 kcal/mol; ΔH_{aq} = -133.81 kcal/mol) as well as the protonation 3 → 4 (ΔH_{gas} = -136.22 kcal/mole; ΔH_{aq} = -29.30 kcal/mol) proceed exothermically. In reactions 2 → 3 and 3 → 4, the enthalpy differences in gas versus aqueous phases is due to the solvation free energy (ΔG_{sol}) of H-clusters 2, 3, and 4, and also from the solvation free energy of the hydronium ion (H_3O^+) in 3 → 4 (Table 2-1). In particular, the solvation free energy is larger for H-cluster 3 because it has a more negative charge (-1 a.u.) relative to 2 and 4 (which are neutral). Regarding gas versus aqueous phases, the above trend in enthalpy differences is observed for all pathways involving O_2 inhibition (Figure 2-4, Figure 2-5, and Figure 2-6), i.e., the reaction enthalpy increases for the electron transfer and decreases for protonation. Furthermore, cluster (4) undergoes reduction, and the reaction 4 → 9 proceeds exothermically as well (ΔH_{gas} = -80.21 kcal/mole; ΔH_{aq} = -109.64 kcal/mol). The iron binding of O_2 (Fe_d^I-O_2) 5 → 3 (path II) is much firmer (ΔH_{gas} = -48.47 kcal/mole; ΔH_{aq} = -44.48 kcal/mol) than the binding in 1 → 2 (Fe_d^{II}-O_2, path I). The remaining two reactions 3 → 4, and 4 → 9 (path II) are identical to the last two steps of path I. In path III, 6 → 7, the heat of reactions (ΔH_{gas} = -48.89 kcal/mole; ΔH_{aq} = -41.67 kcal/mol) are almost identical to the enthalpies of reaction 5 → 3. The enthalpy similarities may ensue from the fact that both loci of oxygen binding (Fe_d^I-O_2) are on similar oxidized species, Fe_d^I. In path III, the protonation reaction (7 → 9) is, once again, exothermic for both phases (ΔH_{gas} = -243.17 kcal/mole; ΔH_{aq} = -60.63 kcal/mol). Finally, in path IV, the protonation 6 → 8 is the second most exothermic reaction in the gas phase (ΔH_{gas} = -

220.08 kcal/mole), compared to 7 → 9, while in the aqueous phase is less exothermic (ΔH_{aq} = -33.53 kcal/mol). The enthalpy differences (ΔH_{gas} = -220.08 kcal/mole vs. ΔH_{aq} = -33.53 kcal/mol), between the above phases in 6 → 8, are attributed to the large solvation free energy (ΔG_{sol} = -167.46 kcal/mol) of cluster 6, which has a –2 a.u. charge.

In the final step 8 → 9 of path IV (ΔH_{gas} = -71.99 kcal/mole; ΔH_{aq} = -68.77 kcal/mol), O_2 is interposed between Fe_d and the exogenous hydride (Fe_d^I-O_2-H, 9).

Furthermore, path IV shows that the oxidation of Fe_p-Fe_d H-cluster is similar* to the Ni_p-Fe_d hydrogenase H-cluster obtained from experimental data[47].

Thus, from the above thermodynamic results, it is observed that every reaction of each path is exothermic and leads to the oxidized species 9. Each vacant H-cluster (1, 5, or 6), regardless of its oxidation state, gets poisoned aerobically.

2.4. NBO Charges and Geometry Modification of Intermediates in the Oxidation of H-cluster

The atoms of the vacant H-clusters 1, 5, and 6 have similar natural bond orbital (NBO) charge distributions. For instance, for cluster 1 the NBO charges of Fe_p-Fe_d are q_{Fep} = 0.137 and q_{Fed} = -0.096 a.u., whereas in 5, the partial charges are somewhat reversed, i.e. -0.024 on Fe_p and 0.078 on Fe_d. Then the NBO charges for the Fe_p-Fe_d in

* The similarity for these clusters is they are first found as hydride containing H-clusters, and then undergo oxidation.

cluster 6 are more negative, q_{Fep} = -0.104, and q_{Fed} = -0.117 a.u. because both metals are in a reduced state (Figure 2-4), unlike clusters 1 and 5.

As for charges on the nitrogen atom, N3, (of the DTMA bridge), one can see even more charge similarities among clusters 1, 5, and 6, than for the Fe_p-Fe_d atoms mentioned above; the partial charges for N3 are approximately -0.700 a.u., which makes this nitrogen a relatively strong base within the H-cluster.

The non-bridging sulfur (S_{nb}) is positively charged for 0.204 a.u. (1), 0.142 a.u. (5), and 0.079 a.u. (6). A drop in NBO charges can be seen for S_{nb} belonging to clusters 1 to 5 and 5 to 6, with a concomitant increase in the negative charge of Fe_p.

When H-cluster 1 is in an oxidized state, Fe_p^{II}- Fe_d^{II}, the CO_b shifts towards the Fe_d^{II}, and becomes bonded to the Fe_d^{II20}. The shifted CO_b (measured from its bridging carbon, C_b, to the iron atoms) bond distance between C_b—Fe_p^{II} is 3.067 Å, whereas C_b—Fe_d^{II} is 1.819 Å. When the carbonyl is close to Fe_d^{II}, CO_b-Fe_d^{II}, the fully oxidized H-cluster 1 becomes more stable which can also be seen from the NBO charge on C in CO_b, (0.664 a.u.). This is caused by charge repulsion between q_{Cb} (0.664 a.u.) and q_{Fep} (0.137 a.u.), whereas the CO_b migration towards Fe_d ensues due to the attraction between q_{Cb} and q_{Fed} (-0.096 a.u.). For clusters 5 and 6, the partial charges (q_{Cb} = 0.462 and q_{Cb} = 0.466 a.u., respectively) are less then in 1 because CO_b is bonded to both iron atoms.

Comparing the heat of reactions for O_2 binding which renders clusters 2, 3, and 7, one may notice that 3 and 7 are more stable than 2. The reason for this stability is mostly due to the formation of a hydrogen bond between the exogenous oxygen and the hydrogen H9 (bonded to N of the DTMA bridge) in 3 and 7. The hydrogen bond length is 2.016 Å in 3, and 1.765 Å in 7, which correlates with the NBO charges on exogenous

oxygen and H9; the partial charges on oxygen are q_{O1} = -0.235 in 3, and q_{O2} = -0.493 a.u. in 7, whereas the charge on H9 is 0.439 in 3, and 0.454 a.u. in 7. Note that CO_b is located almost symmetrically in clusters 2, 3, and 7.

Structurally, clusters 4 and 9 are similar in that both have a hydrogen bond (H9…O1), whereas CO_b is found to reside quasi-symmetrically in 9, but asymmetrically in 4 bound only to Fe_p^{II}.

2.5. Thermodynamics of H_2O Removal from the Oxidized H-cluster

Figure 2-5 depicts a series of reactions (9 → 9', 9' → 10, 10 → 11, 11 → 12, 12 → 13, and 13 → 14) which present the net conversion of 9 to 14.

The compounds 9 and 9' are isomers, with 9' being more stable by +44.17 kcal/mole (due to hydrogen bond formation between H_2O and the N3 of DTMA bridge (N3…H-OH)). The hydrogen bond length, N3…H, is 1.939 Å (and the angle formed by N3…H-O is 168.7°). The distance between the iron atoms is larger in 9' (2.796 Å) than in 9 (2.605 Å). During reaction 9 → 9', CO_b moves away from Fe_p^{II} (i.e., for C_b~Fe_p^{II} 2.225 Å (9) → 2.771 Å (9')). The protonation of 9' (9' → 10) produces a quaternary ammonium (NR_4^+) in the DTMA bridge, and is exothermic for both phases (ΔH_{gas} = -131.60 kcal/mole; ΔH_{aq} = -27.63 kcal/mol). Species 9' possesses a charge of -1.0 a.u., which is responsible for its relatively large proton affinity. In 10 → 11, H_2O is removed from N3 by means of hydrogen bond breaking; this reaction (vs. 9' → 10) proceeds

endothermically in gas phase (ΔH_{gas} = +12.31 kcal/mole), however in the aqueous phase it barely proceeds exothermically (ΔH_{aq} = -1.11 kcal/mol).

The first reduction **11** → **12** (Figure 2-5) is subjected to an increase in the partial charge of the exogenous oxygen (q_{O1} = -0.568 a.u (**11**) → -0.594 a.u. (**12**); ΔH_{gas} = -68.72 kcal/mole; ΔH_{aq} = -99.12 kcal/mol). Regarding geometrical changes in **11** (**11** → **12**), the bond distance between Fe_p^{II}-Fe_d^{II} is increasing from 2.792 Å to 3.261 Å, while the CO_b departs from Fe_p^{II} (for C_b- Fe_p^{II} 2.766 Å (**11**) → 3.183 Å (**12**)). Due to the high negative charge on O1 (**12**), the latter readily captures a proton (**12** → **13**; ΔH_{gas} = -150.55 kcal/mole; ΔH_{aq} = -29.04 kcal/mol). Finally, in Figure 2-5, an e^- is acquired by the OH group (**13** → **14**; ΔH_{gas} = -77.33 kcal/mole; ΔH_{aq} = -115.06 kcal/mol). Note that the H-cluster **14**[19,20] is the starting compound in the reactivation pathway, which ends in the reduced H-cluster **6** (Fe_p^I-Fe_d^I).

In Figure 2-6, an alternative pathway (**9'** → **15**, **15** → **16**, **16** → **12**, **12** → **13**, and **13** → **14**) has been investigated. The pathway starts with an electron transfer rather than a proton transfer. Reaction **9'** → **15** is slightly endothermic for the gas phase (ΔH_{gas} = +1.15 kcal/mole), but highly exothermic for the aqueous phase (ΔH_{aq} = -90.08 kcal/mol), since 15 has higher solvation free energy than **9'** (Table 2-1). Cluster **15** has a high proton affinity (**15** → **16**) particularly for the gas phase (ΔH_{gas} = -201.72 kcal/mole; ΔH_{aq} = -37.99 kcal/mol) because **15** has a charge of -2 a.u. For **16** → **12**, the heat of reaction for the gas phase is endothermic (ΔH_{gas} = +12.57 kcal/mole) whereas for the aqueous phase it is only slightly endothermic (ΔH_{aq} = +0.21 kcal/mol). Note that both **10** (Figure 2-5) and **16** (Figure 2-6) lead to the same compound (**12**) by H_2O elimination. The thermodynamic data are similar for both reactions (**10** → **12** and **16** → **12**) because Fe_d

is found in the same oxidation state (Fe_d^I) in both **10** and **16**, but Fe_p (being further away from the reaction center) has different oxidation states (Fe_p^{II} (**10**); Fe_p^I (**16**)). Next, reactions **12** → **13**, and **13** → **14** proceed exothermically [(ΔH_{gas} = -150.55 kcal/mol; ΔH_{aq} = -29.04 kcal/mol), and (ΔH_{gas} = -77.33 kcal/mol; ΔH_{aq} = -115.06 kcal/mol), respectively], as previously discussed in Figure 2-5. Unlike **10** → **12** (Figure 2-5), **16** → **12** is endothermic in both phases (ΔH_{gas} = +12.57 kcal/mol; ΔH_{aq} = +0.21 kcal/mol) which indicates (Figure 2-6) that the oxidation of H-cluster has difficulties proceeding to **14** in both phases.

From above, it can be seen that there is only one exothermic path from the oxidized H-cluster **9'** to the hydroxylated cluster **14**. A path starts with H^+ transfer, while the other begins by e^- transfer. The gas phase H_2O elimination from the oxidized H-cluster **9'** proceeds endothermically in both pathways, whereas the aqueous phase H_2O removal is slightly exothermic for one path (Figure 2-5) and slightly endothermic for the other path (Figure 2-6).

Table I. H-cluster Quantum Mechanical, E_{QM}, and Solvation Free Energies, ΔG_{sol}

Clusters &ligands	ΔG_{sol}[a]	E_{QM}[b] gas phase	E_{QM} solution	E[a,c]	%[a,d]
1	-24.01	-2141.7418	-2141.7938	-32.64	35.95
2	-27.91	-2292.0094	-2292.0639	-34.23	22.65
3	-47.53	-2292.1845	-2292.2771	-58.11	22.27
4	-21.26	-2292.6753	-2292.7247	-30.97	45.68
5	-53.25	-2141.8412	-2141.9388	-61.22	14.96
6	-167.46	-2141.7980	-2142.0681	-169.49	1.21
7	-158.33	-2292.1419	-2292.4019	-163.15	3.05
8	-55.61	-2142.4224	-2142.5224	-62.73	12.81
9	-50.84	-2292.8032	-2292.8994	-60.40	18.80
9'	-48.38	-2292.8735	-2292.9710	-61.19	26.47
10	-27.45	-2293.3570	-2293.4159	-37.00	34.78
11	-37.31	-2216.9033	-2216.9693	-41.40	10.95
12	-66.92	-2217.0128	-2217.1272	-71.80	7.29
13	-22.27	-2217.5265	-2217.5744	-30.07	35.01
14	-62.57	-2217.6497	-2217.7577	-67.80	8.36
15	-137.81	-2292.8717	-2293.1146	-152.42	10.60
16	-60.00	-2293.4669	-2293.5760	-68.46	14.10
O_2	1.91	-150.2661	-150.2675	-0.88	-146.08
H_3O^+	-87.90	-76.7078	-76.8493	-88.81	1.04
H_2O	-8.06	-76.4340	-76.4484	-9.03	12.03

[a] Kcal/mol

[b] Hartrees/molecule

[c] Between gas and aqueous phases

[d] Percent difference between the solvation free energy and ΔE.

2.6. Study the H-Cluster Electronic Structure to Ascertain the Thermodynamics Analysis

Electronic contributions are now presented which are adduced by the frontier orbitals in conjunction with the previously presented enthalpies of reaction.

Upon reduction of most open-shell H-clusters, it is observed that an e^- is obtained by a virtual molecular orbital (SOMO), while the closed-shell clusters receive an e^- into the lowest virtual molecular orbital (LUMO).

However, when a H^+ is in the proximity of an open-shell H-cluster, it forms a σ-bond through the interaction of the e^- in the highest occupied molecular orbital (HOMO), or through the contributions of both HOMO and SOMO, with the proviso that the SOMO is sufficiently low in energy relative to HOMO. Alternatively, when a H^+ is near a closed-shell cluster, the σ-bond ensues mainly due to the contribution of e^-s from HOMO with the H^+.

Thermodynamic properties, of the reactions in Figures 2-4, 2-5, and 2-6, are now examined with regard to frontier molecular orbitals (FMO). Thus, in **2** the LUMO (Figure 2-7) is localized on the exogenous O_2 and N_{DTMA}, which is also corroborated by an increase of NBO charges on O_2 and N_{DTMA} (N3) in **3** upon reduction of H-cluster **2** (q_{O1} = -0.046 a.u (**2**) → -0.235 a.u. (**3**); q_{N3} = -0.568 a.u (**2**) → -0.717 a.u. (**3**)).

For open-shell clusters, unrestricted B3LYP calculations have been performed which resulted in different quantum mechanical (QM) energies and molecular orbital (MO) coefficients for α and β electrons.

The $HOMO_{\alpha}$ (the lower energy HOMO containing a spin up e^-) of **3** is predominantly localized on the exogenous O_2, where the protonation also occurs. However, the $HOMO_{\beta}$ (the higher energy HOMO with its spin down e^-) is localized on the DTMA bridge (Figure 2-7).

The $SOMO_{\alpha}$ of compound **4** is mostly localized on the DTMA bridge, partially on the exogenous oxygen and the iron atoms. $SOMO_{\beta}$ (the higher energy virtual SOMO) is more delocalized than $SOMO_{\alpha}$ (Figure 2-7). The main change in partial charges occurs on the iron atoms (q_{Fep} = -0.141 a.u (**4**) → -0.003 a.u. (**9**); q_{Fed} = 0.464 a.u (**4**) → 0.025 a.u. (**9**)). The above NBO observed changes in 4 → 9 can be corroborated by $LUMO_{\alpha}$ (**4**; Figure 2-7). It is noteworthy that the e^- is transferred into the $LUMO_{\alpha}$ (-0.15381 Hartrees), for its energy is lower than that of $SOMO_{\beta}$ (-0.14425 Hartrees).

The HOMO of **6** is localized on the Fe_d and the CO_b, whereas the HOMO of **7** is primarily localized on the exogenous O_2 but is less diffused over CO_b (Figure 2-7). The high proton affinity (especially in gas phase) of clusters **6** (Path IV) and **7** is explained because the HOMO orbital is localized on proton binding loci. In particular, **7** shows clearly as to where the protonation ought to occur; the exogenous O_2 captures the H^+ (Figure 2-7). Antithetically, in **6**, in spite of the fact that both Fe_d and the CO_b are engulfed in an about similar size MOs, Fe_d seems to have the propensity for capturing a H^+.

The HOMO of **9'**, which is delocalized throughout the cluster, has a smaller proton affinity than **6** and **7**. However, higher HOMO amplitude is found on the exogenous O1, DTMA bridge, and the two irons and this may explain why the N3 is protonated in this case. For cluster **11**, the LUMO is more localized over the Fe_p than on Fe_d, extending

from the irons towards the CO_b via a linear combination between the e_g orbitals of the iron atoms with the CO_b π orbitals[48], thus the e^- transfer **11** $\rightarrow$ **12** shall change the oxidation state of Fe_p. Both $HOMO_\alpha$ and $HOMO_\beta$ of **12** are generally localized on the Fe_p (Figure 8). However, in this case the protonation does not occur at the Fe_p, instead it occurs at the exogenous O1 since its NBO charge is very negative, i.e., q_{O1} = -0.594 a.u. as opposed to q_{Fep} = 0.126 a.u..

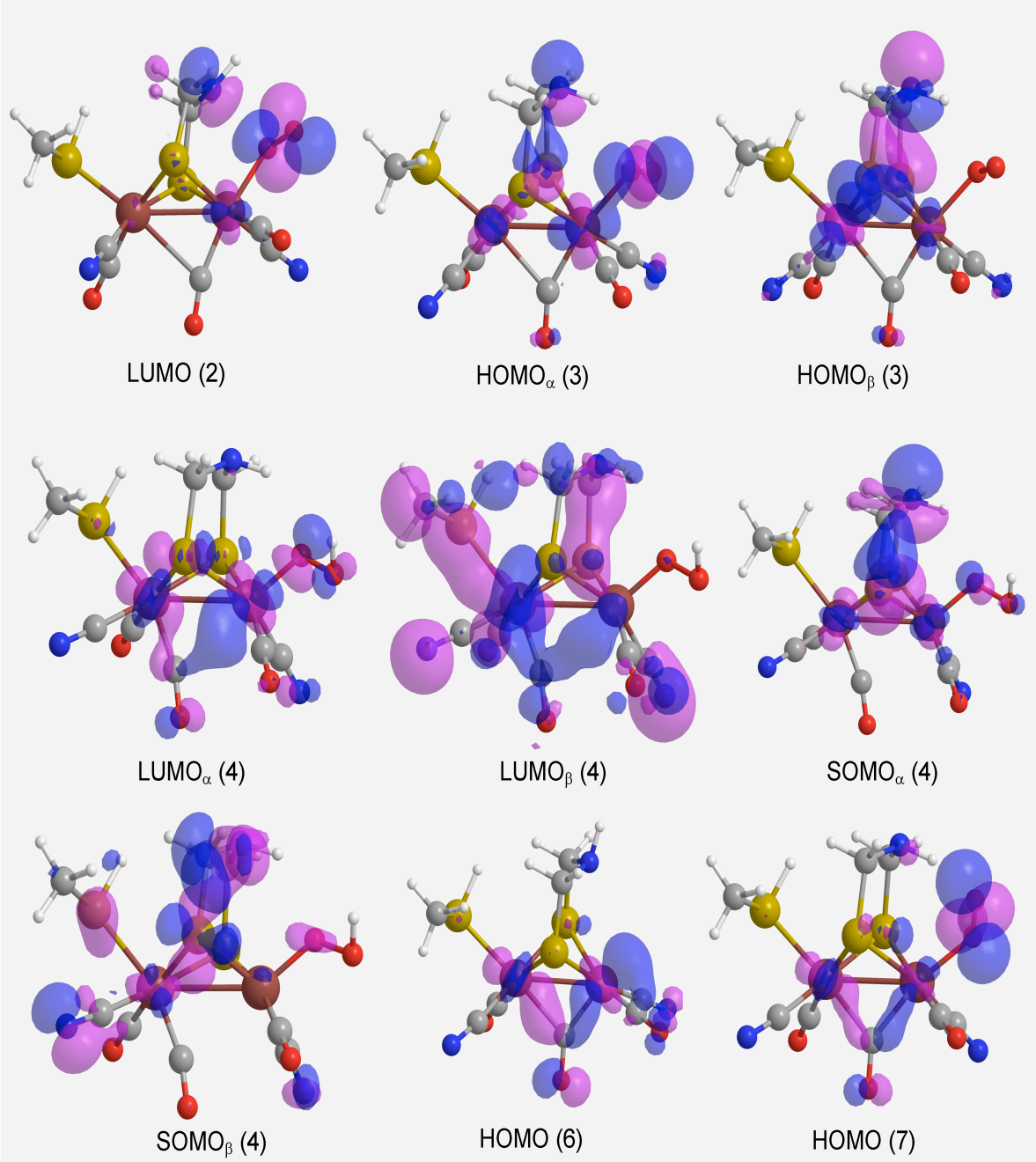

Figure 2-7. Frontier molecular orbitals for H-clusters LUMO (2), $HOMO_{\alpha}$ (3), $HOMO_{\beta}$ (3), $LUMO_{\alpha}$ (4), $LUMO_{\beta}$ (4), $SOMO_{\alpha}$ (4), $SOMO_{\beta}$ (4), HOMO (6), HOMO (7) (where the atom colors, for the H-clusters, are O = red, C = grey, N = blue, S = yellow, Fe = burgundy, and H = white).

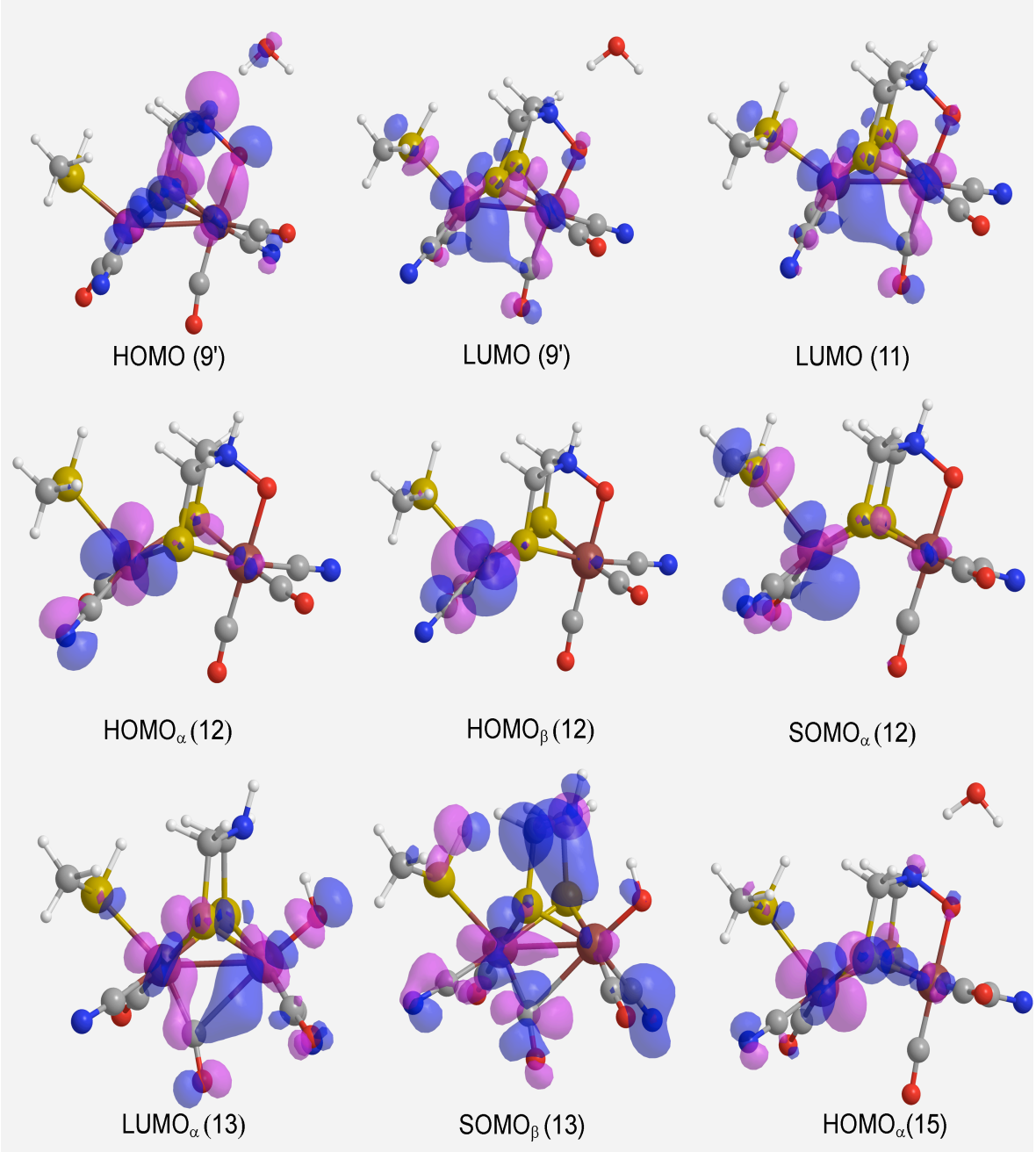

Figure 2-8. Frontier molecular orbitals for H-clusters HOMO (9'), LUMO (9'), LUMO (11), HOMO$_\alpha$ (12), HOMO$_\beta$ (12), SOMO$_\alpha$ (12), LUMO$_\alpha$ (13), SOMO$_\beta$ (13), HOMO$_\alpha$ (15).

In the reduction process of H-cluster **13**, the in silico data clearly shows that the orbital energy of $LUMO_{\alpha}$ ($E_{LUMO_{\alpha}}$ = -0.14850 Hartrees) is lower than the energy of $SOMO_{\beta}$ ($E_{SOMO_{\beta}}$ = -0.13886 Hartrees). Thus, upon reduction of cluster **13**, the e^- goes into $LUMO_{\alpha}$ having lower orbital energy relative to $SOMO_{\beta}$ (Figure 2-8). Analyzing the NBO charges of cluster **13** and **14**, it is noticeable that the OH and Fe_d of **14** acquire most of the partial charge ceded by Fe_p and the reductive process **13** → **14**. H-cluster **15** undergoes a protonation reaction on N_{DTMA}, which is substantiated by the NBO negative charge decrease on N_{DTMA} (q_{N3} = -0.267 a.u (15) → -0.187 a.u. (16)).

2.7. Perform Calculations on the Inhibitory Mechanism of [Fe-Fe]-Hydrogenase by O_2

The subsequent investigation deals with the inhibition mechanism of H-cluster by O_2, which uses the hybrid ONIOM* method on the enzyme matrix.

* ONIOM scheme (Acronym: **O**ur ow**N** n-layered **I**ntegrated molecular **O**rbital + molecular mechanics **M**ethod) is a fast hybrid method developed by Morokuma et al.[2,3] to execute different levels of theory on the same molecule. The algorithm consists of high-level (QM) calculations that are performed on a small part of the system (e.g., active site of an enzyme), and low-level (classical mechanics) calculations for the influence of the rest of the system.

2.7.1. Evaluation of the inhibitory effect of O_2 for the wild type [Fe-Fe]-hydrogenase

The ONIOM method is a QM/MM method. The QM methods of calculations are described above. However, the MM[49-52] method* uses a universal force field[53-55] (UFF**), described by Rappe et al.[56], comprised of simple point charges (SPC). In order to use ONIOM, the enzyme is solvated in water and, then, is subjected to energy minimization procedures via QM/MM algorithm. The total charge of the DdH hydrogenase is –6 a.u., and, therefore, counterions, such as Na^+ cations, are added in order to render the enzyme neutral[57,58]. Within the H-domain, the existent hydrogen bonds, are encountered between the H-cluster and the juxtaposed key amino acids, are monitored implementing Chem3D, Molden, and Pymol software programs[59-61]:

1. Discover the sole amino acids possessing the least O_2 binding potential for [Fe-Fe]-hydrogenase.
2. Monitor the hydrogen bonds during the energy minimization process.

---

* Molecular mechanics makes use of Newtonian mechanics for the purpose of modeling molecular systems. MM (ignores electrons) is based on a model of molecules as a collection of atoms (balls) held together by bonds (springs). By changing the molecular† geometry until the lowest energy is attained, one finds a (molecular) geometry optimization.

† The shapes of molecules - bond lengths, angles, and dihedrals.

** A force field consists of a mathematical form of terms, such as bond stretching, angle bending, dihedral angles, and nonbonded interactions, and the parameters in them describing the potential energy of a system of particles.

2.7.2. Engineer an [Fe-Fe]-hydrogenase which shall not react with O_2 via conservative mutations

QM gives relatively precise results, but it is rather time consuming, hence costly from a computational point of view. However, one can still use this method, especially on small enzyme residues such as the hydrogenase H-cluster. Moreover, for the whole enzyme, ONIOM calculations are performed, and thus intermediate structures of the enzyme are obtained which are energetically minimized. These intermediate structures are then studied implementing QM procedures, such as FMO.

The technique below follows the subsequent steps:

1. Solvate the enzyme by adding H_2O molecules within and around the enzyme, where the surrounding layer is 1 nm.
2. Perform energy minimizations using ONIOM by implementing QM calculations on the H-cluster, and MM computational analysis on whole enzyme.
3. Carry out exploratory mutations on the key amino acids (Figure 2-9, to know which residues posses the least O_2 binding potential for [Fe-Fe]-hydrogenase) of the H-domain by turning off their charges.
4. Within a given class of amino acids, mutations are being tried on the amino acids that was found to have the least O_2 binding potential for the referred to enzyme.

To summarize, mutations deal with amino acid substitutions within the same class, (i.e., amino acids that have similar chemical (polar) properties - conservative mutations)

or residue substitutions in different classes. Such mutations should not drastically change the enzymatic stability and function, but could accelerate the O_2 removal process, which is a desideratum in order to enhance H_2 formation. Once mutations have been achieved (for the purpose of enzymatic stability and proper function) the ambient amino acids have to be studied also in detail[62].

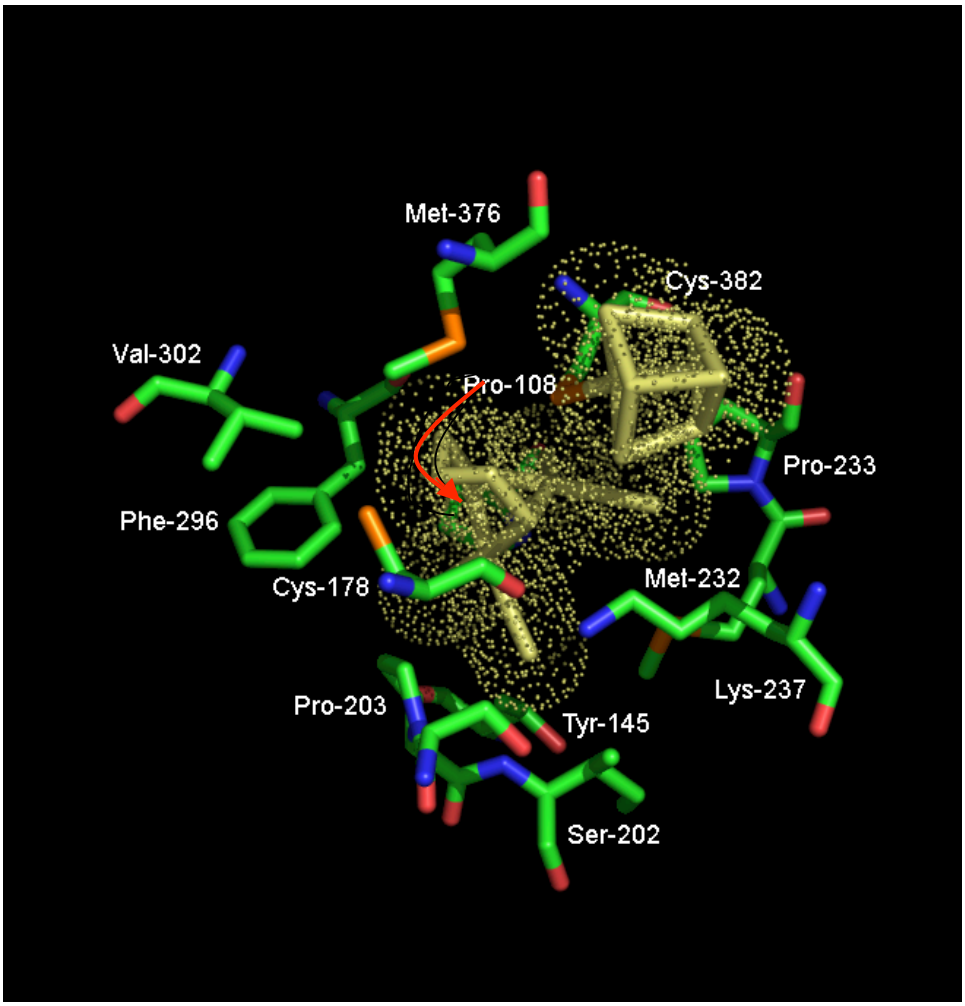

Figure 2-9. The key amino acid residues that are contiguous with the H-cluster (as presented in reference 63)

References

(1) Das, D.; Dutta, T.; Nath, K.; Kotay, S. M.; Das, A. K.; Veziroglu, T. N. *Curr. Sci.* **2006**, *90*, 1627.

(2) Dapprich, S.; Komaromi, I.; Byun, K. S.; Morokuma, K.; Frisch, M. J. *J. Mol. Struct. (Theochem)* **1999**, *1,* 461.

(3) Svensson, M.; Humbel, S.; Froese, R. D. J.; Mastubara, T.; Sieber, S.; Morokuma, K. *J. Phys. Chem.* **1996**, *100*, 19357.

(4) Nicolet, Y.; Lemon, B. J.; Fontecilla-Camps, J. C.; Peters, J. W. *Trends Biochem. Sci.* **2000**, *25*, 138.

(5) Peters, J. W. *Curr. Opin. Struct. Biol.* **1999**, *9*, 670.

(6) Seibert, M.; King, P.; Zhang, L.; Mets, L.; M., G. *Proceedings of the 2002 U.S. DOE Hydrogen Program Review NREL/CP-610-32405* **2002**.

(7) Cohen, J.; Kim, K.; Posewitz, M.; Ghirardi, M. L.; Schulten, M.; Seibert, M.; King, P. *Biochem. Soc. Trans.* **2005**, *33*, 80.

(8) Pierik, A. J.; Hagen, W. R.; Redeker, J. S.; Wolbert, R. B. G.; Boersma, M.; Verhagen, M. F. J. M.; Grande, H. J.; Veeger, C.; Mutsaers, P. H. A.; Sands, R. H.; Dunham, W. R. *Eur. J. Biochem.* **1992**, *209*, 63.

(9) Lemon, B. J.; Peters, J. W. *Biochemistry* **1999**, *38*, 12969.

(10) Lemon, B. J.; Peters, J. W. *J. Am. Chem. Soc.* **2000**, *122*, 3793.

(11) Melis, A.; Zhang, L.; Forestier, M.; Ghirardi, M. L.; Seibert, M. *Plant Physiol.* **2000**, *122*, 127.

(12) Albracht, S. P. J. *Biochim. Biophys. Acta* **1994**, *1118*, 167.

(13) Adams, M. W. W. *Biochim. Biophys. Acta* **1990**, *1020*, 115.

(14) Adams, M. W. W.; Stiefel, E. I. *Science* **1998**, *282*, 1842.

(15) Happe, R. P.; Roseboom, W.; Pierik, A. J.; Albracht, S. P.; Bagley, K. A. *Nature* **1997**, *385*, 126.

(16) Meyer, J.; Gagnon, J. *Biochemistry* **1991**, *30*, 9697.

(17) Peters, J. W.; Lanzilotta, W. N.; Lemon, B. J.; Seefeldt, L. C. *Science* **1998**, *282*, 1853.

(18) Nicolet, Y.; Piras, C.; Legrand, P.; Hatchikian, E. C.; Fontecilla-Camps, J. C. *Structure* **1999**, *7*, 13.

(19) Liu, Z.-P.; Hu, P. *J. Am. Chem. Soc.* **2002**, *124*, 5175.

(20) Motiu, S.; Dogaru, D.; Gogonea, V. *Int. J. Quantum Chem.* **2007**, *107*, 1248.

(21) Cammack, R. *Nature* **1999**, *397*, 214.

(22) Cammack, R.; Frey, M.; R., R. *Hydrogen as a Fuel: Learning from the Nature*; CRC Press, 2001.

(23) Morelli, X.; Czjzek, M.; Hatchikian, E. C.; Bornet, O.; Fontecilla-Camps, J. C.; Palma, N. P.; Moura, J. J. G.; Guerlesquin, F. *J. Biol. Chem.* **2000**, *275*, 23204.

(24) Lee, C.; Yang, W.; Parr, R. G. *Phys. Rev. B* **1988**, *37*, 785.

(25) Becke, A. D. *J. Chem. Phys.* **1993**, *98*, 5648.

(26) Stephens, P. J.; Devlin, F. J.; Chabalowski, C. F.; Frisch, M. J. *J. Phys. Chem.* **1994**, *98*, 11623.

(27) Kohn, W.; Sham, L. J. *Phys. Rev. A* **1965**, *140*, 1133.

(28) Hohenberg, P.; Kohn, W. *Phys. Rev. B* **1964**, *136*, 864.

(29) Cao, Z.; Hall, M. B. *J. Am. Chem. Soc.* **2001**, *123*, 3734.

(30) Fan, H.-J.; Hall, M. B. *J. Am. Chem. Soc.* **2001**, *123*, 3828.

(31) Zampella, G.; Bruschi, M.; Fantucci, P.; Razavet, M.; Pickett, C. J.; De Gioia, L. *Chem. Eur. J.* **2005**, *11*, 509.

(32) Bruschi, M.; Fantucci, P.; De Gioia, L. *Inorg. Chem.* **2004**, *43*, 3733.

(33) Bruschi, M.; Fantucci, P.; De Gioia, L. *Inorg. Chem.* **2003**, *42*, 4773.

(34) Bruschi, M.; Fantucci, P.; De Gioia, L. *Inorg. Chem.* **2002**, *41*, 1421.

(35) Frisch, M. J.; Trucks, G. W.; Schlegel, H. B.; Scuseria, G. E.; Robb, M. A.; Cheeseman, J. R.; Montgomery, J., J. A.; Vreven, T.; Kudin, K. N.; Burant, J. C.; Millam, J. M.; Iyengar, S. S.; Tomasi, J.; Barone, V.; Mennucci, B.; Cossi, M.; Scalmani, G.; Rega, N.; Petersson, G. A.; Nakatsuji, H.; Hada, M.; Ehara, M.; Toyota, K.; Fukuda, R.; Hasegawa, J.; Ishida, M.; Nakajima, T.; Honda, Y.; Kitao, O.; Nakai, H.; Klene, M. L., X.; Knox, J. E.; Hratchian, H. P.; Cross, J. B.; Bakken, V.; Adamo, C.; Jaramillo, J.; Gomperts, R.; Stratmann, R. E.; Yazyev, O.; Austin, A. J.; Cammi, R.; Pomelli, C.; Ochterski, J. W.; Ayala, P. Y.; Morokuma, K.; Voth, G. A.; Salvador, P.; Dannenberg, J. J.; Zakrzewski, V. G.; Dapprich, S. D., A. D.; Strain, M. C.; Farkas, O.; Malick, D. K.; Rabuck, A. D.; Raghavachari, K.; Foresman, J. B.; Ortiz, J. V.; Cui, Q.; Baboul, A. G.; Clifford, S.; Cioslowski, J.; Stefanov, B. B.; Liu, G.; Liashenko, A.; Piskorz, P.; Komaromi, I.; Martin, R. L.; Fox, D. J.; Keith, T.; Al-Laham, M. A.; Peng, C. Y.; Nanayakkara, A.; Challacombe, M.; Gill, P. M. W.; Johnson, B.; Chen, W.; Wong, M. W.; Gonzalez, C.; Pople, J. A. Gaussian 03, Revision C.02; Gaussian, Inc.: Wallingford CT, 2004.

(36) Hay, P. J.; Wadt, W. R. *J. Chem. Phys.* **1985**, *82*, 298.

(37) Wadt, W. R.; Hay, P. J. *J. Chem. Phys.* **1985**, *82*, 284.

(38) Hay, P. J.; Wadt, W. R. *J. Chem. Phys.* **1985**, *82*, 270.

(39) Justice, A. K.; Linck, R. C.; Rauchfuss, T. B.; Wilson, S. R. *J. Am. Chem. Soc.* **2004**, *126*, 13214.

(40) Darensbourg, M. Y.; Lyon, E. J.; Zhao, X.; Georgakaki, I. P. *Proc. Natl. Acad. Sci. U.S.A.* **2003**, *100*, 3683.

(41) Nicolet, Y.; De Lacey, A. L.; Vernede, X.; Fernandez, V. M.; Hatchikian, E. C.; Fontecilla-Camps, J. C. *J. Am. Chem. Soc.* **2001**, *123*, 1596.

(42) De Lacey, A. L.; Stadler, C.; Cavazza, C.; Hatchikian, E. C.; Fernandez, V. M. *J. Am. Chem. Soc.* **2000**, *122*, 11232.

(43) Cossi, M.; Barone, V.; Cammi, R.; Tomasi, J. *Chem. Phys. Lett.* **1996**, *255*, 327.

(44) Miertus, S.; Tomasi, J. *Chem. Phys.* **1982**, *65*, 239.

(45) Miertus, S.; Scrocco, E.; Tomasi, J. *Chem. Phys.* **1981**, *55*, 117.

(46) Dogaru, D.; Motiu, S.; Gogonea, V. *Int. J. Quantum Chem.* **2007**, *107.*

(47) George, S. J.; Kurkin, S.; Thorneley, R. N. F.; Albracht, S. P. J. *Biochemistry* **2004**, *43*, 6808.

(48) Liu, Z.-P.; Hu, P. *J. Chem. Phys.* **2002**, *117*, 8177.

(49) Vernon, G. S. *J. Mol. Model.* **1997**, *3*, 124.

(50) Burkert, U.; Allinger, N. L. *Molecular Mechanics*, **1982**, ACS Monograph 177, American Chemical Society, Washington, D.C**.**

(51) Koehl, P.; Levitt, M. *Nature Struct. Biol.* **1999**, *6*, 108.

(52) Leckband, D.; Israelachvili, J. *Quart. Rev. Biophys.* **2001**, *34*, 105.

(53) Hopfinger, A. J.; Pearlstein, R. A. *J. Comput. Chem.* **1984**, *5*, 486.

(54) MacKerell, A. D., Jr.,. **2004**, *25*, 1584.

(55) Ponder, J. W.; Case, D. A. *Adv. Prot. Chem.* **2003**, *66*, 27.

(56) Rappe, A. K.; Casewit, C. J.; Colwell, K. S.; Goddard, W. A.; Skiff, W. M. *J. Am. Chem. Soc.* **1992**, *113*, 10024.

(57) Lindahl, E.; Hess, B. *J. Mol. Mod.* **2001**, *7*, 306.

(58) Berendsen, H. J. C.; van der Spoel, D. *Comp. Phys. Comm.* **1995**, *91*, 43.

(59) ChemOffice Ultra 9.0; 9.0 ed.; CambridgeSoft: Cambridge, MA, 2005.

(60) DeLano, W. L. PyMOL: Molecular Visualization Program; DeLano Scientific: South San Francisco, CA, 2003.

(61) Schaftenaar, G.; Noordik, J. H. *J. Comput.-Aided Mol. Design* **2000**, *14*, 123.

(62) Jonson, P. H.; Petersen, S. B. *Prot. Eng.* **2001**, *14*, 397.

(63) Nicolet, Y.; Cavazza, C.; Fontecilla-Camps, J. C. *J. Inorg. Biochem.* **2002**, 1.

CHAPTER III

INACTIVATION OF [FE-FE]-HYDROGENASE BY O_2. THERMODYNAMICS AND FRONTIER MOLECULAR ORBITALS ANALYSES

3.1. General Considerations

H-cluster[1-83] oxidation in gas phase, and in aqueous enzyme phase, has been investigated by means of quantum mechanics (QM) and combined quantum mechanics-molecular mechanics (QM/MM). Several potential reaction pathways (in the above mentioned chemical environments) have been studied, wherein only the aqueous enzyme phase has been found to lead to an inhibited hydroxylated cluster. Specifically, the inhibitory process occurs at the distal iron (Fe_d) of the catalytic H-cluster (which is also

the atom involved in H_2 synthesis). The processes involved in the H-cluster oxidative pathways are O_2 binding, e^- transfer, protonation, and H_2O removal.

We found that oxygen binding is non-spontaneous in gas phase, and spontaneous for aqueous enzyme phase where both Fe atoms have oxidation state II; however, it is spontaneous for the partially oxidized and reduced clusters in both phases. Hence, in the protein environment the hydroxylated H-cluster is obtained by means of completely exergonic reaction pathway starting with proton transfer.

A unifying endeavor has been carried out for the purpose of understanding the thermodynamic results vis-à-vis several other performed electronic structural methods, such as frontier molecular orbitals (FMO), natural bond orbital partial charges (NBO), and H-cluster geometrical analysis.

Our investigation is composed of three different parts. 1). Thermodynamic analysis, for every reaction path mechanism (Figures 3-1a, 3-1b, 3-2 and 3-3), implicated in the eventual H-cluster **14** inhibition by means of $O_2 \rightarrow OH^-$. 2). Electronic analysis, for the same paths referred to above, which deals with Natural Bond Orbitals (NBO), as well as Frontier Molecular Orbitals (FMO). 3). Geometrical analysis carried out only for appropriate bond breaking, and bond formation.

From the investigated subdivisions, thermodynamics analysis (Figure 3-2, and 3-3) is of pivotal importance since it shows that there is just an exergonic path from H-cluster **9'** to the hydroxylated cluster **14** occurring in the aqueous enzyme phase. However, from the thermodynamic results (Figure 3-1a), it is observed that most reaction steps proceed exergonically (except **1** → **2**, gas phase), leading to the oxidized cluster **9**. Moreover, at

the end of each path, every vacant H-cluster 1, 5, and 6, in spite of its oxidation states, becomes aerobically inactivated, 9.

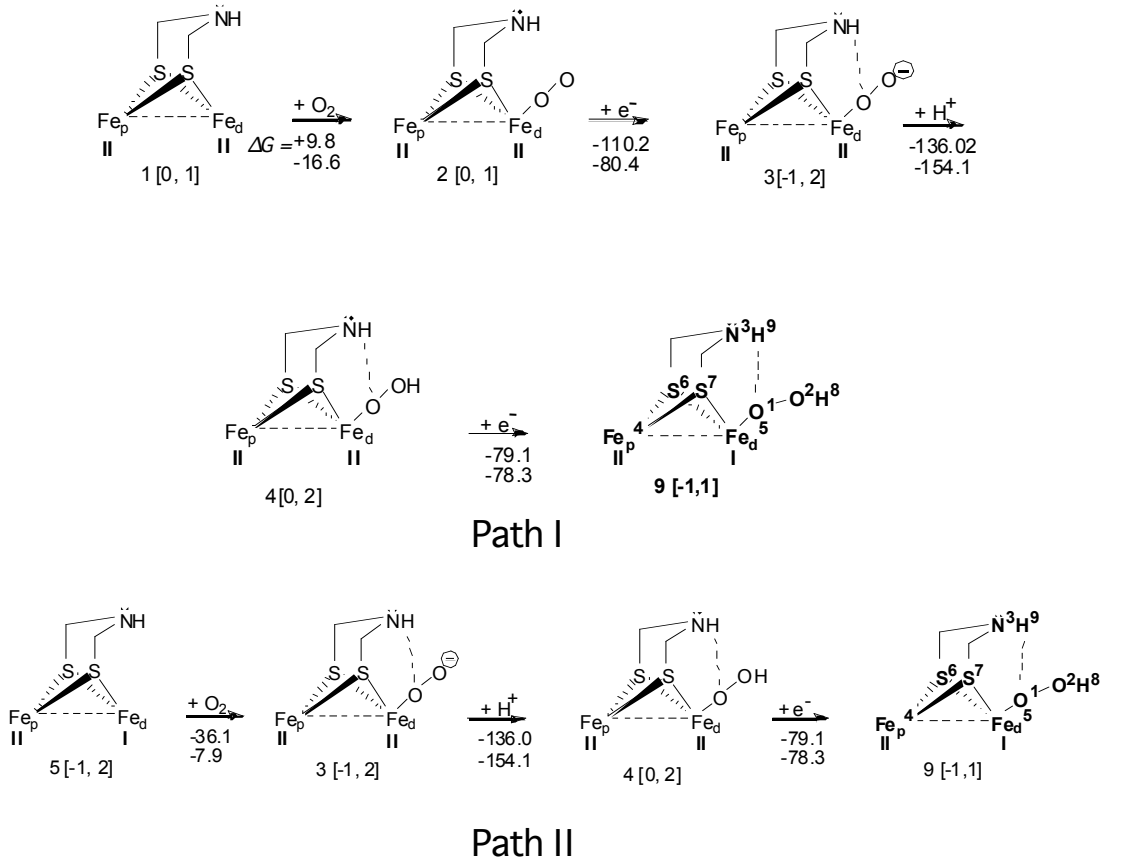

Figure 3-1a. Reaction pathways I and II: Oxidation mechanisms of H-clusters that are fully oxidized (1), partially oxidized (5). The charges and multiplicities are given in square brackets. The first Gibbs' energy value is for gas phase, and the second is for ONIOM calculations. Fe_p is the proximal iron, and Fe_d is the distal iron.

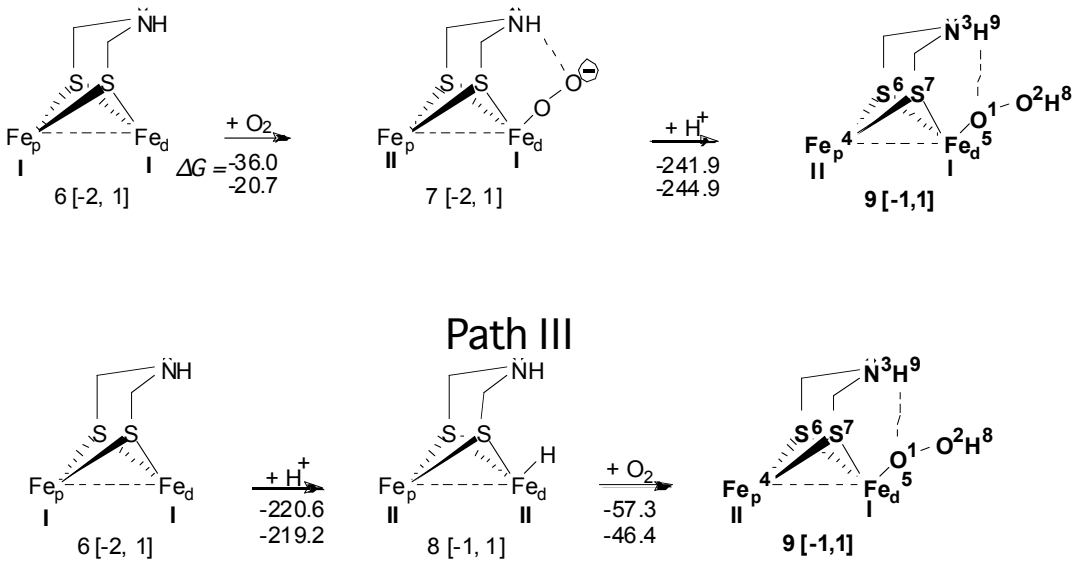

Figure 3-1b. Reaction pathways III and IV: Oxidation mechanisms of H-cluster that is reduced (6). The charges and multiplicities are given in square brackets. The first Gibbs' energy value is for gas phase, and the second is for ONIOM calculations. Fe_p is the proximal iron, and Fe_d is the distal iron.

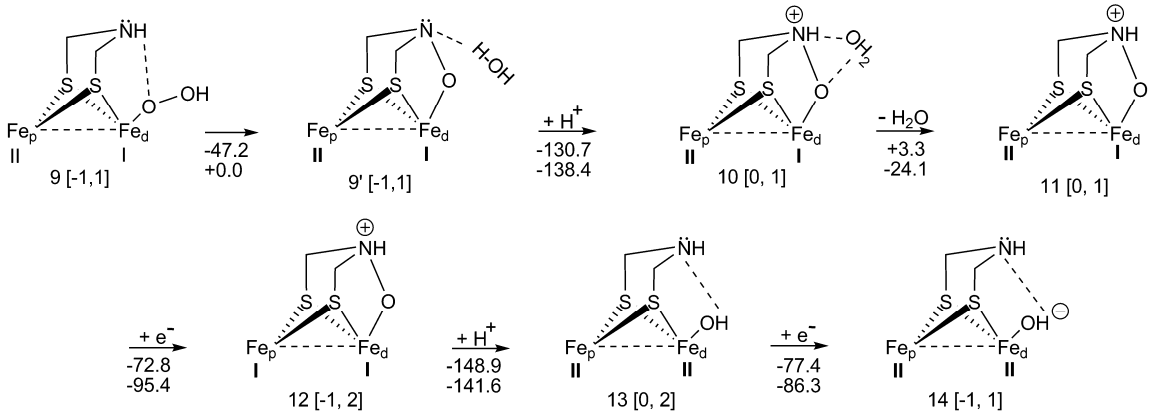

Figure 3-2. Reaction mechanism for isomerization, protonation, H_2O elimination, and reduction of the inhibited [Fe-Fe]-hydrogenase H-cluster. The H_2O is being removed from a closed-shell cluster (the charges, multiplicities, and energy values are presented as in Figure 3-1a).

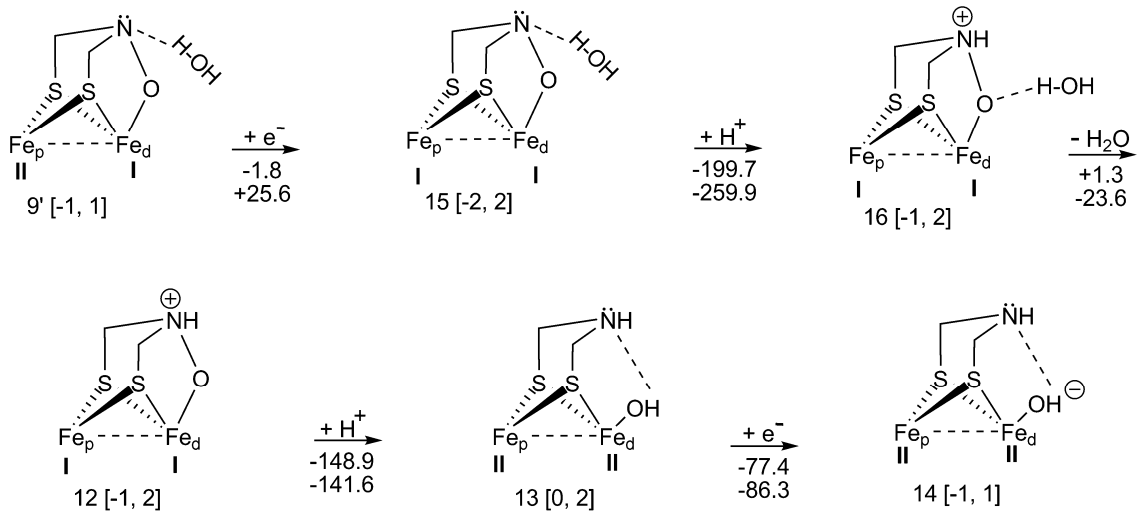

Figure 3-3. Reaction mechanism for reduction, protonation, and H_2O removal from the inhibited [Fe-Fe]-hydrogenase H-cluster. Here, the H_2O is being eliminated from an open-shell cluster (the charges, multiplicities, and energy values are presented as in Figure 3-1a).

3.2. Quantum Mechanics/ Molecular Mechanics Hybrid Method

In the current study, both QM [DFT (in gas phase)] and QM/MM [DFT/UFF[84] (in aqueous enzyme phase)] methodologies have been used. The ONIOM[85] method (DFT for the QM region, and the universal force field, UFF, for the MM region, implemented in Gaussian03[86]) has been applied to determine the reaction thermodynamics, i.e., ΔG, for the inactivation pathways of the H-cluster, and the [Fe-Fe]-hydrogenase H-cluster (positioned within the enzyme matrix). Subsequently, the DFT results have been compared with the ONIOM calculations. The electronic structure of the hydrogenase active site (except the proximal cubane) is investigated by quantum mechanics (Gaussian 03) using DFT method (B3LYP functional[87,88]), and QM/MM with 6-31+G(d,p) basis set. For Fe an effective-core potential with a double zeta polarization basis set (LANL2DZ[89,90]) was used for DFT gas phase calculations, and a 6-31+G(d,p) basis set for the ONIOM calculations. In accordance with experimental and in-silico data low spin states (singlet, and doublet), and low oxidation states (I, and II) have been selected for the Fe atoms[2,14,35]. Gromacs program[91,92] was employed to add hydrogen atoms, water, and counter ions to the X-ray crystal structure of DdH [Brookhaven Protein Data Bank id.1HFE]. Hydrogen atoms and a 1 nm layer of water (2043 molecules) have been added to the PDB DdH structure. Moreover, Na^+ ions have been randomly inserted* into the solvent to neutralize the negative charges encountered therein, e.g., the -2 a.u. found on

* In a real biological system, a protein has counter ions in its proximity.

the cubane/cysteine moieties[*93]. For both basic and acidic amino acids, charges were assigned by Gromacs algorithm to be at pH 7. ONIOM geometry optimizations have been performed on the DdH, with the low layer (MM region) being frozen[**], with the exception of the proximal cubane, while the high layer (QM) had only the iron atoms, Fe_p-Fe_d, and the N3, (of the DTMA bridge) kept frozen; "freezing atoms" is practiced to reduce computational time. The low layer consists of all the hydrogenase amino acids as well as its constituent cubanes, i.e., proximal, medial, and distal. The high layer is comprised of 2Fe subunit, (which is the moiety of the H-cluster), and C_β and S_γ (appertaining to the bridging Cys^{382}). Moreover, two linking hydrogen atoms were added between C_α and C_β of Cys^{382}, and between S_γ and an Fe atom of the proximal cubane. The charge equilibration method of the UFF was used to describe the electrostatic interactions within the low layer of the system[94]. The DdH partial charges were obtained using the charge equilibration method, whereas the solvent charges were acquired from literature[94] (q_O = -0.706 a.u. and q_H = 0.353 a.u.).

3.3. H-cluster Thermodynamics for O_2 Binding, Reduction, and Protonation

Figure 3-1a illustrates different O_2 inhibition pathways of the hydrogenase H-cluster; the H-clusters, **1**, **5**, **6**, and **8**[2,9,21], of the pathways are obtained in the reversible catalysis of H_2. Reaction **1** → **2** (path I) is endergonic for the gas phase (ΔG_{gas} = +9.8 kcal/mol; gas = gas phase) when O_2 binds to the fully oxidized H-cluster (**1**). ONIOM

[*] Each of the three cubane/cysteine moieties (found in DdH) is comprised of a cubane plus four surrounding, depotonated cysteines which are bound to the four iron atoms of every cubane.

[**] Where "frozen" means that the x, y, z coordinates for the atoms are kept fixed

calculations, on the other hand, show that O_2 binding occurs exergonically ($\Delta G_{QM/MM}$ = -16.6 kcal/mol), shedding light on the sensitivity of hydrogenases to O_2[95].

Reduction **2** → **3** (ΔG_{gas} = -110.2 kcal/mol) as well as protonation **3** → **4** (ΔG_{gas} = -136.0 kcal/mol) proceed exergonically; ONIOM calculations, for the hydrogenase matrix, show that e^- transfer is considerably less exergonic ($\Delta G_{QM/MM}$ = -80.4 kcal/mol) relative to protonation which is more exergonic ($\Delta G_{QM/MM}$ = -154.1 kcal/mol). The free energy differences, in gas vs. aqueous enzyme phases for reactions **2** → **3** and **3** → **4**, ensue from the effect of the electric field of the protein on the H-clusters **2**, **3**, and **4**, and from the different phase geometries.

Cluster **4** undergoes reduction, and it (**4** → **9**) proceeds exergonically in both gas and aqueous hydrogenase phase (ΔG_{gas} = -79.1 kcal/mol; $\Delta G_{QM/MM}$ = -78.3 kcal/mol).

Path II starts with the partially oxidized H-cluster **5**, (Fe_p^{II}-Fe_d^{I}). The binding of O_2 to Fe^I (Fe_d^{I}-O_2), **5** → **3**, is firmer (ΔG_{gas} = -36.1 kcal/mol) than for Fe^{II} in **1** → **2** (Fe_d^{II}-O_2, path I). In contrast, ONIOM results show that O_2 binds to the partially oxidized H-cluster (Fe_p^{II}-Fe_d^{I}, $\Delta G_{QM/MM}$ = -7.9 kcal/mol) as well as to the fully oxidized cluster (Fe_p^{II}-Fe_d^{II}, $\Delta G_{QM/MM}$ = -16.6 kcal/mol, **1** → **2,** path I). The remaining two reactions **3** → **4**, and **4** → **9** (path II) are the same as the last two steps of path I.

In path III (Figure 3-1b), **6** → **7**, which starts with the fully reduced H-cluster **6**, (Fe_p^{I}-Fe_d^{I}), the reaction spontaneity (ΔG_{gas} = -36.0 kcal/mol) is almost identical to the free energies of reaction **5** → **3**. The gas phase free energy similarity may ensue because both loci of oxygen binding (Fe_d^{I}-O_2) are on similar oxidized species, Fe_d^{I}. However, ONIOM calculations show smaller reaction spontaneity difference between aqueous enzyme ($\Delta G_{QM/MM}$ = -20.7 kcal/mol) and gas phase results (ΔG_{gas} = -36.0 kcal/mol, **6** → **7**), than

for O_2 binding in path I and II. In path III, protonation (**7** → **9**) is, once again, largely exergonic for both phases (ΔG_{gas} = -241.9 kcal/mol; $\Delta G_{QM/MM}$ = -244.9 kcal/mol). Moreover, from Figures 3-1a and 3-1b, the above ONIOM calculations show the highest H^+ affinity because H-cluster **7** has a charge of -2 a.u., and also the H^+ binds to a rather electronegative atom, viz., oxygen.

In the final path (IV), protonation **6** → **8** is the second most exergonic reaction in gas phase (ΔG_{gas} = -220.6 kcal/mol) mostly because of the over-all charge of -2 on the H-cluster **6**. ONIOM data (as in **7** → **9**) show very high H^+ affinity ($\Delta G_{QM/MM}$ = -219.2 kcal/mol) for the hydrogenase H-cluster (in spite of the fact that the H^+ is seized by the Fe_d as opposed to the more electronegative Fe_d-O_2, **7** → **9**), which is comparatively similar to the gas phase result (ΔG_{gas} = -220.6 kcal/mol).

In the last step (**8** → **9**; path IV), O_2 is interposed between Fe_d and the hydride (Fe_d^I-O_2-H, **9**). For this insertion reaction, the O_2 binding occurs exergonically in both ONIOM ($\Delta G_{QM/MM}$ = -46.4 kcal/mol) and the gas phase (ΔG_{gas} = -57.3 kcal/mol) results.

N.B., path IV shows that oxidation of Fe_p-Fe_d H-cluster is similar* to the Ni_p-Fe_d hydrogenase H-cluster obtained from experimental data[96].

From the above thermodynamic results, most reaction steps proceed exergonically (except **1** → **2**, gas phase), leading to oxidized cluster **9**. At the end of every path, each vacant H-cluster **1**, **5**, or **6**, in spite of its oxidation states, becomes aerobically inactivated.

* The similarity for these clusters is they are first found as hydride containing H-clusters, and then undergo oxidation.

3.4 NBO Charges and Geometry Adjustment of Intermediates in the Oxidation of H-cluster

The atoms of the vacant H-clusters 1, 5, and 6 have slightly different natural bond orbital (NBO) charge distributions. For instance, for cluster 1 the NBO charges of Fe_p-Fe_d are q^g_{Fep}[**] = 0.137 a.u. (q^e_{Fep} = -0.230 a.u.) and q^g_{Fed} = -0.096 a.u. (q^e_{Fed} = 0.187 a.u.), whereas in 5, the sign of the partial charges are reversed only in gas phase, i.e. q^g_{Fep} = -0.024 a.u. (q^e_{Fep} = -0.227 a.u.) and q^g_{Fed} = 0.078 a.u. (q^e_{Fed} = 0.061 a.u.). Then, the NBO charges for the Fe_p-Fe_d in cluster 6 (in both phases) are more negative, q^g_{Fep} = -0.104 a.u. (q^e_{Fep} = -0.297 a.u.), and q^g_{Fed} = -0.117 a.u. (q^e_{Fed} = -0.160 a.u.) because both metals are in a reduced state, unlike clusters 1 and 5. Regarding charges on the nitrogen, N3, (of the DTMA bridge), similarities are seen amongst clusters 1, 5, and 6; the NBO charges for N3 are approximately -0.700 a.u., making this amine (within the above H-clusters) a relatively important H^+ acceptor/donor (vs. amino acids with similar function in the juxtaposed enzyme matrix, e.g., Lys^{237}) as suggested by Liu and Hu[9]. The non-bridging S_γ (of Cys^{382}) has the following charges: for 1 $q^g_{S\gamma}$ = 0.204 a.u. ($q^e_{S\gamma}$ = 0.474 a.u.), for 5 $q^g_{S\gamma}$ = 0.142 a.u. ($q^e_{S\gamma}$ = 0.425 a.u.), and for 6 $q^g_{S\gamma}$ = 0.079 a.u. ($q^e_{S\gamma}$ = 0.285 a.u.). Comparing clusters 1, 5 and 6, a sequential drop in NBO charges for Fe_p and S_γ is observed.

When H-cluster 1 is in an oxidized state (in gas phase), Fe_p^{II}- Fe_d^{II}, the CO_b shifts[9] towards the Fe_d^{II}, and becomes bonded to Fe_d^{II}. The shifted CO_b bond distance (measured from its bridging carbon, C_b, to the iron atoms) between C_b—Fe_p^{II} is 3.067 Å, whereas

[**] The NBO charges and bond lengths are found in the supporting information addendum. q^g represents the charges for the gas phase, while q^e stands for the aqueous enzyme phase charges.

C_b—Fe_d^{II} is 1.819 Å. When the carbonyl is close to Fe_d^{II}, CO_b-Fe_d^{II}, the fully oxidized H-cluster **1** becomes relatively stable vs. the quasi-symmetric cluster[21] (ΔH = 14 kcal/mol), which is also shown by the NBO charge on C_b in CO_b, (0.664 a.u.). This may be due to repulsion of charges between q^g_{Cb} (0.664 a.u.) and q^g_{Fep} (0.137 a.u.), whereas for the clusters **5** and **6**, the partial charges (q^g_{Cb} = 0.462 a.u., and q^g_{Cb} = 0.466 a.u., respectively) are less then in **1** because CO_b is bonded to both iron atoms. However, in the enzyme phase less shifting of the bridging carbonyl occurs, with the charges on C_b being similar (q^e_{Cb} = 0.536 a.u. for **1**, q^e_{Cb} = 0.497 a.u. for **5**, and q^e_{Cb} = 0.493 a.u. for **6**). Comparing the reaction spontaneity for O_2 binding (in gas phase), which renders clusters **2**, **3**, and **7**, one may observe that **3** and **7** are more stable than **2**. The reason for this stability is essentially due to the formation of a hydrogen bond between the exogenous O_2 and the hydrogen H9 (bonded to N3 of the DTMA bridge) in both **3** and **7**. The O1—H9 bond distance is 2.016 Å in **3**, and O2—H9 bond distance is 1.765 Å in **7**, which correlates with the NBO charges on the mentioned oxygens and hydrogens; the partial charges on oxygens are q^g_{O1} = -0.235 a.u. in **3**, and q^g_{O2} = -0.493 a.u. in **7**, whereas the charge on H9 is 0.439 a.u. in **3**, and 0.454 a.u. in **7**. Note that CO_b is located almost symmetrically in clusters **2**, **3**, and **7**. Structurally, clusters **4** and **9** are similar in view of the fact that both possess a hydrogen bond (H9...O1), whereas CO_b is found to reside quasi-symmetrically in **9**, but asymmetrically in **4** bonded only to Fe_p^{II}. In the enzyme phase both hydrogen bonds (in clusters 3 and 7) are formed between H9 and O2 of the exogenous oxygen (q^e_{O2} = -0.210 a.u. in **3**, q^e_{O2} = -0.452 a.u. in **7**, q^e_{H9} = 0.443 a.u. in **3**, and q^e_{H9} = 0.445 a.u. in **7**; O2—H9 bond distance is 1.890 Å in **3**, and O2—H9 bond distance is 1.760 Å in **7**).

3.5. Thermodynamics and NBO Charges Relationship for H_2O Removal from the Oxidized H-cluster

Figure 3-2 depicts a series of reactions (9 → 9', 9' → 10, 10 → 11, 11 → 12, 12 → 13, and 13 → 14), which present the net conversion of 9 to 14. The compounds 9 and 9' are isomers; 9' is more stable by 47.2 kcal/mol, [which may be, to a certain extent, attributed to the hydrogen bond formation between H_2O and the N3 of DTMA bridge (N3…H-OH; i.e., 2 bonds being broken vs. 3 being formed for 9 → 9', respectively)]. The hydrogen bond length, N3…H, is 1.939 Å (and the angle formed by N3…H-O is 168.7°). The distance between the iron atoms is larger in 9' (2.796 Å) than in 9 (2.605 Å). During reaction 9 → 9', CO_b moves away from Fe_p^{II} [i.e., for C_b-Fe_p^{II} 2.225 Å (9) → 2.771 Å (9')]. Also, in Figure 3-2 (hydrogenase H-cluster 9, and 9'), ONIOM geometry optimizations for 9, and 9' resulted in in the same structure for the hydrogenase H-clusters ($\Delta G_{QM/MM}$ corresponding to 9 → 9' is 0 kcal/mol). The protonation of 9' (9' → 10) produces a quaternary ammonium ion (NR_4^+) within the DTMA bridge, which is exergonic for both phases, viz., ΔG_{gas} = -130.7 kcal/mol, and $\Delta G_{QM/MM}$ = -138.4 kcal/mol. To wit, the observed high reaction spontaneity for both phases is attributed to the negatively charged H-cluster 9'. In 10 → 11, H_2O is removed from N3 by means of hydrogen bond breaking; this reaction (vs. 9' → 10) occurs slightly endergonically in gas phase (ΔG_{gas} = +3.3 kcal/mol), while for QM/MM results, the H_2O removal step, 10 → 11, is exergonic ($\Delta G_{QM/MM}$ = -24.1 kcal/mol).

Reduction 11 → 12 (Figure 3-2) is subjected to an increase in the partial charge of the exogenous oxygen (q^g_{O1} = -0.568 a.u. (11) → -0.594 a.u. (12); ΔG_{gas} = -72.8

kcal/mol). Regarding geometrical changes in **11** → **12**, the bond distance between Fe_p^{II}-Fe_d^{I} is increasing from 2.792 Å to 3.261 Å, while the CO_b departs from Fe_p^{II} [for C_b-Fe_p^{II} 2.766 Å (**11**) → 3.183 Å (**12**)]. For the aqueous enzyme phase result, **11** → **12** occurs with a relatively large free energy ($\Delta G_{QM/MM}$ = -95.4 kcal/mol; compared to other neutral H-cluster reductions), versus the gas phase outcome (ΔG_{gas} = -72.8 kcal/mol); the charge remains constant on the exogenous oxygen [q^e_{O1} = -0.530 a.u. (**11**) → -0.527 a.u. (**12**)]. Due to excess electron density accumulation on O1 (**12**), the latter readily captures a proton (**12** → **13**; ΔG_{gas} = -148.9 kcal/mol). ONIOM calculations, **12** → **13**, confirm the high H^+ affinity (in Figure 3-2, $\Delta G_{QM/MM}$ = -141.6 kcal/mol) for the hydrogenase H-cluster, which is close to the gas phase result (ΔG_{gas} = -148.9 kcal/mol). The free energy differences between the given protonations, **12** → **13** vs. **9'** → **10**, may arise because of the greater stability of cluster **13** vs.**10**.

Finally, in Figure 3-2, an e^- is acquired by the hydroxyl group (**13** → **14**; ΔG_{gas} = -77.4 kcal/mol; $\Delta G_{QM/MM}$ = -86.3 kcal/mol). Note that the H-cluster **14**[2,21] is the starting compound in the reactivation pathway that ends in the reduced H-cluster **6** (Fe_p^{I}-Fe_d^{I}).

In Figure 3-3, an alternative pathway (**9'** → **15**, **15** → **16**, **16** → **12**, **12** → **13**, and **13** → **14**) has been investigated. The pathway starts with a reductive step, rather than with a protonation. Reaction **9'** → **15** is slightly exergonic for the gas phase (ΔG_{gas} = -1.8 kcal/mol), while ONIOM calculations indicate an endergonic process ($\Delta G_{QM/MM}$ = +25.6 kcal/mol). **9'** → **15** is another O_2 inhibitory step (in addition to **10** → **11** for the gas phase, Figure 3-2) which seems to explain the O_2 sensitivity of wild type DdH. Therefore, mutagenic studies ought to be performed on [Fe-Fe]-hydrogenase H-cluster **9'** to eliminate its inhibitory path (viz., **9'** → **15**). When a H^+ is in the vicinity of H-cluster

15, 15 → 16 proceeds with the greatest spontaneity (of Figures 3-2 and 3-3) in gas phase (ΔG_{gas} = -199.7 kcal/mol) because 15 has a net charge of -2 a.u. Note that the ONIOM findings, for step 15 → 16, confirm the highest free energy ($\Delta G_{QM/MM}$ = -259.9 kcal/mol) of all the potential reaction mechanisms analyzed for the [Fe-Fe]-hydrogenase H-cluster, while the gas phase result is about 60 kcal/mol less exergonic. Water elimination in gas phase, (16 → 12) is slightly endergonic (ΔG_{gas} = +1.3 kcal/mol), whereas for the aqueous enzyme phase it is significantly exergonic ($\Delta G_{QM/MM}$ = -23.6 kcal/mol). Note that both 10 (Figure 3-2) and 16 (Figure 3-3) lead to the same compound (12) by H_2O elimination. The thermodynamic data are similar for both reactions, 10 → 11 and 16 → 12, because Fe_d is found in the same oxidation state (Fe_d^I) in both 10 and 16, but Fe_p (being further away from the focal catalytic locus, Fe_d) has different oxidation states [Fe_p^{II} (10); Fe_p^I (16)]. The in silico ONIOM result of the H_2O removal step (Figure 3, 16 → 12), is exergonic ($\Delta G_{QM/MM}$ = -23.6 kcal/mol), just like in step 10 → 11, (Figure 3-2, $\Delta G_{QM/MM}$ = -24.1 kcal/mol). Also, close free energies are observed for the gas phases of 16 → 12 (ΔG_{gas} = +1.3 kcal/mol) and 10 → 11 (ΔG_{gas} = +3.3 kcal/mol). Next, reactions 12 → 13, and 13 → 14 proceed exergonically [(ΔG_{gas} = -148.9 kcal/mol; $\Delta G_{QM/MM}$ = -141.6 kcal/mol), and (ΔG_{gas} = -77.4 kcal/mol; $\Delta G_{QM/MM}$ = -86.3 kcal/mol), respectively], just as (previously discussed) in Figure 3-2. The following reactions, 10 → 11 (Figure 3-2) and 16 → 12 (Figure 3-3), show that the entire (oxidative inhibitory H-cluster) path has difficulties proceeding to 14 in gas phase.

From the above, it can be seen that there is only one exergonic path (Figure 3-2) from the oxidized H-cluster 9' to the hydroxylated cluster 14 in aqueous enzyme phase. A path starts with H^+ transfer (Figure 3-2), while the other begins by e^- transfer (Figure

3). The gas phase H_2O elimination, from the oxidized H-cluster, proceeds endergonically in both pathways (Figure 3-2 and 3-3).

3.6. Frontier Molecular Orbital Analysis

Electronic contributions are now presented for both phases, which are adduced by the frontier molecular orbitals in conjunction with the previously presented free energies.

Upon reduction of open-shell H-clusters, it is observed that an e^- is obtained by a semi-occupied molecular orbital (SOMO), while the closed-shell clusters receive an e^- into the lowest virtual molecular orbital (LUMO). However, when a H^+ is in the proximity of an open-shell H-cluster, it can form a σ-bond probably through the interaction of the e^- in the highest occupied molecular orbital (HOMO), or through the contributions of both HOMO and SOMO, with the proviso that the SOMO is sufficiently low in energy relative to HOMO. Alternatively, when a H^+ is near a closed-shell cluster, the σ-bond probably ensues mainly due to the contribution of e^-s from HOMO with the H^+.

Gas phase thermodynamic properties, of the reactions in Figures 3-1a, 3-1b, 3-2, and 3-3, are being examined with regard to frontier molecular orbitals (FMO). Thus, in **2** the LUMO (Figure 3-4) is mostly localized on the exogenous O_2 and N3, which is also corroborated by an increase of NBO charges on O_2 and N3 in **3** upon reduction of H-cluster **2** [q^g_{O1} = -0.046 a.u. (**2**) → -0.235 a.u. (**3**); q^g_{N3} = -0.568 a.u. (**2**) → -0.717 a.u. (**3**)].

Aqueous enzyme phase thermodynamic properties are next being examined for the reactions of Figs. 3-1, 3-2, and 3-3 relative to the frontier molecular orbitals (FMO).

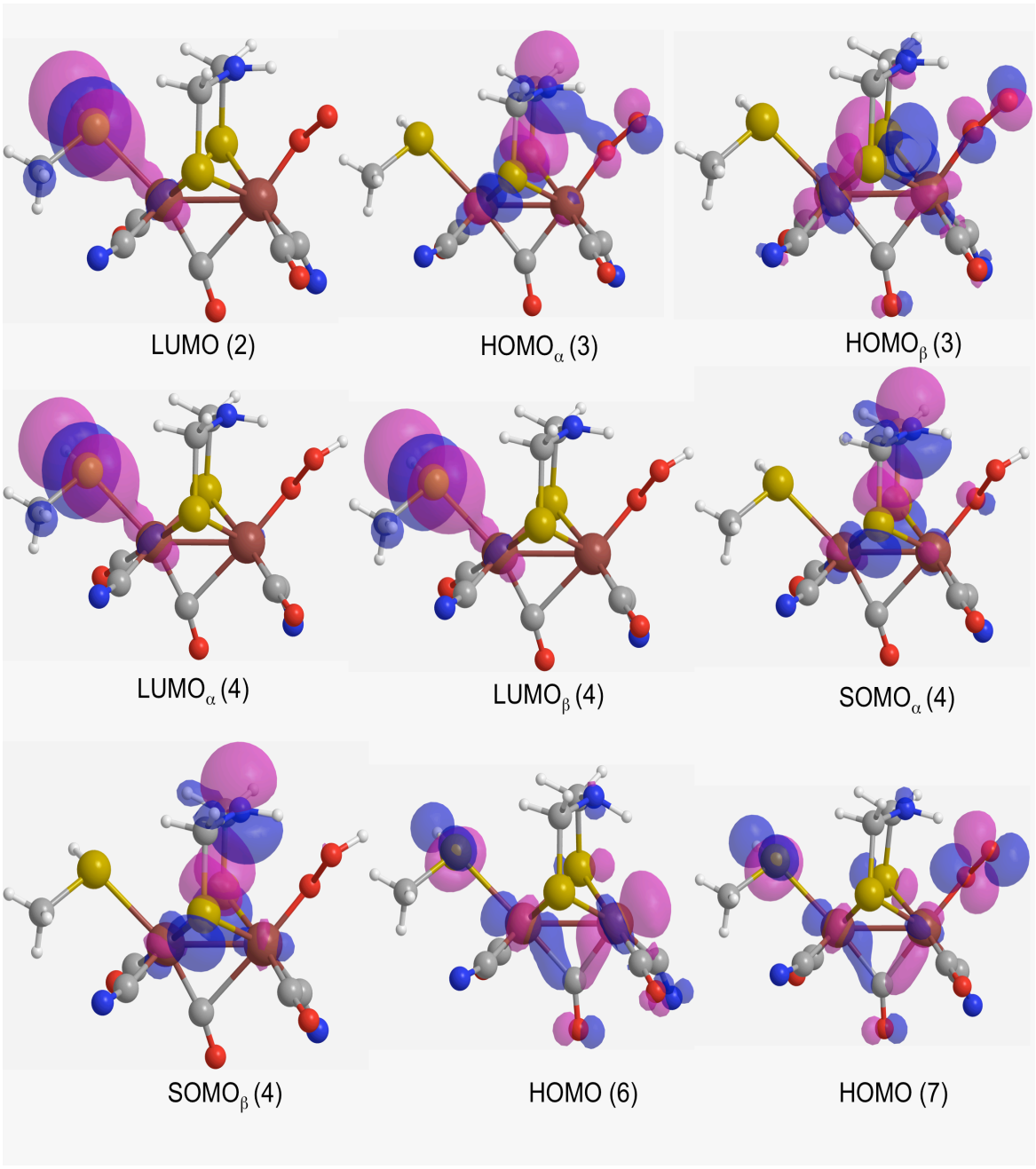

Figure 3-4. Frontier molecular orbitals (aqueous enzyme phase) for H-clusters LUMO (2), HOMO$_\alpha$ (3), HOMO$_\beta$ (3), LUMO$_\alpha$ (4), LUMO$_\beta$ (4), SOMO$_\alpha$ (4), SOMO$_\beta$ (4), HOMO (6), and HOMO (7).

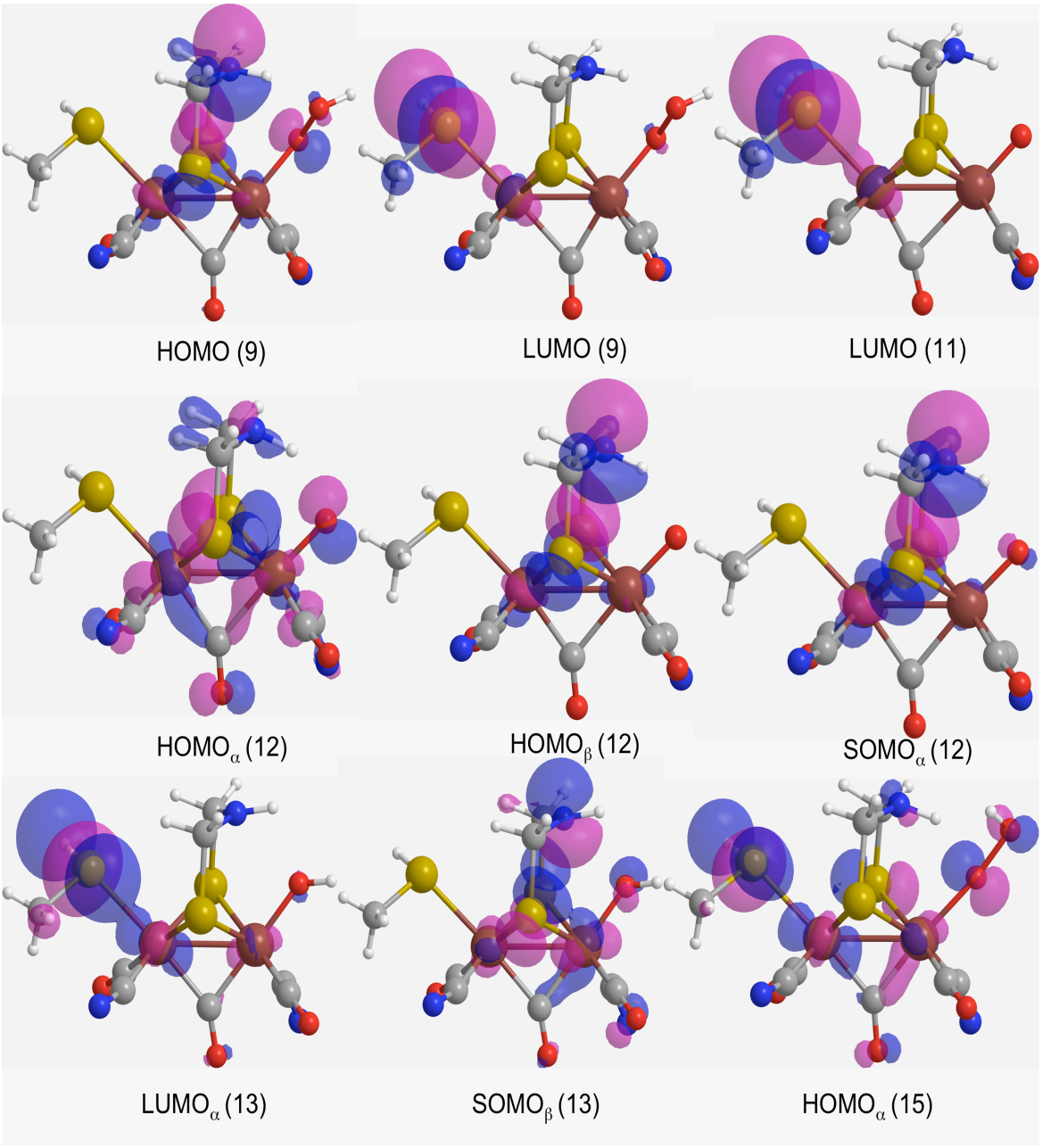

Figure 3-5. Frontier molecular orbitals (aqueous enzyme phase) for H-clusters HOMO (9), LUMO (9), LUMO (11), HOMO$_\alpha$ (12), HOMO$_\beta$ (12), SOMO$_\alpha$ (12), LUMO$_\alpha$ (13), SOMO$_\beta$ (13), and HOMO$_\alpha$ (15).

For **2**, LUMO [Figure 3-4, (compare gas phase)] is mostly localized on Sγ of Cys^{382} (as opposed to cluster **2** in gas phase) owing to the electronic contribution of the proximal cubane. Additionally, the localization of LUMO is supported by a decrease of NBO charge on Sγ in **3** upon reduction of H-cluster **2** [$q^{e}_{S\gamma}$ = 0.471 a.u. (**2**) → 0.388 a.u. (**3**)].

For open-shell clusters, unrestricted B3LYP calculations have been performed which resulted in different quantum mechanical (QM) energies and molecular orbital (MO) coefficients for α and β electrons.

In gas phase, the $HOMO_{\alpha}$ (the lower energy HOMO containing a spin up e^{-}) of **3** is predominantly localized on the exogenous O_2, where the protonation also occurs. However, the $HOMO_{\beta}$ (the higher energy HOMO with its spin down e^{-}) is localized on the DTMA bridge (Chapter II).

For the aqueous enzyme phase, the $HOMO_{\alpha}$ of **3** is less localized on the exogenous O_2 (relative to the gas phase situation), but this orbital is essentially localized on the DTMA bridge.

The $HOMO_{\beta}$, relative to the gas phase electronic distribution, is more localized on the exogenous O_2 (Figure 3-4), supporting the greater spontaneity of H^{+} transfer (**3** → **4**).

The $SOMO_{\alpha}$ of compound **4**, in gas phase, is mostly localized on the DTMA bridge, and, to some extent, on the exogenous O_2 and the Fe atoms (Figure 4). $SOMO_{\beta}$ is more delocalized than $SOMO_{\alpha}$. Following the e^{-} transfer **4** → **9**, the main change in partial charges occurs on the iron atoms [q^{g}_{Fep} = -0.141 a.u. (**4**) → -0.003 a.u. (**9**); q^{g}_{Fed} = 0.464 a.u. (**4**) → 0.025 a.u. (**9**)]. The change in NBO charges in **4** → **9** can be corroborated by $LUMO_{\alpha}$. It is noteworthy that the e^{-} is transferred into the $LUMO_{\alpha}$ (-0.15381 Hartrees), for its energy is lower than that of $SOMO_{\beta}$ (-0.14425 Hartrees). For

the hydrogenase, $LUMO_{\alpha}$ (4, Figure 3-4) is also lower in energy than $SOMO_{\beta}$ (4, Figure 3-4) ($E_{LUMO\alpha}^{Enzyme}$ = -0.35944 Hartrees, $E_{SOMO\beta}^{Enzyme}$ = -0.35907 Hartrees), implying that the e^- is transferred to and localized on S_{γ} of Cys^{382}. However, this difference in electron localization is not reflected in the reaction thermodynamics, because 4 → 9 is similarily exergonic in both phases.

The HOMO of 6, in gas phase, is localized on the Fe_d and the CO_b, whereas the HOMO of 7 is primarily localized on the exogenous O_2 but is less diffused over CO_b (Chapter II). The proton binds with high affinity to Fe_d of H-clusters 6 (Path IV) and 7 (Path III) because the HOMO orbitals of these clusters are localized on Fe_d and exogenous O_2, respectively. In particular, 7 manifestly displays where protonation occurs, viz., on the exogenous O_2 (Figure 3-1b).

In aqueous enzyme phase, similar electron orbital distributions are encountered for clusters 6 (Path IV) and 7 (Path III), except that S_{γ} (of Cys^{382}) incurs MO distributions, which may be sustained by the proximal cubane (that facilitates the e^- transfer).

The HOMO of 9', is delocalized throughout the cluster and, has smaller proton affinity in comparison to 6 and 7. However, higher HOMO 9' amplitude is found on the exogenous O1, DTMA bridge, and the two irons which may explain why the N3 is being protonated in this case.

For cluster 11, the LUMO is more localized over the Fe_p than on Fe_d, extending from the irons towards the CO_b via a linear combination between the e_g orbitals of the iron atoms with the CO_b π orbitals[9], thus the e^- transfer, 11 → 12, changes the oxidation state of Fe_p. However, for ONIOM, the LUMO is localized on S_{γ} which is being bereft of

e⁻s via an inductive effect of the vicinal cubanes [$q^e_{S\gamma}$ = 0.464 a.u. (11) vs. 0.333 a.u. (12)].

Both $HOMO_\alpha$ and $HOMO_\beta$, of 12, are generally localized on the Fe_p (Figure 5). However, in this case, the protonation does not occur at the Fe_d, instead it occurs at the exogenous O1 since its NBO charge is very negative, i.e., q^g_{O1} = -0.594 a.u. as opposed to q^g_{Fed} = 0.126 a.u. On the other hand, for the aqueous enzyme phase, both $HOMO_\alpha$ and $HOMO_\beta$, of 12, differ in their distribution, especially $HOMO_\alpha$ having orbital amplitude on the exogenous oxygen, making it a good H^+ acceptor.

Cluster 13 is an open-shell cluster, so upon its reduction an e^- may either enter a $LUMO_\alpha$, or a $SOMO_\beta$ depending on their relative orbital energies. In the reductive process of H-cluster 13 (for gas phase), the in silico data explicitly shows that the orbital energy of $LUMO_\alpha$ ($E_{LUMO\alpha}^{gas}$ = -0.14850 Hartrees) is lower than the energy of $SOMO_\beta$ ($E_{SOMO\beta}^{gas}$ = -0.13886 Hartrees). Nevertheless, these energies are almost identical in the aqueous enzyme phase ($E_{LUMO\alpha}^{enzyme}$ = -0.35177 Hartrees, $E_{SOMO\beta}^{enzyme}$ = -0.35185 Hartrees). Thus, upon reduction of cluster 13, the e^- could enter into $LUMO_\alpha$ (Figures 5 and 7 of both phases). Upon analysis of the NBO charges of clusters 13 and 14, the OH^- and Fe_d of 14 acquire most of the partial charge ceded by Fe_p during the reductive process 13 → 14.

Finally, in gas phase H-cluster 15 undergoes a protonation reaction on N3, which is substantiated by the NBO negative charge decrease, for both phases, on N3 [q^g_{N3} = -0.267 a.u. (15) → -0.187 a.u. (16)], while in protein environment the exogenous O_2 is protonated [q^e_{O2} = -0.510 a.u. (15) → -1.024 a.u. (16)].

In conclusion, several possible pathways have been investigated for the oxidation of [Fe-Fe]-hydrogenase H-cluster, and they all proceed spontaneously to cluster, **9**. Each pathway is initiated by an intermediate (**1**, **5**, **6**, and **8**) of the catalytic cycles in H_2 metabolism.

In gas phase, O_2 binding is endergonic for the fully oxidized H-cluster **1** and exergonic for **8**; however, it is exergonic for the partially oxidized **5** and reduced **6** clusters. But for aqueous enzyme phase, the O_2 binding is exergonic for all oxidation states. This suggests that the fully oxidized state of the H-cluster **1** in enzyme environment is more sensitive to O_2 inhibition.

Our calculations show that in the protein environment (Figure 3-2, and 3-3) the hydroxylated H-cluster **14**, which is the end product of hydrogenase inhibition, is obtained from **9** via the fully exergonic reaction pathway that starts by means of protonation (Figure 3-2). Antithetically, the reaction pathway that is initiated by means of reduction (Figure 3-3, aqueous enzyme phase) does not proceed to the hydroxylated H-cluster 14 due to this very endergonic step ($\Delta G_{QM/MM}$ = +25.6 kcal/mol).

The inhibitory steps in gas phase (Figure 3-2, and 3-3) consist of water removal from a closed shell, **10**, and an open shell, **16**, H-cluster (ΔG_{gas} = +3.3 and +1.3 kcal/mol, respectively), while in the aqueous enzyme phase there is one inhibitory step, i.e., an e^- transfer from an open shell H-cluster (**9'**, $\Delta G_{QM/MM}$ = +25.6 kcal/mol).

From gas phase geometrical analysis CO_b shows a displacement away from Fe_p^{II} (**9** → **9'**), but in the aqueous enzyme phase this CO_b translocation is not observed; the observed different phase behavior in the protein environment may be due to the imposed immobility on the iron atoms (by means of "freezing" them).

For the gas phase, cluster **11**, LUMO is more localized over the Fe_p than on Fe_d, extending from the iron atoms towards the CO_b via a linear combination between the e_g orbitals of the iron atoms with the CO_b π orbitals[9], thus the e^- transfer, **11** → **12**, changes the oxidation state of Fe_p. However, for the protein environment, the LUMO is localized on S_γ which is being bereft of e^-s via an inductive effect of the vicinal cubanes [$q^e_{S\gamma}$ = 0.464 a.u. (**11**) vs. 0.333 a.u. (**12**)].

Lastly, an interesting result from the FMO gas phase analysis is that an e^- is transferred to a virtual α orbital rather than to the virtual β orbital. We also found that O_2 inhibited [Fe-Fe]-hydrogenase H-cluster has OH^- bonded to the Fe_d, and that OH^- is the end product of O_2 metabolism, with all aqueous enzyme phase reaction pathways proceeding exergonically.

References

(1) Das, D.; Dutta, T.; Nath, K.; Kotay, S. M.; Das, A. K.; Veziroglu, T. N. *Curr. Sci.* **2006**, *90*, 1627.

(2) Liu, Z.-P.; Hu, P. *J. Am. Chem. Soc.* **2002**, *124*, 5175.

(3) Vignais, P. M.; Billoud, B.; Meyer, J. *FEMS Microbiol. Rev.* **2001**, *25*, 455–501.

(4) Melis, A.; Zhang, L.; Forestier, M.; Ghirardi, M. L.; Seibert, M. *Plant Physiol.* **2000**, *122*, 127.

(5) Albracht, S. P. J. *Biochim. Biophys. Acta* **1994**, *1118*, 167.

(6) Adams, M. W. W. *Biochim. Biophys. Acta* **1990**, *1020*, 115.

(7) Adams, M. W. W.; Stiefel, E. I. *Science* **1998**, *282*, 1842.

(8) Happe, R. P.; Roseboom, W.; Pierik, A. J.; Albracht, S. P.; Bagley, K. A. *Nature* **1997**, *385*, 126.

(9) Liu, Z.-P.; Hu, P. *J. Chem. Phys.* **2002**, *117*, 8177.

(10) Bruschi, M.; Fantucci, P.; De Gioia, L. *Inorg. Chem.* **2002**, *41*, 1421.

(11) Bruschi, M.; Fantucci, P.; De Gioia, L. *Inorg. Chem.* **2003**, *42*, 4773.

(12) Bruschi, M.; Fantucci, P.; De Gioia, L. *Inorg. Chem.* **2004**, *43*, 3733.

(13) Zampella, G.; Bruschi, M.; Fantucci, P.; Razavet, M.; Pickett, C. J.; De Gioia, L. *Chem. Eur. J.* **2005**, *11*, 509.

(14) Cao, Z.; Hall, M. B. *J. Am. Chem. Soc.* **2001**, *123*, 3734.

(15) Fan, H.-J.; Hall, M. B. *J. Am. Chem. Soc.* **2001**, *123*, 3828.

(16) Greco, C.; Bruschi, M.; De Gioia, L.; Ryde, U. *Inorg. Chem.* **2007**, *46*, 5911.

(17) Trohalaki, S.; Pachter, R. *ENERG. FUEL.* **2007**, *21*, 2278.

(18) Greco, C.; Bruschi, M.; Heimdal, J.; Fantucci, P.; De Gioia, L.; Ryde, U. *Inorg. Chem.* **2007**, *46*, 7256.

(19) Greco, C.; Bruschi, M.; Fantucci, P.; De Gioia, L. *Eur. J. Inorg. Chem.* **2007**, *13*, 1835.

(20) Greco, C.; Zampella, G.; Bertini, L.; Bruschi, M.; Fantucci, P.; De Gioia, L. *Inorg. Chem.* **2007**, *46*, 108.

(21) Motiu, S.; Dogaru, D.; Gogonea, V. *Int. J. Quantum Chem.* **2007**, *107*, 1248.

(22) Bruschi, M.; Zampella, G.; Fantucci, P.; De Gioia, L. *Coord. Chem. Rev.* **2005**, *15-16*, 1620.

(23) Liu, X.; Ibrahim, S. K.; Tard, C.; Pickett, C. J. *Coord. Chem. Rev.* **2005**, *15-16*, 1641.

(24) Armstrong, F. A. *Curr. Opin. Chem. Biol.* **2004**, *8*, 133.

(25) Rauchfuss, T. B. *Inorg. Chem.* **2004**, *43*, 14.

(26) Evans, D. J.; Pickett, C. J. *Chem. Soc. Rev.* **2003**, *35*, 268.

(27) Chen, Z.; Lemon, B. J.; Huang, S.; Swartz, D. J.; Peters, J. W.; Bagley, K. A. *Biochemistry* **2002**, *41*, 2036.

(28) Horner, D. S.; Heil, B.; Happe, T.; Embley, T. M. *Trends Biochem. Sci.* **2002**, *27*, 148.

(29) Nicolet, Y.; Cavazza, C.; Fontecilla-Camps, J. C. *J. Inorg. Biochem.* **2002**, 1.

(30) Lyon, E. J.; Georgakaki, I. P.; Reibenspies, J. H.; Darensbourg, M. Y. *Angew. Chem., Int. Ed.* **1999**, *38*, 3178.

(31) Nicolet, Y.; Piras, C.; Legrand, P.; Hatchikian, E. C.; Fontecilla-Camps, J. C. *Structure* **1999**, *7*, 13.

(32) Cloirec, A. L.; Best, S. P.; Borg, S.; Davies, S. C.; Evans, D. J.; Hughes, D. L.; Pickett, C. J. *Chem. Commun.* **1999**, 2285.

(33) Rauchfuss, T. B.; Contakes, S. M.; Schmidt, M. *J. Am. Chem. Soc.* **1999**, *121*, 9736.

(34) Lai, C.-H.; Lee, W.-Z.; Miller, M. L.; Reibenspies, J. H.; Darensbourg, D. J.; Darensbourg, M. Y. *J. Am. Chem. Soc.* **1998**, *120*, 10103.

(35) Pierik, A. J.; Hulstein, M.; Hagen, W. R.; Albracht, S. P. *Eur. J. Biochem.* **1998**, *258*, 572.

(36) Pierik, A. J.; Hagen, W. R.; Redeker, J. S.; Wolbert, R. B. G.; Boersma, M.; Verhagen, M. F.; Grande, H. J.; Veeger, C.; Mustsaers, P. H. A.; Sand, R. H.; Dunham, W. R. *Eur. J. Biochem.* **1992**, *209*, 63.

(37) Zambrano, I. C.; Kowal, A. T.; Mortenson, L. E.; Adams, M. W. W.; Johnson, M. K. *J. Biol. Chem.* **1989**, *264*, 20974.

(38) Patil, D. S.; Moura, J. J. G.; He, S. H.; Teixeira, M.; Prickril, B. C.; Der Vartanian, D. V.; Peck, H. D., Jr.; Legall, J.; Huynh, B. H. *J. Biol. Chem.* **1988**, *263*, 18732.

(39) Rusnak, F. M.; Adams, M. W. W.; Mortenson, L. E.; Munck, E. *J. Biol. Chem.* **1987**, *262*, 38.

(40) Adams, M. W. W. *J. Biol. Chem.* **1987**, *262*, 15054.

(41) Adams, M. W. W.; Mortenson, L. E. *J. Biol. Chem.* **1984**, *259*, 7045.

(42) Roseboom, W.; De Lacey, A. L.; Fernandez, V. M.; Hatchikian, E. C.; Albracht, S. P. J. *J. Biol. Inorg. Chem.* **2006**, *11*, 102.

(43) Peters, J. W.; Lanzilotta, W. N.; Lemon, B. J.; Seefeldt, L. C. *Science* **1998**, *282*, 1853.

(44) Tye, J. W.; Darensbourg, M. Y.; Hall, M. B. *J. Mol. Struct. (Theochem)* **2006**, *771*, 123.

(45) Eilers, G.; Schwartz, L.; Stein, M.; Zampella, G.; Gioia, L. d.; Ott, S.; Lomoth, R. *Chem. Eur. J.* **2007**, *13*, 7075.

(46) Tye, J. W.; Darensbourg, M. Y.; Hall, M. B. *Inorg. Chem.* **2008**, *47*, 2380.

(47) Felton, G. A. N.; Vannucci, A. K.; Chen, J.; L. Tori Lockett; Okumura, N.; Petro, B. J.; Zakai, U. I.; Evans, D. H.; Glass, R. S.; Lichtenberger, D. L. *J. Am. Chem. Soc.* **2007**, *129*, 12521.

(48) Siegbahn, P. E. M.; Tye, J. W.; Hall, M. B. *Chem. Rev.* **2007**, *107*, 4414.

(49) Borg, S. J.; Tye, J. W.; Hall, M. B.; Best, S. P. *Inorg. Chem.* **2007**, *46*, 384.

(50) Zilberman, S.; Stiefel, E. I.; Cohen, M. H.; Car, R. *Inorg. Chem.* **2007**, *46*, 1153.

(51) Woodward, J.; Cordray, K. A.; Edmonston, R. J.; Blanco-Rivera, M.; Mattingly, S. M.; Evans, B. R. *Energy Fuels* **2000**, *14*, 197.

(52) Wolpher, H.; Borgstrom, M.; Hammarstrom, L.; Bergquist, J.; Sundstrom, V.; Stenbjorn, S.; Sun, L. C.; Akermark, B. *Inorg. Chem. Commun.* **2003**, *6*, 989.

(53) Winter, A.; Zsolnai, L.; Huttner, G. Z. *Naturforsch., B: Chem. Sci.* **1982**, *37B*, 1430.

(54) Windhager, J.; Rudolph, M.; Brautigan, S.; Gorls, H.; Weigand, W. *Eur. J. Inorg. Chem.* **2007**, *18*, 2748.

(55) Wang, Z.; Liu, J.; He, C.; Jiang, S.; Akermark, B.; Sun, L. *Inorg. Chim. Acta.* **2007**, *360*, 2411.

(56) Jiang, S.; Liu, J.; Shi, Y.; Wang, Z.; Akermark, B.; Sun, L. *Polyhedron* **2007**, *26*, 1499.

(57) Tsuda, M.; Dino, W. A.; Kasai, H. *Solid State Commun.* **2005**, *133*, 589.

(58) Treichel, P. M.; Rublein, E. K. J. *Organomet. Chem.* **1989**, *359*, 195.

(59) Tard, C.; Liu, X. M.; Ibrahim, S. K.; Bruschi, M.; De Gioia, L.; Davies, S. C.; Yang, X.; Wang, L. S.; Sawers, G.; Pickett, C. J. *Nature* **2005**, *433*, 610.

(60) Sun, L.; Akermark, B.; Ott, S. *Coord. Chem. Rev.* **2005**, *249*, 1653.

(61) van der Vlugt, J. I.; Rauchfuss, T. B.; Wilson, S. R. *Chem. Eur. J.* **2006**, *12*, 90.

(62) Song, L.-C.; Ge, J.-H.; Zhang, X.-G.; Liu, Y.; Hu, Q.-M. *Eur. J. Inorg. Chem.* **2006**, 3204.

(63) Song, L. C.; Yang, Z. Y.; Hua, Y. J.; Wang, H. T.; Liu, Y.; Hu, Q. M. *Organometallics* **2007**, *26*, 2106.

(64) Smith, M. C.; Barclay, J. E.; Davies, S. C.; Hughes, D. L.; Evans, D. J. *Dalton Trans.* **2003**, 4147.

(65) Seyferth, D.; Womack, G. B.; Gallagher, M. K.; Cowie, M.; Hames, B. W.; Fackler, J. P., Jr.; Mazany, A. M. *Organometallics* **1987**, *6*, 283.

(66) Seyferth, D.; Henderson, R. S.; Song, L. C. *Organometallics* **1982**, *1*, 125.

(67) Schwartz, L.; Ekstrom, J.; Lomoth, R.; Ott, S. *Chem. Commun.* **2006**, 4206.

(68) Ott, S.; Kritikos, M.; Akermark, B.; Sun, L.; Lomoth, R. *Angew. Chem., Int. Ed.* **2004**, *43*, 1006.

(69) Ott, S.; Borgstrom, M.; Kritikos, M.; Lomoth, R.; Bergquist, J.; Akermark, B.; Hammarstrom, L.; Sun, L. C. *Inorg. Chem.* **2004**, *43*, 4683.

(70) Nandi, R.; Sengupta, S. *Crit. Rev. Microbiol.* **1998**, *24*, 61.

(71) Morvan, D.; Capon, J. F.; Gloaguen, F.; Le Goff, A.; Marchive, M.; Michand, F.; Schollhammer, P.; Talarmin, J.; Yaouanc, J. J. *Organometallics* **2007**, *26*, 2042.

(72) Morozov, S. V.; Karyakina, E. E.; Zorin, N. A.; Varfolomeyev, S. D.; Cosnier, S.; Karyakin, A. A. *Bioelectrochemistry* **2002**, *55*, 169.

(73) Mejia-Rodriguez, R.; Chong, D.; Reibenspies, J. H.; Soriaga, M. P.; Darensbourg, M. Y. *J. Am. Chem. Soc.* **2004**, *126*, 12004-12014.

(74) Liaw, W. F.; Lee, J. H.; Gau, H. B.; Chen, C. H.; Jung, S. J.; Hung, C. H.; Chen, W. Y.; Hu, C. H.; Lee, G. H. *J. Am. Chem. Soc.* **2002**, *124*, 1680.

(75) Li, P.; Wang, M.; He, C.; Li, G.; Liu, X.; Chen, C.; Akermark, B.; Sun, L., . *Eur. J. Inorg. Chem.* **2005**, 2506.

(76) Lamle, S. E.; Halliwell, L. M.; Armstrong, F. A.; Albracht, S. P. J. *Inorg. Biochem.* **2003**, *96*, 174.

(77) Karyakin, A. A.; Morozov, S. V.; Karyakina, E. E.; Zorin, N. A.; Perelygin, V. V.; Cosnier, S. *Biochem. Soc. Trans*. **2005**, *33*, 73.

(78) Karyakin, A. A.; Morozov, S. V.; Karyakina, E. E.; Varfolomeyev, S. D.; Zorin, N. A.; Cosnier, S. *Electrochem. Commun.* **2002**, *4*, 417.

(79) Jiang, S.; Liu, J.; Shi, Y.; Wang, Z.; Akermark, B.; Sun, L. *Dalton Trans.* **2007**, 896.

(80) Homann, P. H. *Photosynth. Res.* **2003**, *76*, 93.

(81) Hieber, W.; Spacu, P. Z. Z. *Anorg. Allg. Chem.* **1937**, *233*, 353

(82) Duan, L.; Wang, M.; Li, P.; Na, Y.; Wang, N.; Sun, L. *Dalton Trans.* **2007**, 1277.

(83) Gloaguen, F.; Lawrence, J. D.; Schmidt, M.; Wilson, S. R.; Rauchfuss, T. B. *J. Am. Chem. Soc.* **2001**, *123*, 12518.

(84) Rappe, A. K.; Casewit, C. J.; Colwell, K. S.; Goddard, W. A., III.; Skiff, W. M. *J. Am. Chem. Soc.* **1992**, *113*, 10024.

(85) Dapprich, S.; Komaromi, I.; Byun, K. S.; Morokuma, K.; Frisch, M. J. *J. Mol. Struct. (Theochem)* **1999**, *1*, 461.

(86) Frisch, M. J.; Trucks, G. W.; Schlegel, H. B.; Scuseria, G. E.; Robb, M. A.; Cheeseman, J. R.; Montgomery, J., J. A.; Vreven, T.; Kudin, K. N.; Burant, J. C.; Millam, J. M.; Iyengar, S. S.; Tomasi, J.; Barone, V.; Mennucci, B.; Cossi, M.; Scalmani, G.; Rega, N.; Petersson, G. A.; Nakatsuji, H.; Hada, M.; Ehara, M.; Toyota, K.; Fukuda, R.; Hasegawa, J.; Ishida, M.; Nakajima, T.; Honda, Y.; Kitao, O.; Nakai, H.; Klene, M. L., X.; Knox, J. E.; Hratchian, H. P.; Cross, J. B.; Bakken, V.; Adamo, C.; Jaramillo, J.; Gomperts, R.; Stratmann, R. E.; Yazyev, O.; Austin, A. J.; Cammi, R.; Pomelli, C.; Ochterski, J. W.; Ayala, P. Y.; Morokuma, K.; Voth, G. A.; Salvador, P.; Dannenberg, J. J.; Zakrzewski, V. G.; Dapprich, S. D., A. D.; Strain, M. C.; Farkas, O.; Malick, D. K.; Rabuck, A. D.; Raghavachari, K.; Foresman, J. B.; Ortiz, J. V.; Cui, Q.; Baboul, A. G.; Clifford, S.; Cioslowski, J.; Stefanov, B. B.; Liu, G.; Liashenko, A.; Piskorz, P.; Komaromi, I.; Martin, R. L.; Fox, D. J.; Keith, T.; Al-Laham, M. A.; Peng, C. Y.; Nanayakkara, A.; Challacombe, M.; Gill, P. M. W.; Johnson, B.; Chen, W.; Wong, M. W.; Gonzalez, C.; Pople, J. A. Gaussian 03, Revision C.02; Gaussian, Inc.: Wallingford CT, 2004.

(87) Becke, A. D. *J. Chem. Phys.* **1993**, *98*, 5648.

(88) Lee, C.; Yang, W.; Parr, R. G. *Phys. Rev. B* **1988**, *37*, 785.

(89) Hay, P. J.; Wadt, W. R. *J. Chem. Phys.* **1985**, *82*, 270.

(90) Wadt, W. R.; Hay, P. J. *J. Chem. Phys.* **1985**, *82*, 284.

(91) Berendsen, H. J. C.; van der Spoel, D. *Comp. Phys. Comm.* **1995**, *91*, 43.

(92) Lindahl, E.; Hess, B. *J. Mol. Mod.* **2001**, *7*, 306.

(93) Popescu, C. V.; Munck, E. *J. Am. Chem. Soc.* **1999**, *121*, 7877.

(94) Rappe, A. K.; Goddard, W. A., III. *J. Phys. Chem.* **1991**, *95*, 3358.

(95) Peters, J. W. *Curr. Opin. Struct. Biol.* **1999**, *9*, 670.

(96) George, S. J.; Kurkin, S.; Thorneley, R. N. F.; Albracht, S. P. J. *Biochemistry* **2004**, *43*, 6808.

CHAPTER IV

RESIDUE MUTATED [FE-FE]-HYDROGENASE IMPEDES O_2 BINDING: A QM/MM INVESTIGATION

4.1. General Considerations

[Fe-Fe]-hydrogenases are enzymes that catalyze the reversible reduction of protons to hydrogen ($2H^+ + 2e^- \rightleftarrows H_2$) in anaerobic media[2,3], and are considered one of the oldest enzymes in nature[4].The eventual elucidation of the catalytic mechanism of hydrogen synthesis may avail researches produce clean hydrogen fuel, using certain prokaryotes and eukaryotes[5-50].

The hydrogenase H-cluster (Figure 2-1) is the active site and is comprised of two iron atoms (Fe_p-Fe_d, i.e., proximal and distal iron). The di-iron atoms are coordinated by endogenous ligands, i.e., two cyanides, two terminal carbonyls, and a bridging carbonyl

(CO_b). Also, 1,3-di(thiomethyl)amine (DTMA) and propanedithiolate (PDT) are considered potential bidentate ligands of the di-iron subcluster[51-53].

A cubane cluster, [4Fe-4S] (which also belongs to the H-cluster), is bonded to S_γ of Cys^{382}, while the former (S_γ) is bound to Fe_p of the H-cluster.

Previous Density Functional Theory (DFT) as well as hybrid quantum mechanics/molecular mechanics (QM/MM) calculations[2,54-62] have been successful in clarifying some aspects of the catalytic properties of the H-cluster. As in similar computational studies[2,55], CH_3-S is substituted for cysteine, and a H^+ is exchanged for the proximal cubane. Furthermore, computational and experimental[1,2,51,53,55,60,62-88] [Fe-Fe]-hydrogenase H-cluster (and synthetic H-cluster-like compounds) research sheds light on the mechanism and the potential redox states of the [Fe-Fe]-hydrogenase H-cluster subunit, Fe_p-Fe_d; Fe_p^{I}-Fe_d^{I} is the reduced hydrogenase H-cluster subunit, Fe_p^{II}-Fe_d^{I} is the partially oxidized enzyme subunit, and Fe_p^{II}-Fe_d^{II} is the fully oxidized, inactive enzyme H-cluster subunit.

The oxidized H-cluster, Fe_p^{II}-Fe_d^{II}, has a OOH^-, H_2O molecule or an OH^- bound to the Fe_d^{II}[1,55]. In our previous investigation[67], we have inferred that a vacant Fe_p^{II}-Fe_d^{II} could also be a viable intermediate in H_2 synthesis. Regardless of [Fe-Fe]-hydrogenase H-cluster subunit redox states, the proximal cubane always retains a 2+ oxidation state, $[Fe_4S_4]^{2+}$. The partially oxidized H-cluster (containing Fe_p^{II}-Fe_d^{I}), H_{ox}, is also the active species of the hydrogenase enzyme. According to Liu and Hu[55], Fe_p^{I}-Fe_d^{I} is also the cluster having a tendency for protonation, when a proton is captured from the side chain of a near by amino acid, such as Lys^{237}.

Hydrogenase X-ray crystallography and spectroscopic studies, with the latter having been obtained from *Clostridium pasteurianum* (CP)[52] and *Desulfovibrio desulfuricans* (Dd)[53], led to a more detailed understanding of the biochemical role of these enzymes.

The X-ray crystal structure of CPI hydrogenase shows an oxygen species that may be OH^-, or H_2O bound to Fe_d of the H-cluster. However, based on computational results of Tye et al.[1], and according to X-ray crystal structure, CPI has OOH^- in its inactive form. Hence, we attempt to ascertain if oxygen binding to distal iron (Fe_d-O_2) can be hindered by residue mutations within the surrounding apoprotein of the catalytic site.

The current investigation is comprised of three parts. (1) Wild-type and residue mutated [Fe-Fe]-hydrogenase thermodynamic analysis for O_2 hindering reactions (from binding to Fe_d) for the three different oxidation states of the di-iron subcluster, viz., Fe_p^{I}-Fe_d^{I}, Fe_p^{II}-Fe_d^{I}, and Fe_p^{II}-Fe_d^{II}. (2) Geometrical analyses that were carried out for significant interatomic distances of Fe_d-O_2 and the extrinsic ligand, O-O, and of CO_b bond distances to the di-iron atoms. The remaining subdivision, (3), is the electronic analysis which discusses the frontier molecular orbitals.

4.2. Methodology

In the current investigation, QM/MM [DFT/UFF[89]] methodologies have been used for [Fe-Fe]-hydrogenase. The ONIOM[90] method (DFT for the QM region, and the universal force field, UFF, for the MM region, implemented in Gaussian03[91]) has been

used to determine the reaction thermodynamics, i.e., ΔG, for the oxygen binding reactions to the [Fe-Fe]-hydrogenase H-cluster (situated within the enzyme matrix).

The electronic structure of H-cluster (except the proximal cubane) is investigated by QM (Gaussian 03) using DFT method (B3LYP functional[92,93]), with 6-31+G(d,p) basis set. In accordance with experimental and in silico data, low spin states (singlet, and doublet) and low oxidation states (I, and II) have been selected for the Fe atoms[2,60].

The Gromacs software program[94,95] was employed to add hydrogen atoms, water, and counter ions to the X-ray crystal structure of DdH [Brookhaven Protein Data Bank (id.1HFE)]. Hydrogen atoms and 1 nm layer of water (2043 H_2O molecules) have been added to the PDB DdH structure. Na cations have been randomly inserted into the solvent to neutralize the negative charges encountered in DdH, e.g., the -2 a.u. found on the cubane/cysteine moieties, or in the H-cluster (when needed)[96]. For both basic and acidic amino acids, charges were assigned by Gromacs algorithm to be at pH 7. ONIOM geometry optimizations have been performed on DdH, with the low layer (MM region) being frozen*, with the exception of the proximal cubane; for the high layer (QM), only the iron atoms, Fe_p-Fe_d, and the N (of the DTMA bridge) have been kept frozen**.

The low layer consists of all metalloenzyme residues as well as its constituent cubanes, i.e., proximal, medial, and distal. The high layer is comprised of 2Fe subunit,

---

*Where "frozen" means that x, y, z atom coordinates are kept fixed to reduce computational time.

** For the fully and partially oxidized vacant di-iron subunits, additional optimizations have been carried out by freezing these atoms: Fe_p-CO_t (where CO_t stands for terminal carbonyl). The extra optimizations have been done because the above mentioned di-iron subunits are more likely to undergo CO_b migration.

(which is a moiety of the H-cluster), and C_β and S_γ (of the bridging Cys^{382}). Two linking hydrogen atoms were added between C_α and C_β of Cys^{382}, and between S_γ and an Fe atom of the proximal cubane.

The charge equilibration method of the UFF was used to describe the electrostatic interactions within the low layer of the system[97]. The DdH partial charges were obtained using the charge equilibration method (QEq), whereas the solvent charges were acquired from literature[97] (q_O = -0.706 a.u. and q_H = 0.353 a.u.).

Residue mutations were carried out within the adjacent apoenzyme environment (to H-cluster) in order to hinder O_2 from binding to the open coordination site (Fe_d) of DdH H-cluster.

Residue mutations are comprised of deletions and substitutions which are performed 8 Å radially outward from Fe_d. In order to screen the thirty polar residues located in the 8 Å apoenzyme layer, individual residue deletions are carried out to ascertain what residue substitutions should be made in order to impede O_2 from bonding to Fe_d.

Residue deletions and substitutions are performed for the three di-iron subcluster oxidation states, viz., Fe_p^{II}-Fe_d^{II}, Fe_p^{II}-Fe_d^{I}, and Fe_p^{I}-Fe_d^{I} of [Fe-Fe]-hydrogenase H-cluster.

4.3. [Fe-Fe]-hydrogenase H-cluster Thermodynamics for O_2 Binding

In Table II, two values are given for the wild-type DdH. The first row presents Gibbs' energies ($\Delta G^c_{QM/MM}$) for the wild-type enzyme with all the charges obtained by means of QEq method for the MM layer, which include the neighboring charges of 2Fe

subunit, viz., over proximal cubane*, MM section of Cys^{382}, C (of the peptide bond) from Gly^{381}, and over N of Val^{383} (all MM charges are provided in the supplementary material). The second wild-type DdH energy values ($\Delta G_{QM/MM}$) have also been calculated [by the same QM/MM method as in the first row calculations], but the neighboring charges of the 2Fe subunit have been deleted.

The deletion of the neighboring charges of the 2Fe subunit is carried out in order to remove the wavefunction distortions. However, the effects of the neighboring charges are investigated because they exist in the studied enzyme.

The difference in the wave function polarization (with or without neighboring charges) is quantified by natural bond orbital charges (NBO, Figure 1a, and 1b). The strongest effect of the MM electric field is on the NBO charges of S_γ of Cys^{382}, and the linking atom (H_L) attached to it.

First, in the presence of the neighboring charges, abnormal NBO charge differences are observed between S_γ and H_L. This charge differences provide highly positive charges on S_γ (ranging from 0.285 to 0.474 a.u.) and highly negative charges on H_L (ranging from -0.443 to -0.262 a.u.), which is essentially due to the negatively charged sulfurs of the proximal cubane. When no neighboring charges are used for MM layer, the charge differences between S_γ and H_L are much smaller [than in the presence of the neighboring charges; (NBO charges of H_L range from 0.219 to 0.288 a.u.; NBO charges of S_γ range from 0.051 to 0.148 a.u.)], for the electronegativity of H is ca. 2.1 and for S is ca. 2.5[98].

---

* Except for the cubane sulfur ($S_{c,d}$) situated diagonally from the cubane Fe, which is bound to cysteinyl sulfur of Cys^{382}.

Table II. Wild-type and Residue Removed DdH - First 14 Amino Acids - Gibbs' Energies for O_2 Binding

Reaction:	**FeII-FeII $+O_2$**	**FeII-FeI $+O_2$**	**FeI-FeI $+O_2$**
Wild-type DdH*	**-16.6**	**-7.9**	**-20.7**
Wild-type DdH	**-10.6**	**+2.6**	**-20.5**
$\Delta Ser^{62}s$**	-9.0	+2.5	-20.4
ΔArg^{111}	-11.2	+2.2	-22.9
ΔTyr^{112}	-10.8	-3.2	-21.1
ΔAsp^{144}	-8.4	+4.6	-20.5
ΔThr^{145}	-11.1	+3.9	-21.5
ΔGlu^{146}	-8.7	+2.7	-21.6
ΔThr^{148}	-10.9	+2.1	-21.2
ΔAsp^{150}	-9.4	+1.9	-22.8
ΔThr^{152}	**-9.2**	**+4.1**	**-18.6**
ΔGlu^{155}	-11.1	+2.2	-21.0
ΔThr^{176}	-10.1	+3.0	-19.6
ΔSer^{177}	-10.8	+4.4	-21.3
ΔGln^{183}	-10.8	+2.9	-19.7
ΔSer^{198}	-10.5	+2.7	-20.3

*Gibbs' energies (kcal/mol) for the wild-type enzyme; the MM layer include the neighboring charges of 2Fe subunit, viz., over proximal cubane (except $S_{c,d}$), MM section of Cys^{382}, C (of the peptide bond) from Gly^{381}, and over N of Val^{383}.

**Residue removed DdH; s = small chain.

Table III. Residue Removed DdH - Next 16 Amino Acids - Gibbs' Energies for O_2 Binding

Reaction:	**FeII-FeII $+O_2$**	**FeII-FeI $+O_2$**	**FeI-FeI $+O_2$**
ΔLys^{201}*	-10.6	+2.5	-20.9
ΔSer^{202}	**-7.9**	**+3.9**	**-17.3**
ΔAsn^{207}	-10.3	+2.6	-21.1
ΔSer^{230}	-10.3	+2.9	-19.8
ΔLys^{237}	-10.0	-2.7	-24.5
ΔLys^{238}	-11.7	+2.2	-21.0
ΔGlu^{240}	-10.7	+3.6	-20.9
ΔThr^{257}	-10.7	-2.9	-20.5
ΔThr^{259}	-11.2	-3.0	-20.7
ΔThr^{260}	-10.5	+2.7	-20.3
ΔSer^{289}	-10.3	-2.9	-20.7
ΔThr^{294}	-10.1	+3.2	-20.1
ΔThr^{299}	-10.5	-2.8	-20.5
ΔGlu^{374}	-10.1	+4.7	-21.5
ΔTyr^{375}	-10.4	+2.7	-20.7
ΔGln^{388}	-10.8	+2.5	-20.4

*Residue removed DdH; the Gibbs' energies are given in kcal/mol.

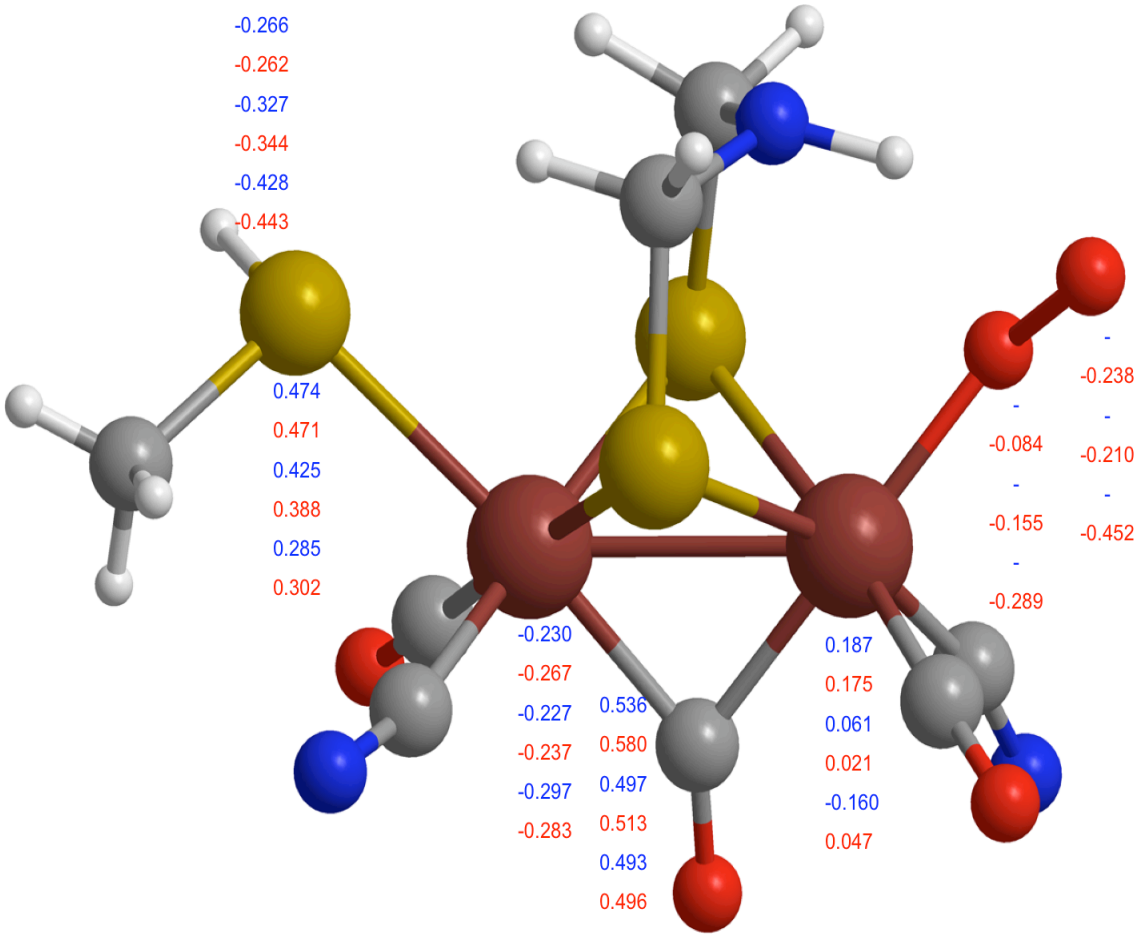

Figure 4-1a. The NBO charges of 2Fe subunit with (MM layer) neighboring charges.

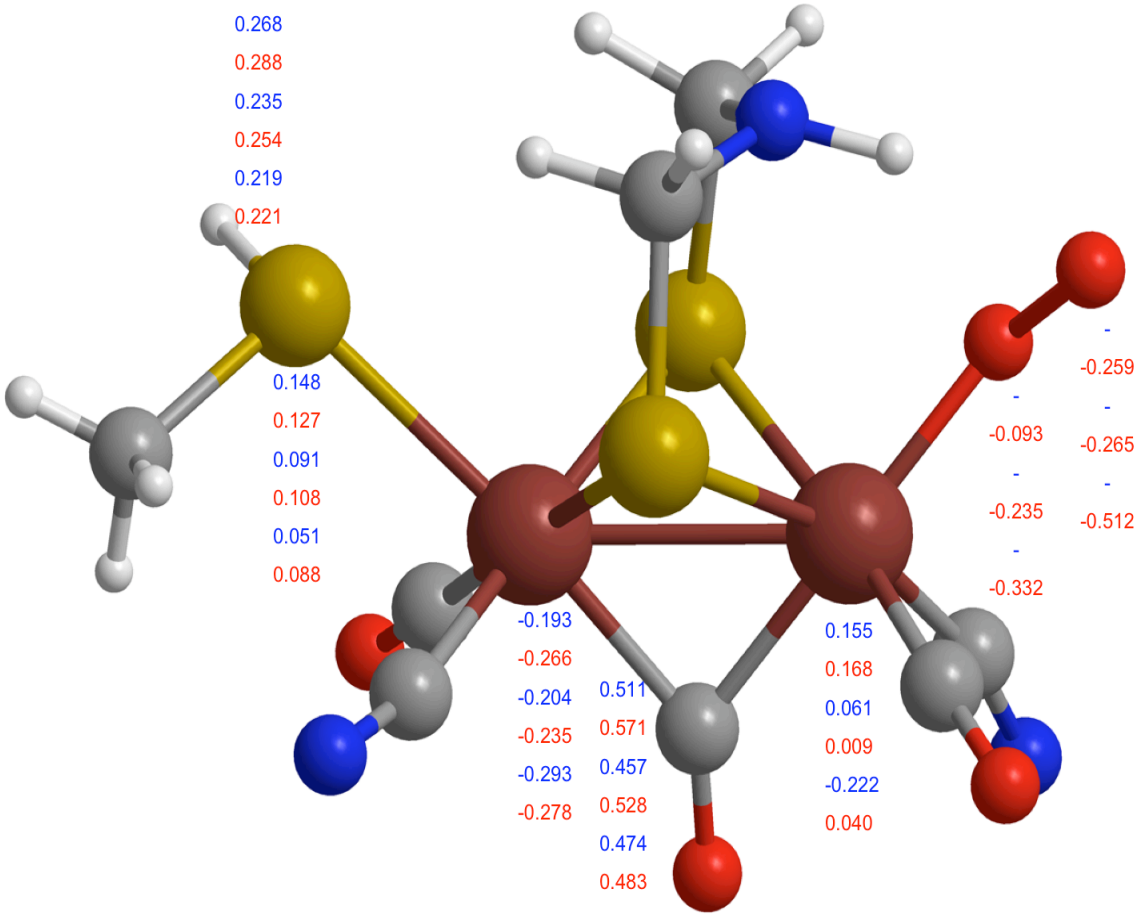

Figure 4-1b. The NBO charges of 2Fe subunit without (MM layer) neighboring charges.

For the Fe atoms of the vacant di-iron subunits, Fe_p^{I}-Fe_d^{I}, Fe_p^{II}-Fe_d^{I}, and Fe_p^{II}-Fe_d^{II}, the following trend is observed. When using neighboring charges, the NBO charges of Fe_p (for all di-iron subunit oxidation states) become more negative. However, the opposite NBO charge trend is observed for Fe_d (with neighboring charges).

On the other hand, for the Fe atoms of the O_2 inactivated di-iron subunits, Fe_p^{I}-Fe_d^{I}, Fe_p^{II}-Fe_d^{I}, and Fe_p^{II}-Fe_d^{II}, a similar trend is observed for NBO charges (as for the vacant di-iron subunits) of both Fe_p and Fe_d, except that NBO charges shift less.

In both cases, with or without neighboring charges, the NBO charges found on the exogenous O_2, of Fe_p^{II}-Fe_d^{II}, remain relatively constant. However, for the Fe_p^{I}-Fe_d^{I}, Fe_p^{II}-Fe_d^{I}, the NBO charges located on the extrinsic O_2, become less negative due to neighboring charge induction, hence hindering O_2 from leaving.

Finally, for both vacant and O_2 inactivated di-iron subunits, the C charges of CO_b remain relatively constant upon utilizing neighboring charges.

Generally, the effect of the neighboring charges on Gibbs' energy (for Fe_p^{I}-Fe_d^{I}, Fe_p^{II}-Fe_d^{I}, and Fe_p^{II}-Fe_d^{II}) is to increase the spontaneity for O_2 binding. However, this effect is rather small for the reduced di-iron subcluster.

Thus, the more realistic approach of O_2 inactivation for the di-iron subunits, is when the MM layer is bereft of neighboring charges, for, as shown in the crystal structure of DdH, Fe_p^{II}-Fe_d^{I} has little propensity for O_2 bonding[53].

In Figure 4-2, O_2 inhibition pathways are presented, in which three different oxidation states, for the examined H-clusters, are studied, i.e., Fe_p^{II}-Fe_d^{II} (1), Fe_p^{II}-Fe_d^{I} (3), and Fe_p^{I}-Fe_d^{I} (5), where (1), (3), and (5), are the cluster identifiers.

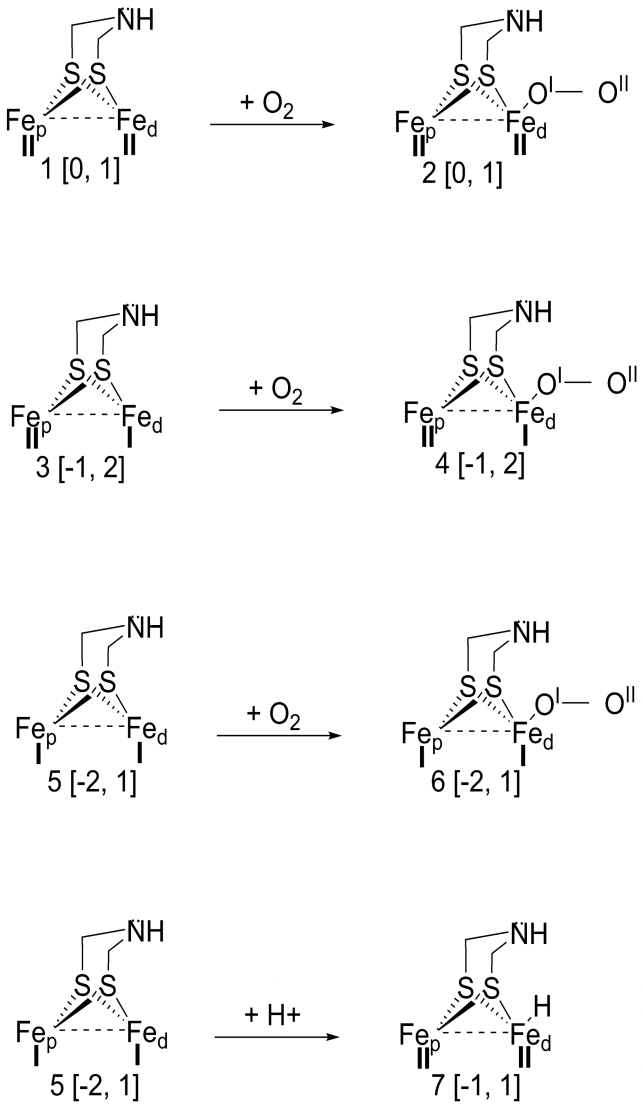

Figure 4-2. Oxidation reactions of O_2 with the fully oxidized (1), partially oxidized (3), and reduced (5) di-iron subunits. Also the protonation with the reduced (5) di-iron subunit is depicted. The charge and multiplicity are provided in square brackets.

In gas phase, the 1st reaction, 1 → 2, is endergonic (ΔG_{gas} = +9.8 kcal/mol; gas = gas phase) when O_2 binds to the fully oxidized H-cluster (1). Hybrid QM/MM calculations in aqueous enzyme phase, on the other hand, show that O_2 binding occurs exergonically ($\Delta G^{c}_{QM/MM}$ = -16.6 kcal/mol; $\Delta G_{QM/MM}$ = -10.6 kcal/mol), reconfirming the affinity of hydrogenases for O_2[99].

In gas phase, the 2nd reaction, 3 → 4, starts with the partially oxidized H-cluster (3), (Fe_p^{II}-Fe_d^{I}), and the bonding of O_2 to Fe_d^{I}, in this case, occurs rather exergonically (ΔG_{gas} = -36.1 kcal/mol) relative to step 1 → 2.

Alternatively, ONIOM results show that O_2 binding occurs spontaneously when neighboring charges are used (Fe_p^{II}-Fe_d^{I}, $\Delta G^{c}_{QM/MM}$ = -7.9 kcal/mol) to the partially oxidized H-cluster, but when the MM layer is deprived neighboring charges, then O_2 is barred from binding to the coordination site ($\Delta G_{QM/MM}$ = +2.6 kcal/mol).

In gas phase, the 3nd reaction, 5 → 6, starts with the reduced H-cluster 5, (Fe_p^{I}-Fe_d^{I}); the process occurs spontaneously (ΔG_{gas} = -36.0 kcal/mol), which is almost identical to the Gibbs' energy of reaction 3 → 4. The gas phase Gibbs' energy similarity (between 5 → 6 and 3 → 4) may result because both loci of oxygen binding (Fe_d^{I}-O_2) are on similar oxidized species, Fe_d^{I}.

However, the hybrid QM/MM calculations 5 → 6 show a small free energy difference between the aqueous enzyme ($\Delta G^{c}_{QM/MM}$ = -20.7 kcal/mol; $\Delta G_{QM/MM}$ = -20.5 kcal/mol) and gas phase results (ΔG_{gas} = -36.0 kcal/mol).

In gas phase, Figure 4-2, the protonation reaction, 5 → 7, is very exergonic (ΔG_{gas} = -220.6 kcal/mol), essentially because the charge on H-cluster 5 is -2 a.u.. ONIOM calculations also show a very high H^+ affinity ($\Delta G^{c}_{QM/MM}$ = -219.2 kcal/mol) for the

hydrogenase H-cluster, which is considerably close to the gas phase result (ΔG_{gas} = -220.6 kcal/mol).

From Figure 4-2, thermodynamic results show that most reactions considered proceed exergonically with the exception of 1 → 2 (gas phase).

Residue screening on an 8 Å layer surrounding the H-cluster has been carried out. First residue deletions and then residue substitutions were performed.

For O_2 binding to Fe_d^{II} (of the oxidized biferrous hydrogenase H-cluster subsite, Fe_p^{II}-Fe_d^{II}, (1)), results were obtained that are a function of stereoelectronic effects from the juxtaposed residues on the catalytic site. Both neutral polar and charged polar residue deletions gave good results, e.g., $\Delta Ser^{62}s^{*}$, ΔAsp^{144}, ΔGlu^{146}, ΔAsp^{150}, ΔThr^{152}, and ΔSer^{202}, with $\Delta G_{QM/MM}$ = -9.0 kcal/mol, $\Delta G_{QM/MM}$ = -8.4 kcal/mol, $\Delta G_{QM/MM}$ = -8.7 kcal/mol, $\Delta G_{QM/MM}$ = -9.4 kcal/mol, $\Delta G_{QM/MM}$ = -9.2 kcal/mol, and $\Delta G_{QM/MM}$ = -7.9 kcal/mol, respectively.

Moreover, by carrying out residue deletions within the previously mentioned apoenzyme layer, it is observed that O_2 is hindered from binding to Fe_d^{I} of the partially oxidized di-iron subsite (Fe_p^{II}-Fe_d^{I}).

Specifically, successful and, therefore, endergonic residue deletion results have been obtained for all tried residues (Table II and III), except for the following: ΔTyr^{112}, ΔLys^{237}, ΔThr^{257}, ΔThr^{259}, ΔSer^{289}, and ΔThr^{299}, with $\Delta G_{QM/MM}$ = -3.2 kcal/mol, $\Delta G_{QM/MM}$ = -2.7 kcal/mol, $\Delta G_{QM/MM}$ = -2.9 kcal/mol, $\Delta G_{QM/MM}$ = -3.0 kcal/mol, $\Delta G_{QM/MM}$ = -2.9 kcal/mol, and $\Delta G_{QM/MM}$ = -2.8 kcal/mol, respectively.

---

*s = DdH small chain

An improving trend has been observed (towards impeding O_2 binding) for residue deletions, relative to the wild-type enzyme (Table II and III), that hinder O_2 from binding to Fe_d^I, of the fully reduced di-iron subsite (Fe_p^I-Fe_d^I), which gave the following results: ΔThr^{152}, and ΔSer^{202}, with $\Delta G_{QM/MM}$ = -18.6 kcal/mol, and $\Delta G_{QM/MM}$ = -17.3 kcal/mol, respectively.

With the positive results obtained from residue deletions, we were now enabled to carry out residue substitutions (Table IV).

Therefore, by carrying out the two residue deletions, ΔThr^{152} and ΔSer^{202}, favorable Gibbs' energy have been obtained, which were followed by mutations to alanine, i.e., Thr^{152}Ala, and Ser^{202}Ala.

The dual residue deletions, ΔThr^{152} and ΔSer^{202}, gave successful Gibbs' energy results ($\Delta G_{QM/MM}$ = +5.4 kcal/mol) for the H-cluster subsite Fe_p^{II}-Fe_d^I, which obviously impede O_2 binding. However, for the H-cluster subsite, in oxidation states Fe_p^{II}-Fe_d^{II} and Fe_p^I-Fe_d^I, only a slight (O_2 inhibition) improvement for Gibbs' energy has been observed, viz., +2.2 kcal/mol and +4.4 kcal/mol respectively.

For the simultaneous mutations to alanine, i.e., Thr^{152}Ala, and Ser^{202}Ala, of the di-iron H-cluster subsite, improved Gibbs' energy results ($\Delta G_{QM/MM}$ = -9.2 kcal/mol for Fe_p^{II}-Fe_d^{II}, $\Delta G_{QM/MM}$ = +4.2 kcal/mol for Fe_p^{II}-Fe_d^I and $\Delta G_{QM/MM}$ = -18.1 kcal/mol for Fe_p^I-Fe_d^I), were also obtained for O_2 inhibition.

The rationale for choosing the two residues (Thr^{152} and Ser^{202}) is that their deletions gave good results for all oxidation states of the di-iron H-cluster subsite.

Table IV. Wild-type and Residue Mutated DdH Gibbs' Energies for O_2 Binding

Reaction:	**FeII-FeII +O_2**	**FeII-FeI +O_2**	**FeI-FeI +O_2**
Wild-type DdH	**-10.6***	**+2.6**	**-20.5**
ΔThr^{152},ΔSer^{202}	-8.4	+5.4	-16.1
ΔThr^{152},ΔSer^{202} (at 100°C)	-5.6	+7.9	-12.9
$Thr^{152}Ala$,$Ser^{202}Ala$	-9.2	+4.2	-18.1

*The Gibbs' energies are given in kcal/mol

Additionally, it is known that certain organisms containing [Fe-Fe]-hydrogenases thrive around suboceanic thermal vents[4]. Hence, at a temperature of 100 °C intercalated with hydrogenase mutations (Table IV), QM/MM results indicate that the extrinsic O_2 metalloenzyme inactivation is reduced ($\Delta G_{QM/MM}$ = -5.6 kcal/mol for Fe_p^{II}-Fe_d^{II}, $\Delta G_{QM/MM}$ = +7.9 kcal/mol for Fe_p^{II}-Fe_d^{I} and $\Delta G_{QM/MM}$ = -12.9 kcal/mol for Fe_p^{I}-Fe_d^{I}),

4.4. DdH Geometrical readjustment upon Oxidation

Here, the wild-type DdH Gibbs' energies are correlated with geometrical parameters, such as interatomic distances and bond angles.

The iron-carbon distances, Fe_p-CO_b, are now assessed for the three oxidation states of the di-iron subsites (Table V).

For the Fe_p^{II}-Fe_d^{II} subsite, the iron-carbon distance, Fe_p-CO_b, becomes smaller (1.925 Å (1) → 1.807 Å (2)) upon enzyme oxidation, occurring with a concomitant bond elongation (1.942 Å (1) → 2.287 Å (2)) between Fe_d-CO_b, which generally indicates an increased bonding strength for an exogenous ligand[67].

For the oxidation state of the di-iron subsite, Fe_p^{II}-Fe_d^{I}, the interatomic bond distance, Fe_p-CO_b, becomes smaller (1.939 Å (3) → 1.924 Å (4)), once again, upon enzyme oxidation, while a bond elongation is observed (1.908 Å (3) → 1.924 Å (4)) for Fe_d-CO_b.

Upon DdH oxidation, for the reduced di-iron subcluster (Fe_p^{I}-Fe_d^{I}), the Fe_p-CO_b interatomic bond distance becomes smaller (1.942 Å (5) → 1.935 Å (6)), as the bond Fe_d-CO_b increases (1.826 Å (5) → 1.945 Å (6)).

Table V. Interatomic Distances for Wild-Type Ddh, Between Fe_p and Co_b, Fe_d and Co_b, Fe_d and O_I, And O_I-O_{II} Before and After O_2 Binding - the Angle (Fe_d-O_I-O_{II}) Is also Given

Before O_2 binding	$Fe^{II}Fe^{II}$	$Fe^{II}Fe^{I}$	$Fe^{I}Fe^{I}$
CO_b-Fe_p	1.925*	1.939	1.942
CO_b-Fe_d	1.942	1.908	1.826
After O_2 binding			
CO_b-Fe_p	1.807	1.924	1.935
CO_b-Fe_d	2.287	1.924	1.945
O_I-Fe_d	1.729	1.840	1.808
O_I-O_{II}	1.276	1.281	1.373
Fe_d-O_I-O_{II}	137.0	160.6	126.0

*The distances are given in Å

From the above considerations, it is observed that a similar trend occurs for fully and partially oxidized, and reduced di-iron subcluster. That is, the bond between the carbon of the bridging carbonyl and the distal iron becomes longer upon O_2 binding to the catalytic site.

Following, an analysis is presented for interatomic distances between distal iron and oxygen, and between oxygen atoms, Fe_d-O_I-O_{II}, relative to Gibbs' energy for all three di-iron oxidation states.

For the Fe_p^{II}-Fe_d^{II} subcluster, the iron-oxygen distance, Fe_d-O_I, is rather small (1.729 Å; Table V), which suggests a strong bonding ($\Delta G_{QM/MM}$ = -10.6 kcal/mol; 1 → 2) between the distal iron and the oxygen atom bound to it. The inter-oxygen (O_I-O_{II}) bond distance is 1.276 Å, which corresponds to a bond order between a single and double bond.

In the case of the active di-iron subcluster, Fe_p^{II}-Fe_d^{I}, the Fe_d-O_I bond distance is ca. 6% longer (1.840 Å) than Fe_d-O_I interatomic distance of the fully oxidized di-iron subcluster, giving rise to a weaker bond ($\Delta G_{QM/MM}$ = +2.6 kcal/mol; 3 → 4) between the distal iron and the oxygen. The O_I-O_{II} bond distance is 1.281 Å, which is relatively close to the O_I-O_{II} bond for Fe_p^{II}-Fe_d^{II} subcluster.

The O_I-O_{II} bond distance is relatively larger, 1.373 Å, which suggests that π-backdonation occurs between a filled d-orbital of Fe_d and the empty π* orbital on O_2.

Out of the three di-iron oxidation states, the reduced di-iron subcluster (Fe_p^{I}-Fe_d^{I}) has most attributes of π-backdonation, i.e., the O_2 bond order has been reduced, and lengthening of the O_I-O_{II} bond to 1.373 Å.

The more e^--rich Fe_p and Fe_d, can explain why the reduced di-iron subcluster has more π-backdonation than any of the other*.

Finally, the Fe_d-O_I-O_{II} angle varies as the oxidation states decrease, viz., for Fe_p^{II}-Fe_d^{II}-O_I-O_{II} the ∠ = 137.0°, for Fe_p^{II}-Fe_d^{I}-O_I-O_{II} the ∠ = 160.6°, and for Fe_p^{I}-Fe_d^{I}-O_I-O_{II} the ∠ = 126.0° in conjunction with effects of the nearby electric field of the apoprotein.

4.5. Frontier Molecular Orbital Analysis

Here, the electronic contributions of the frontier molecular orbitals, for the aqueous enzyme phase, are presented relative to the formerly presented Gibbs' energies.

Upon O_2 binding to Fe_d of the closed-shell H-cluster (1), Figure 4-3, the lone pair of electrons residing on the incoming O_2 are transferred into the vacant Fe_d d-orbital.

For Fe_p^{II}-Fe_d^{II} subcluster (Figure 4-2, 1 → 2), the empty lowest unoccupied molecular orbital (LUMO) is essentially composed of an empty d-orbital of Fe_d (where O_2 bonding occurs); it also extends over the π-orbital of CO_b (Figure 4-3). Therefore, LUMO for Fe_p^{II}-Fe_d^{II} subcluster is favorable for O_2 bonding (which is confirmed by Gibbs' energy, viz., -10.6 kcal/mole, 1 → 2).

---

* This π-backdonation agrees with Gibbs' energy results form Table II. For example, the Fe_p^{II}-Fe_d^{II} subcluster has an exergonic Gibbs' energy ($\Delta G_{QM/MM}$ = -16.6 kcal/mol), which can be improved however by DdH mutations such as residue deletions and substitutions, since there is only slight π-backdonation present. The bond Fe_d-O_I is still relatively weak (ΔG = -7.9 kcal/mol) for Fe_p^{II}-Fe_d^{I} subsite. However, for the reduced Fe_p^{I}-Fe_d^{I} subsite, the π-backdonation makes the oxygen bond very strong, thus making its elimination rather difficult (even by means of DdH mutations, Table IV).

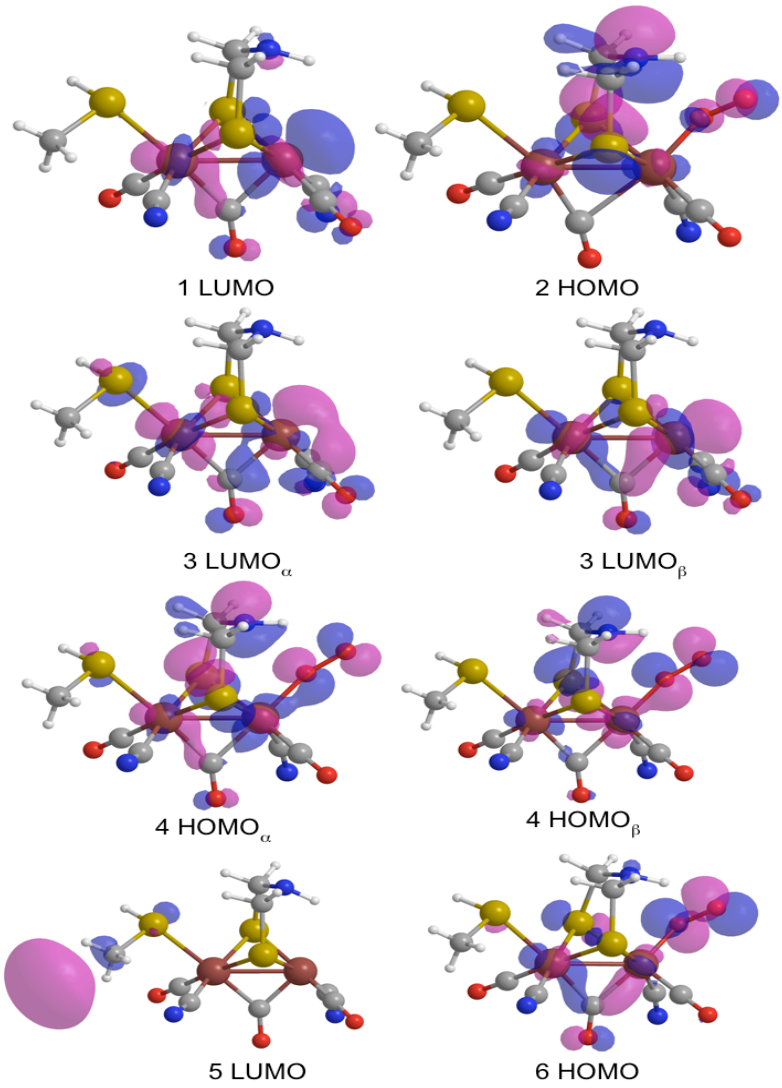

Figure 4-3. Frontier molecular orbitals (aqueous enzyme phase) for H-clusters LUMO (1), HOMO (2), LUMO$_\alpha$ (3), LUMO$_\beta$ (3), HOMO$_\alpha$ (4), HOMO$_\beta$ (4), LUMO (5), and HOMO (6) (where the atom colors, of the H-clusters, are O = red, C = grey, N = blue, S = yellow, Fe = burgundy, and H = white).

Once the O_2 binding has occurred, the e^-s do not necessarily remain localized on Fe_d^{100}, Figure 4-3, as the e^- density is predominantly delocalized on the DTMA bidentate ligand.

For the open shell Fe_p^{II}-Fe_d^{I} subcluster, both $LUMO_\alpha$ and $LUMO_\beta$ show large virtual orbitals surrounding their Fe_d, some e^- delocalization over the terminal ligands of Fe_d, CO_b, and over Fe_p. As for $LUMO_\alpha$, some e^- delocalization is observed on cysteinyl sulfur of Cys^{382}.

It seems, in retrospect, that LUMO of Fe_p^{II}-Fe_d^{II} subcluster, having a more localized orbital on Fe_d, than $LUMO_\alpha$ and $LUMO_\beta$ (of Fe_p^{II}-Fe_d^{I} subcluster), favors the above mentioned spontaneous reaction ($\Delta G_{QM/MM}$ = -10.6 kcal/mole, 1 → 2) with O_2.

Again, (Figure 4-2, 3 → 4) once O_2 bonding occurs, for the open shell Fe_p^{II}-Fe_d^{I} subcluster, $HOMO_{\alpha,,}$ and $HOMO_\beta$ are delocalized over the DTMA bridge, over the bonded O_2 (slightly more by $HOMO_\beta$), and over Fe_p^{II}-Fe_d^{I} (especially by $HOMO_\alpha$). Thus, again, once O_2 bonding occurs, the e^-s migrate away from Fe_d (Figure 4-3) in the Fe_p^{II}-Fe_d^{I} subcluster.

For Fe_p^{I}-Fe_d^{I} subcluster (Figure 4-2, 5), LUMO is found to be delocalized near the cubane/cysteines moiety. Nevertheless, in spite of the empty orbital shape (LUMO, Figure 4-3), the binding occurs between the distal iron and exogenous ligand, Fe_d^{I}-O_2 (5). In cluster 6 (Figure 4-3), π-backdonation seems to occur between the filled d-orbitals of Fe_p^{I}-Fe_d^{I} and the π*-orbital of the exogenous O_2.

As formerly mentioned, the (electron lone pair) π-backdonation for the reduced Fe_p^{I}-Fe_d^{I} subsite makes the iron-oxygen bond (in Fe_d^{I}-O_2) rather strong ($\Delta G_{QM/MM}$ = -20.5 kcal/mol), thus making its removal difficult even by means of DdH mutations, Table IV.

4.6. Conclusion

Because it is expensive to work with the wild-type DdH in anaerobic conditions, we have in silico mutated [Fe-Fe]-hydrogenase, thus preventing or weakening the bonding of exogenous O_2 to the active site.

The [Fe-Fe]-hydrogenase mutations have been carried out in two steps on an 8 Å layer surrounding the H-cluster using residue screening. First, residue deletions have been performed, one by one. Then, from clues obtained from these residue deletions, residue substitutions have been performed on the wild-type DdH.

For DdH residue deletions, regarding O_2 binding to Fe_d^{II} (of hydrogenase H-cluster subsite, Fe_p^{II}-Fe_d^{II}), both neutral polar residue and charged residue deletions gave enhanced results ΔSer^{62}s, ΔAsp^{144}, ΔGlu^{146}, ΔAsp^{150}, ΔThr^{152}, and ΔSer^{202}, with $\Delta G_{QM/MM}$ = -9.0 kcal/mol, $\Delta G_{QM/MM}$ = -8.4 kcal/mol, $\Delta G_{QM/MM}$ = -8.7 kcal/mol, $\Delta G_{QM/MM}$ = -9.4 kcal/mol, $\Delta G_{QM/MM}$ = -9.2 kcal/mol, and $\Delta G_{QM/MM}$ = -7.9 kcal/mol, respectively.

Then, by carrying out residue deletions, on the partially oxidized di-iron subcluster (Fe_p^{II}-Fe_d^{I}), it is observed that O_2 is hindered from binding to Fe_d^{I}, in most cases.

Specifically, successful (or endergonic) residue deletions have been obtained for most assessed residues; several of the endergonic (successful) residue deletions are ΔGlu^{374}, ΔAsp^{144}, ΔSer^{177}, and ΔThr^{152}, giving $\Delta G_{QM/MM}$ = +4.7 kcal/mol, $\Delta G_{QM/MM}$ = +4.6 kcal/mol, $\Delta G_{QM/MM}$ = +4.4 kcal/mol, and $\Delta G_{QM/MM}$ = +4.1 kcal/mol, respectively (Table II).

For several residue deletions, a successful trend has been observed in hindering O_2 binding to Fe_d^{I} (Fe_p^{I}-Fe_d^{I}), relative to the wild-type enzyme (Table II), which gave the

following results for ΔThr^{152}, and ΔSer^{202} DdH mutants, giving $\Delta G_{QM/MM}$ = -18.6 kcal/mol, and $\Delta G_{QM/MM}$ = -17.3 kcal/mol, respectively.

Results for residue substitutions are now presented (for they were carried out after residue deletions with clues thereof). Therefore, by carrying out residue deletions for ΔThr^{152} and ΔSer^{202}, and finding improvements in Gibbs' energy, the subsequent mutations to alanine were carried out, viz., $Thr^{152}Ala$, and $Ser^{202}Ala$.

The two-residue deletions, $\Delta Thr^{152}$and ΔSer^{202}, on Fe_p^{II}-Fe_d^{I} hydrogenase, gave successful Gibbs' energy; the O_2 binding is hindered by +5.4 kcal/mol. Also, for Fe_p^{I}-Fe_d^{I} hydrogenase, a small (O_2 inhibition) improvement for Gibbs' energy has been found, viz., +4.4 kcal/mol.

The difference between the two residue deletions ($\Delta Thr^{152}$and ΔSer^{202}) and two residue substitutions ($Thr^{152}Ala$, and $Ser^{202}Ala$) with alanine is small ($\Delta G_{QM/MM} \sim +2$ kcal/mol), for O_2 binding, and it is attributed to the overall charge of alanine which is approximately zero. However, this closeness in Gibbs' energy for deletions and substitutions is unlikely to be found for mutations using charged amino acids (e.g. $Thr^{152}Glu$, and $Ser^{202}Glu$). Hence, DdH mutations open up new research opportunities along these lines.

Finally, from FMO and geometrical analysis, evidence exists for π-backdonation, especially for Fe_p^{I}-Fe_d^{I} species. The strong observed Fe_d^{I}-O_2 bonding is likely to be influenced by π-backbonding between the filled d-orbitals of distal iron and π* orbital on oxygen.

References

(1) Tye, J. W.; Darensbourg, M. Y.; Hall, M. B. *Inorg. Chem.* **2008**, *47*, 2380.

(2) Liu, Z.-P.; Hu, P. *J. Am. Chem. Soc.* **2002**, *124*, 5175.

(3) Das, D.; Dutta, T.; Nath, K.; Kotay, S. M.; Das, A. K.; Veziroglu, T. N. *Curr. Sci.* **2006**, *90*, 1627.

(4) Cammack, R.; Frey, M.; R., R. *Hydrogen as a Fuel: Learning from the Nature*; CRC Press, 2001.

(5) Melis, A.; Zhang, L.; Forestier, M.; Ghirardi, M. L.; Seibert, M. *Plant Physiol.* **2000**, *122*, 127.

(6) Albracht, S. P. J. *Biochim. Biophys. Acta* **1994**, *1118*, 167.

(7) Woodward, J.; Cordray, K. A.; Edmonston, R. J.; Blanco-Rivera, M.; Mattingly, S. M.; Evans, B. R. *Energy Fuels* **2000**, *14*, 197.

(8) Wolpher, H.; Borgstrom, M.; Hammarstrom, L.; Bergquist, J.; Sundstrom, V.; Stenbjorn, S.; Sun, L. C.; Akermark, B. *Inorg. Chem.Commun.* **2003**, *6*, 989.

(9) Winter, A.; Zsolnai, L.; Huttner, G. Z. *Naturforsch., B: Chem. Sci.* **1982**, *37B*, 1430.

(10) Windhager, J.; Rudolph, M.; Brautigan, S.; Gorls, H.; Weigand, W. *Eur. J. Inorg. Chem.* **2007**, *18*, 2748.

(11) Wang, Z.; Liu, J.; He, C.; Jiang, S.; Akermark, B.; Sun, L. *Inorg. Chim. Acta.* **2007**, *360*, 2411.

(12) Jiang, S.; Liu, J.; Shi, Y.; Wang, Z.; Akermark, B.; Sun, L. *Polyhedron* **2007**, *26*, 1499.

(13) Tsuda, M.; Dino, W. A.; Kasai, H. *Solid State Commun.* **2005**, *133*, 589.

(14) Treichel, P. M.; Rublein, E. K. *J. Organomet. Chem.* **1989**, *359*, 195.

(15) Tard, C.; Liu, X. M.; Ibrahim, S. K.; Bruschi, M.; De Gioia, L.; Davies, S. C.; Yang, X.; Wang, L. S.; Sawers, G.; Pickett, C. J. *Nature* **2005**, *433*, 610.

(16) Sun, L.; Akermark, B.; Ott, S. *Coord. Chem. Rev.* **2005**, *249*, 1653.

(17) van der Vlugt, J. I.; Rauchfuss, T. B.; Wilson, S. R. *Chem. Eur. J.* **2006**, *12*, 90.

(18) Song, L.-C.; Ge, J.-H.; Zhang, X.-G.; Liu, Y.; Hu, Q.-M. *Eur. J. Inorg. Chem.* **2006**, 3204.

(19) Song, L. C.; Yang, Z. Y.; Hua, Y. J.; Wang, H. T.; Liu, Y.; Hu, Q. M. *Organometallics* **2007**, *26*, 2106.

(20) Smith, M. C.; Barclay, J. E.; Davies, S. C.; Hughes, D. L.; Evans, D. J. *Dalton Trans.* **2003**, 4147.

(21) Seyferth, D.; Womack, G. B.; Gallagher, M. K.; Cowie, M.; Hames, B. W.; Fackler, J. P., Jr.; Mazany, A. M. *Organometallics* **1987**, *6*, 283.

(22) Seyferth, D.; Henderson, R. S.; Song, L. C. *Organometallics* **1982**, *1*, 125.

(23) Schwartz, L.; Ekstrom, J.; Lomoth, R.; Ott, S. *Chem. Commun.* **2006**, 4206.

(24) Ott, S.; Kritikos, M.; Akermark, B.; Sun, L.; Lomoth, R. *Angew. Chem., Int. Ed.* **2004**, *43*, 1006.

(25) Ott, S.; Borgstrom, M.; Kritikos, M.; Lomoth, R.; Bergquist, J.; Akermark, B.; Hammarstrom, L.; Sun, L. C. *Inorg. Chem.* **2004**, *43*, 4683.

(26) Nandi, R.; Sengupta, S. *Crit. Rev. Microbiol.* **1998**, *24*, 61.

(27) Morvan, D.; Capon, J. F.; Gloaguen, F.; Le Goff, A.; Marchive, M.; Michand, F.; Schollhammer, P.; Talarmin, J.; Yaouanc, J. J. *Organometallics* **2007**, *26*, 2042.

(28) Morozov, S. V.; Karyakina, E. E.; Zorin, N. A.; Varfolomeyev, S. D.; Cosnier, S.; Karyakin, A. A. *Bioelectrochemistry* **2002**, *55*, 169.

(29) Mejia-Rodriguez, R.; Chong, D.; Reibenspies, J. H.; Soriaga, M. P.; Darensbourg, M. Y. *J. Am. Chem. Soc.* **2004**, *126*, 12004.

(30) Liaw, W. F.; Lee, J. H.; Gau, H. B.; Chen, C. H.; Jung, S. J.; Hung, C. H.; Chen, W. Y.; Hu, C. H.; Lee, G. H. *J. Am. Chem. Soc.* **2002**, *124*, 1680.

(31) Li, P.; Wang, M.; He, C.; Li, G.; Liu, X.; Chen, C.; Akermark, B.; Sun, L., . *Eur. J. Inorg. Chem.* **2005**, 2506.

(32) Lamle, S. E.; Halliwell, L. M.; Armstrong, F. A.; Albracht, S. P. *J. Inorg. Biochem.* **2003**, *96*, 174.

(33) Karyakin, A. A.; Morozov, S. V.; Karyakina, E. E.; Zorin, N. A.; Perelygin, V. V.; Cosnier, S. *Biochem. Soc. Trans.* **2005**, *33*, 73.

(34) Karyakin, A. A.; Morozov, S. V.; Karyakina, E. E.; Varfolomeyev, S. D.; Zorin, N. A.; Cosnier, S. *Electrochem. Commun.* **2002**, *4*, 417.

(35) Jiang, S.; Liu, J.; Shi, Y.; Wang, Z.; Akermark, B.; Sun, L. *Dalton Trans.* **2007**, 896.

(36) Homann, P. H. *Photosynth. Res.* **2003**, *76*, 93.

(37) Hieber, W.; Spacu, P. Z. *Z. Anorg. Allg. Chem.* **1937**, *233*, 353.

(38) Duan, L.; Wang, M.; Li, P.; Na, Y.; Wang, N.; Sun, L. *Dalton Trans.* **2007**, 1277.

(39) Gloaguen, F.; Lawrence, J. D.; Schmidt, M.; Wilson, S. R.; Rauchfuss, T. B. *J. Am. Chem. Soc.* **2001**, *123*, 12518.

(40) Gloaguen, F.; Lawrence, J. D.; Rauchfuss, T. B.; Be´nard, M.; Rohmer, M.-M. *Inorg. Chem.* **2002**, *41*, 6573.

(41) Gao, W.; Ekstrom, J.; Liu, J.; Chen, C.; Eriksson, L.; Weng, L.; Akermark, B.; Sun, L. *Inorg. Chem.* **2007**, *46*, 1981.

(42) Fauvel, K.; Mathieu, R.; Poilblanc, R. *Inorg. Chem.* **1976**, *15*, 976.

(43) De Lacey, A. L.; Pardo, A.; Fernandez, V. M.; Dementin, S.; Adryanczyk-Perrier, G.; Hatchikian, E. C.; Rousset, M. *J. Biol. Inorg. Chem.* **2004**, *9*, 636.

(44) De Lacey, A. L.; Detcheverry, M.; Moiroux, J.; Bourdillon, C. *Biotechnol. Bioeng.* **2000**, *68*, 1.

(45) Capon, J.-F.; Gloaguen, F.; Schollhammer, P.; Talarmin, J. *J. Electroanal. Chem.* **2004**, *566*, 241.

(46) Borg, S. J.; Behrsing, T.; Best, S. P.; Razavet, M.; Liu, X.; Pickett, C. J. *J. Am. Chem. Soc.* **2004**, *126*, 16988.

(47) Vignais, P. M.; Billoud, B.; Meyer, J. *FEMS Microbiol. Rev.* **2001**, *25*, 455.

(48) Adams, M. W. W. *Biochim. Biophys. Acta* **1990**, *1020*, 115.

(49) Adams, M. W. W.; Stiefel, E. I. *Science* **1998**, *282*, 1842.

(50) Happe, R. P.; Roseboom, W.; Pierik, A. J.; Albracht, S. P.; Bagley, K. A. *Nature* **1997**, *385*, 126.

(51) Nicolet, Y.; Cavazza, C.; Fontecilla-Camps, J. C. *J. Inorg. Biochem.* **2002**, *91*, 1.

(52) Peters, J. W.; Lanzilotta, W. N.; Lemon, B. J.; Seefeldt, L. C. *Science* **1998**, *282*, 1853.

(53) Nicolet, Y.; Piras, C.; Legrand, P.; Hatchikian, E. C.; Fontecilla-Camps, J. C. *Structure* **1999**, *7*, 13.

(54) Dogaru, D.; Motiu, S.; Gogonea, V. *Int J Quantum Chem* **2009**, *109*.

(55) Liu, Z.-P.; Hu, P. *J. Chem. Phys.* **2002**, *117*, 8177.

(56) Bruschi, M.; Fantucci, P.; De Gioia, L. *Inorg. Chem.* **2002**, *41*, 1421.

(57) Bruschi, M.; Fantucci, P.; De Gioia, L. *Inorg. Chem.* **2003**, *42*, 4773.

(58) Bruschi, M.; Fantucci, P.; De Gioia, L. *Inorg. Chem.* **2004**, *43*, 3733.

(59) Zampella, G.; Bruschi, M.; Fantucci, P.; Razavet, M.; Pickett, C. J.; De Gioia, L. *Chem. Eur. J.* **2005**, *11*, 509.

(60) Cao, Z.; Hall, M. B. *J. Am. Chem. Soc.* **2001**, *123*, 3734.

(61) Fan, H.-J.; Hall, M. B. *J. Am. Chem. Soc.* **2001**, *123*, 3828.

(62) Greco, C.; Bruschi, M.; De Gioia, L.; Ryde, U. *Inorg. Chem.* **2007**, *46*, 5911.

(63) Trohalaki, S.; Pachter, R. *ENERG. FUEL.* **2007**, *21*, 2278.

(64) Greco, C.; Bruschi, M.; Heimdal, J.; Fantucci, P.; De Gioia, L.; Ryde, U. *Inorg. Chem.* **2007**, *46*, 7256.

(65) Greco, C.; Bruschi, M.; Fantucci, P.; De Gioia, L. *Eur. J. Inorg. Chem.* **2007**, *13*, 1835.

(66) Greco, C.; Zampella, G.; Bertini, L.; Bruschi, M.; Fantucci, P.; De Gioia, L. *Inorg. Chem.* **2007**, *46*, 108. (67) Motiu, S.; Dogaru, D.; Gogonea, V. *Int. J. Quantum Chem.* **2007**, *107*, 1248.

(68) Bruschi, M.; Zampella, G.; Fantucci, P.; De Gioia, L. *Coord. Chem. Rev.* **2005**, *15-16*, 1620.

(69) Liu, X.; Ibrahim, S. K.; Tard, C.; Pickett, C. J. *Coord. Chem. Rev.* **2005**, *15-16*, 1641.

(70) Armstrong, F. A. *Curr. Opin. Chem. Biol.* **2004**, *8*, 133.

(71) Rauchfuss, T. B. *Inorg. Chem.* **2004**, *43*, 14.

(72) Evans, D. J.; Pickett, C. J. *Chem. Soc. Rev.* **2003**, *35*, 268.

(73) Chen, Z.; Lemon, B. J.; Huang, S.; Swartz, D. J.; Peters, J. W.; Bagley, K. A. *Biochemistry* **2002**, *41*, 2036.

(74) Horner, D. S.; Heil, B.; Happe, T.; Embley, T. M. *Trends Biochem. Sci.* **2002**, *27*, 148.

(75) Borg, S. J.; Tye, J. W.; Hall, M. B.; Best, S. P. *Inorg. Chem.* **2007,**, *46*, 384.

(76) Zilberman, S.; Stiefel, E. I.; Cohen, M. H.; Car, R. *Inorg. Chem.* **2007**, *46*, 1153.

(77) Tye, J. W.; Darensbourg, M. Y.; Hall, M. B. *J. Mol. Struct. (Theochem)* **2006**, *771*, 123–128.

(78) Eilers, G.; Schwartz, L.; Stein, M.; Zampella, G.; Gioia, L. d.; Ott, S.; Lomoth, R. *Chem. Eur. J.* **2007**, *13*, 7075 –7084.

(79) Lyon, E. J.; Georgakaki, I. P.; Reibenspies, J. H.; Darensbourg, M. Y. *Angew. Chem., Int. Ed.* **1999**, *38*, 3178.

(80) Cloirec, A. L.; Best, S. P.; Borg, S.; Davies, S. C.; Evans, D. J.; Hughes, D. L.; Pickett, C. J. *Chem. Commun.* **1999**, 2285.

(81) Rauchfuss, T. B.; Contakes, S. M.; Schmidt, M. *J. Am. Chem. Soc.* **1999**, *121*, 9736.

(82) Lai, C.-H.; Lee, W.-Z.; Miller, M. L.; Reibenspies, J. H.; Darensbourg, D. J.; Darensbourg, M. Y. *J. Am. Chem. Soc.* **1998**, *120*, 10103.

(83) Pierik, A. J.; Hagen, W. R.; Redeker, J. S.; Wolbert, R. B. G.; Boersma, M.; Verhagen, M. F.; Grande, H. J.; Veeger, C.; Mustsaers, P. H. A.; Sand, R. H.; Dunham, W. R. *Eur. J. Biochem.* **1992**, *209*, 63.

(84) Zambrano, I. C.; Kowal, A. T.; Mortenson, L. E.; Adams, M. W. W.; Johnson, M. K. *J. Biol. Chem.* **1989**, *264*, 20974.

(85) Patil, D. S.; Moura, J. J.; He, S. H.; Teixeira, M.; Prickril, B. C.; DerVartanian, D. V.; Jr., P. H. D.; LeGall, J.; Huynh, B. H. *J. Biol. Chem.* **1988**, *263*, 18732.

(86) Rusnak, F. M.; Adams, M. W. W.; Mortenson, L. E.; Munck, E. *J. Biol. Chem.* **1987**, *262*, 38.

(87) Adams, M. W. W. *J. Biol. Chem.* **1987**, *262*, 15054.

(88) Adams, M. W. W.; Mortenson, L. E. *J. Biol. Chem.* **1984**, *259*, 7045.

(89) Rappe, A. K.; Casewit, C. J.; Colwell, K. S.; Goddard, W. A.; Skiff, W. M. *J. Am. Chem. Soc.* **1992**, *113*, 10024.

(90) Dapprich, S.; Komaromi, I.; Byun, K. S.; Morokuma, K.; Frisch, M. J. *J. Mol. Struct. (Theochem)* **1999**, *461*, 1.

(91) Frisch, M. J.; Trucks, G. W.; Schlegel, H. B.; Scuseria, G. E.; Robb, M. A.; Cheeseman, J. R.; Montgomery, J., J. A.; Vreven, T.; Kudin, K. N.; Burant, J. C.; Millam, J. M.; Iyengar, S. S.; Tomasi, J.; Barone, V.; Mennucci, B.; Cossi, M.; Scalmani, G.; Rega, N.; Petersson, G. A.; Nakatsuji, H.; Hada, M.; Ehara, M.; Toyota, K.; Fukuda, R.; Hasegawa, J.; Ishida, M.; Nakajima, T.; Honda, Y.; Kitao, O.; Nakai, H.; Klene, M. L., X.; Knox, J. E.; Hratchian, H. P.; Cross, J. B.; Bakken, V.; Adamo, C.; Jaramillo, J.; Gomperts, R.; Stratmann, R. E.; Yazyev, O.; Austin, A. J.; Cammi, R.; Pomelli, C.; Ochterski, J. W.; Ayala, P. Y.; Morokuma, K.; Voth, G. A.; Salvador, P.; Dannenberg, J. J.; Zakrzewski, V. G.; Dapprich, S. D., A. D.; Strain, M. C.; Farkas, O.; Malick, D. K.; Rabuck, A. D.; Raghavachari, K.; Foresman, J. B.; Ortiz, J. V.; Cui, Q.; Baboul, A. G.; Clifford, S.; Cioslowski, J.; Stefanov, B. B.; Liu, G.; Liashenko, A.; Piskorz, P.; Komaromi, I.; Martin, R. L.; Fox, D. J.; Keith, T.; Al-Laham, M. A.; Peng, C. Y.;

Nanayakkara, A.; Challacombe, M.; Gill, P. M. W.; Johnson, B.; Chen, W.; Wong, M. W.; Gonzalez, C.; Pople, J. A. Gaussian 03, Revision C.02; Gaussian, Inc.: Wallingford CT, 2004.

(92) Becke, A. D. *J. Chem. Phys.* **1993**, *98*, 5648.

(93) Lee, C.; Yang, W.; Parr, R. G. *Phys. Rev. B* **1988**, *37*, 785.

(94) Berendsen, H. J. C.; van der Spoel, D. *Comp. Phys. Comm.* **1995**, *91*, 43.

(95) Lindahl, E.; Hess, B. *J. Mol. Mod.* **2001**, *7*, 306.

(96) Popescu, C. V.; Munck, E. *J. Am. Chem. Soc.* **1999**, *121*, 7877.

(97) Rappe, A. K.; Goddard, W. A. *J. Phys. Chem.* **1991**, *95*, 3358.

(98) Zumdahl, S. S.; Zumdahl, S. A. *Chemistry*; Houghton Mifflin Company: Boston, 2000.

(99) Peters, J. W. *Curr. Opin. Struct. Biol.* **1999**, *9*, 670.

(100) Roseboom, W.; De Lacey, A. L.; Fernandez, V. M.; Hatchikian, E. C.; Albracht, S. P. J. *J. Biol. Inorg. Chem.* **2006**, *11*, 102.